Universidade Federal do Rio de Janeiro – UFRJ

Centro de Ciências da Saúde

Faculdade de Odontologia

ESTUDO DA ANATOMIA DO SEPTO NASAL E SUA RELAÇÃO COM A MORFOLOGIA DO COMPLEXO NASOMAXILAR

Sarah Braga Sayão de Paula

CD

Dissertação submetida ao corpo docente da Faculdade de Odontologia da Universidade Federal do Rio de Janeiro - UFRJ, como parte dos requisitos, para a obtenção do Título de Mestre em Odontologia (Ortodontia).

Rio de Janeiro

2021

ESTUDO DA ANATOMIA DO SEPTO NASAL E SUA RELAÇÃO COM A MORFOLOGIA DO COMPLEXO NASOMAXILAR

SARAH BRAGA SAYÃO DE PAULA, CD

Orientadora: Profª. Drª. AMANDA CUNHA REGAL DE CASTRO

Dissertação submetida ao corpo docente da Faculdade de Odontologia da Universidade Federal do Rio de Janeiro - UFRJ, como parte dos requisitos, para a obtenção do Título de Mestre em Odontologia (Ortodontia).

Comissão Examinadora:

Profª. Drª. Matilde da Cunha Gonçalves Nojima
CD, MO, DO

Prof. Dr. Eduardo Franzotti Sant'Anna
CD, MO, DO

Prof. Dr. Rodrigo Lopes de Lima
CD, MO, DO

Rio de Janeiro

2021

Ficha Catalográfica

DE PAULA, Sarah Braga Sayão

Estudo da anatomia do septo nasal e sua relação com a morfologia do complexo nasomaxilar. Rio de Janeiro: UFRJ/Faculdade de Odontologia, 2021.

xxvii, 80 f.

Dissertação: Mestrado em Odontologia (Ortodontia) – Universidade Federal do Rio de Janeiro – UFRJ, Faculdade de Odontologia, 2021.

1 Septo nasal **2 Complexo nasomaxilar**

3 Tomografia Computadorizada de Feixe Cônico **4 Teses**

I Título
II Dissertação (Mestrado – UFRJ/Faculdade de Odontologia)

Linha de Pesquisa do Programa de Pós-graduação em Odontologia da Faculdade de Odontologia da UFRJ (Área de Concentração em Ortodontia): Avaliação do crescimento e do desenvolvimento da face e do aparelho mastigador.

Plataforma Sucupira

Projeto: Aspectos moduladores da morfologia craniofacial, fisiologia do movimento dentário, diagnóstico e tratamento ortodônticos.

Comitê de Ética em Pesquisa do Hospital Universitário Clementino Fraga Filho (CEP-HUCFF) da UFRJ (Rio de Janeiro, Brasil)

Projeto: Estudo da relação do septo nasal com as características do complexo nasomaxilar (Cadastro na Plataforma Brasil).

Parecer de aprovação: 3.888.756

CAAE: 27431319.4.0000.5257

DEDICO

Dedico ao **Mauro Sérgio de Paula Santos**, meu esposo, que é meu companheiro em todas as situações, que me ajuda e me apoia em todos os momentos, e que está sempre presente nas minhas maiores conquistas.

AGRADECIMENTOS

Agradeço primeiramente à **Deus**, que é meu escudo e fortaleza, e meu forças para continuar mesmo nos momentos mais difíceis.

Ao meu esposo **Mauro Sérgio de Paula Santos**, que esteve comigo durante todo o curso, me apoiando e foi meu maior incentivador.

Aos meus pais, **Eliane dos Santos Braga Sayão e Ricardo Beda de Amorim Sayão,** juntamente com minha irmã **Mariana Braga Sayão**, que estão sempre por perto dando apoio e porque sempre me incentivam a dar o melhor de mim.

Aos meus grandes amigos da turma 55, **Ericles Otávio Santos, Letícia Iandeyara Dantas de Andrade Sant'Anna, Mariana Braz Herzog, Marina Viudes Bruder Câmara e Rafael Cunha de Bittencourt**, que passaram por momentos tanto difíceis quanto alegres comigo durante essa jornada que foi a Ortodontia da UFRJ, por ouvirem meus desabafos e choros, e por estarem sempre presentes. Passamos por essa pandemia juntos e por 3 anos de mestrado. Obrigada por tudo, quero levá-los por toda a vida.

À turma 54, minhas veteranas, **Annanda Pinheiro Martins, Daniela Gomes Rezende de Azevedo, Luísa Schubach da Costa Barreto, Luíza Trindade Vilela, Taiane dos Santos Lopes e Thais Prates Vieira** por terem sido um segundo ano maravilhoso, por me incentivarem e ajudarem muito. Nossa convivência foi maravilhosa e levo todas vocês com muito carinho.

Agradeço também à turma 56, **Joberth Rainner Baliza de Paula, Líris Cristina Nepomuceno Pinto, Marcelly Dias Silva, Mariana Fernandes Meirelles Azevedo, Michelle da Silveira Guimarães e Thalita Teixeira Santana**, por todos os momentos bons que compartilhamos, pelas trocas e aprendizados, foi muito bom conviver com vocês.

Um agradecimento muito especial à minha orientadora, professora **Dra. Amanda Cunha Regal de Castro**, que foi muito presente, me ajudou muito, e sem ela essa dissertação com certeza não teria sido concluída. Agradeço por todo incentivo, paciência e parceria, não só como minha orientadora, mas também nas clínicas e laboratórios. A senhora é motivo de inspiração para mim.

À professora e coordenadora do curso **Dra. Mônica Tirre de Souza Araújo** por todo cuidado e carinho comigo e minha turma, por nos ajudar e ensinar muito além da ortodontia.

Ao professor **Dr. Antônio Carlos de Oliveira Ruellas**, pelas aulas online, por todos os seminários que fizemos e aprendemos tanto, por toda paciência conosco e vontade de nos ensinar. Agradeço pela ajuda que me deu diversas vezes em relação à minha dissertação. Obrigada por ser um profissional e professor incrível, todos somos inspirados por você.

À professora **Dra. Matilde da Cunha Gonçalves Nojima**, por todo carinho e preocupação que sempre demostrou conosco, por todos os ensinamentos em Ortodontia e também de vida, por ser uma mãezona para nós.

Ao professor **Dr. Lincoln Issamu Nojima**, pelos valiosos ensinamentos em clínica, laboratório, seminários, e por tentar sempre trazer o que temos de mais tecnológico e sempre nos incentivar em melhorar e aprender.

Ao professor **Dr. Eduardo Franzotti Sant'Anna**, pelos ensinamentos transmitidos em clínica e laboratório, e pela vontade de fazer o melhor para os pacientes.

À professora **Dra. Ana Maria Bolognese,** por todos os ensinamentos passados, por me ensinar a ser uma melhor aluna e futura professora, por toda paciência e zelo conosco.

À professora **Dra. Margareth Maria Gomes de Souza**, por todo companheirismo, por me passar não só muito conhecimento em Ortodontia, mas também em relação à vida. Por muitas vezes pegar na minha mão e fazer junto comigo. Pela força de vontade e por me inspirar a ser uma pessoa tão disposta a fazer sempre o melhor.

Ao professor **Dr. José Fernando Stangler Brazzalle,** que se tornou uma grande admiração para mim, com seu fascínio e amor pela Ortodontia e por nos ensinar e incentivar sempre a ser o melhor que pudermos. Obrigada pela sua

dedicação e paciência, e pelos valiosos ensinamentos que guardarei sempre com muito carinho.

Ao professor **Dr. Rodrigo Lopes de Lima**, por toda paciência, atenção e carinho, por nos ensinar tanto e sempre de muito bom grado. Por ter me ajudado diversas vezes no laboratório e me ajudado a melhorar sempre.

Ao professor **Dr. Luiz Felipe Cardoso de Araújo**, que pegou na minha mão e acreditou no meu potencial, mesmo quando eu mesma não acreditava. Que me incentivou e me ensinou muito, sempre com muita paciência e dedicação. Me inspiro no profissional que você é e sempre lembrarei de todos os seus ensinamentos com muito carinho.

Ao professor **Dr. Sérgio Luiz Mota Júnior,** que chegou assim que nossa turma entrou, e nos ajudou tanto, sempre nos incentivando a dar nosso melhor. Agradeço por toda sua paciência, dedicação e vontade em nos ensinar. Você foi um presente para a nossa turma.

À professora **Luciana Rougemont Squeff**, por todo carinho e ajuda em algumas clínicas que tivemos. Gostaria que nossa convivência tivesse sido maior, mas nesse tempo que tivemos, foi muito bom poder contar com a senhora.

À professora **Lorena Andrade Nunes**, da Bahia, que me ajudou muito em diversas partes da minha dissertação, por toda paciência, reuniões online e pela parceria que criamos. Você foi essencial para a conclusão deste trabalho.

Aos professores das disciplinas de áreas conexas **Dr. Bruno Santos de Barros Dias, Dr. Carlos Nelson Elias, Dr. David Normando, Dr. Fábio Ribeiro Guedes, Dr^{a}. Andreia Cristina Breda de Souza, Dr^{a}. Maria Augusta Visconti, Dra. Maria Cynésia Medeiros de Barros, Dr. Rafael Seabra Louro, Dr. Ramiro Beato Souza, Dr. Elson Braga de Mello, Dr. Ivo Carlos Corrêa, Dr. Alexandre Rezende Vieira, Dr. Jonatas Esteves Caldeira**, pelas aulas importantíssimas para complementar à minha formação acadêmica e profissional.

Aos amigos do doutorado, **Bruna Caroline Tomé Barreto, Eduardo Otero Amaral Vargas, Karoline de Melo Magalhães, Flávio de Mendonça Copello, Guido Artemio Marañon Vasquez, Katherine J. de C. M. P. Silver, Kelly Galisteu Luiz, Sylvia de Araújo Paes Souza, Carolina Ribeiro Starling, Lilian Siqueira de Lima, Pedro Lima Emmerich Oliveira, Alice Spitz, Fernanda Blaudt Carvalho Marques, Johnny de Gawn, Ana Paula Tenório**

de Sá, Luciana Duarte Caldas e Teresa Cristina Pereira de Oliveira, pelos dias compartilhados e amizade criada no departamento.

Aos professores **Dra. Mariana Martins e Martins, Dra. Beatriz Vilella e Dr. Oswaldo Vilella, da Universidade Federal Fluminense,** por despertarem meu interesse pela Ortodontia ainda na Graduação, e por serem fonte de inspiração e incentivo.

Aos funcionários, **Diane Esteves de Souza Gomes, Laís Paiva Monteiro, Mônica Mello do Nascimento Gonçalves, Guilhermino Estanhe Saturnino e Edinaldo da Silva**, pelo ótimo convívio e disponibilidade.

Aos **alunos da graduação** da turma 2021/1, que me ajudaram na minha formação como Mestre.

Aos queridos **pacientes** do **Departamento de Ortodontia e Odontopediatria da UFRJ**, obrigada por fazerem parte dessa história, pelo carinho e paciência em todas as consultas. Vocês me tornaram uma profissional melhor.

À **Coordenação de Aperfeiçoamento de Pessoal de Nível Superior (CAPES)**, pela bolsa de estudos concedida, auxiliando na minha formação acadêmica e profissional. “O presente trabalho foi realizado com o apoio da Coordenação de Aperfeiçoamento de Pessoal de Nível Superior – Brasil (CAPES) – Código de Financiamento 001.”

A **todos** que contribuíram direta e indiretamente para essa vitória, meus sinceros agradecimentos!

“Tudo posso naquele que me fortalece.”

(Filipenses 4:13)

RESUMO

DE PAULA, Sarah Braga Sayão. **Estudo da anatomia do septo nasal e sua relação com a morfologia do complexo nasomaxilar.** Orientadora: Profª. Drª Amanda Cunha Regal de Castro. Rio de Janeiro: UFRJ/Faculdade de Odontologia, 2021. Dissertação (Mestrado em Odontologia – Ortodontia) 80 f.

O presente estudo teve como objetivo investigar a influência do desvio do septo nasal (DSN) na morfologia do complexo nasomaxilar quanto a confiabilidade e precisão na marcação de pontos craniofaciais bidimensionais (2D) e tridimensionais (3D) em imagens de tomografia computadorizada de feixe cônico (TCFC), verificação de assimetrias do complexo nasomaxilar em indivíduos com diferentes níveis de DSN em estágios de maturação esquelética distintos, e analisar a associação entre o grau de severidade do DSN e o grau de assimetria do complexo nasomaxilar. Este foi um estudo observacional retrospectivo que utilizou um total de 60 TCFC alocadas em 4 grupos (n = 15) de acordo com o grau de desvio septal e maturação esquelética (DSN <10°, desvio de septo nasal leve, e DSN >10°, desvio de septo nasal moderado a severo, ambos antes e depois do surto de crescimento). A etapa de validação do estudo compreendeu a utilização de 30 TCFC e demarcação de 25 pontos craniofaciais, a fim de avaliar a confiabilidade e precisão desses pontos nas regiões nasal, palatina e facial lateral. Dois métodos foram utilizados: 2D, em cortes

multiplanares de TCFC no programa CS 3D Imaging; e 3D, com a segmentação 3D do crânio com visualização simultânea dos cortes multiplanares no programa ITK Snap. Os dados das coordenadas foram analisados por meio do Índice de Correlação Intraclasse (ICC), média das diferenças entre os tempos das medições, fórmula de Dahlberg e gráficos de Bland-Altman. A análise da relação entre a anatomia do septo nasal e morfologia do complexo nasomaxilar, compreendeu a utilização de 60 TCFC e a demarcação de 23 pontos bidimensionais e, avaliados quanto a presença de assimetria flutuante, por meio da análise de Procrustes ANOVA, comparação intergrupos com o teste de Mann-Whitney, além do teste de correlação de Spearman e regressão multivariada (α=0,05). Os resultados obtidos nas avaliações da reprodutibilidade dos pontos craniofaciais nos mostraram que o ICC variou de 0,95 a 1,0 no método 2D e foi maior ou igual a 0,99 no método 3D, indicando que ambos os métodos tiveram alta confiabilidade. A fórmula de Dahlberg, juntamente com Bland-Altman indicaram menor precisão nos pontos zigomáticomaxilar e orbitário no método 3D, e sutura zigomáticotemporal no método 2D. Os pontos ímpares (a maioria no plano sagital mediano) e os pontos frontozigomático temporal e frontozigomático orbital tiveram os melhores resultados de precisão. Com relação a influência do DSN e assimetrias no complexo nasomaxilar, nossos resultados principais mostraram que não foram observadas diferenças estatisticamente significativas entre as distâncias de Procrustes e Mahalanobis (assimetria flutuante) do complexo nasomaxilar entre os grupos avaliados (*P>0.05*). Entretanto, com os resultados da regressão multivariada, relacionado aos aspectos mais específicos de assimetria (componente assimétrico), houve uma correlação positiva entre o ângulo DSN e componente assimétrico das

regiões palatinas (*P=0.035 e P=0.047*, média e posterior, respectivamente), e também com a forma do SN e componente assimétrico da região palatina anterior (*P=0.039*). Sendo assim, concluímos que, ambos os métodos 2D e 3D de marcação de pontos craniofaciais no complexo nasomaxilar e facial lateral apresentaram alta confiabilidade, entretanto, o método 2D apresentou maiores valores de precisão na maioria dos pontos avaliados. Além disso, todos os pontos avaliados neste estudo foram considerados aceitáveis para fins clínicos. Com relação a análise da anatomia do septo nasal e morfologia do complexo nasomaxilar, todos os grupos avaliados apresentaram níveis significativos de assimetria flutuante. Entretanto, não foram observadas diferenças significativas na assimetria flutuante do complexo nasomaxilar nos grupos com DSN leve em relação aos grupos com DSN moderado a severo, em ambos os estágios de maturação esquelética. Por fim, foi observada correlação positiva entre o ângulo DSN e o componente de assimetria nas regiões palatinas média e posterior e entre a forma do septo nasal e a região palatina anterior. Não foram observadas correlações significativas com as regiões nasal e lateral do complexo nasomaxilar.

SUMMARY

DE PAULA, Sarah Braga Sayão. **Estudo da anatomia do septo nasal e sua relação com a morfologia do complexo nasomaxilar.** Orientadora: Profª. Drª Amanda Cunha Regal de Castro. Rio de Janeiro: UFRJ/Faculdade de Odontologia, 2021. Dissertação (Mestrado em Odontologia – Ortodontia) 80 f.

The present study aimed to investigate the influence of nasal septum deviation (NSD) on the morphology of the nasomaxillary complex regarding reliability and accuracy in two-dimensional (2D) and three-dimensional (3D) craniofacial landmarks in cone beam computed tomography images (CBCT), verification of asymmetries of the nasomaxillary complex in individuals with different levels of NSD at different stages of skeletal maturation, and to analyze the association between the degree of severity of the NSD and the degree of asymmetry of the nasomaxillary complex. This was a retrospective, cross-sectional observational study that used a total of 60 CBCT. For the validation study, 30 CTBC were used and 25 craniofacial landmarks were marked, in order to compare the reliability and precision of these landmarks in the nasal, palatal and lateral facial regions. Two methods were used: 2D, in CBCT multiplanar sections using CS 3D Imaging Software; and 3D, from the 3D segmentation of the skull in the software ITK Snap associated with multiplanar sections. Coordinates data were analyzed using the Intraclass Correlation Coefficient

(ICC), Dalhberg's formula, Bland-Altman plots and mean differences between measurement trials. To study the relationship between nasal septum and nasomaxillary complex, the 60 CBCT were divided into 4 groups (n = 15) according to the degree of septal deviation and skeletal maturation (NSD <10°, mild nasal septum deviation, e NSD >10°, moderate to severe nasal septum deviation, both before and after the growth spurt). 23 two-dimensional landmarks were marked and, to assess asymmetries, we used Procrustes ANOVA, intergroups comparisons with the Mann-Whitney test, in addition to the Spearman's correlation test and multivariate regression. The results obtained in the evaluations of the reliability and precision of craniofacial landmarks showed that the ICC ranged from 0.95 to 1.0 in the 2D method and was greater than or equal to 0.99 in the 3D method, indicating that both methods had high reliability. Dahlberg's formula, together with Bland-Altman, indicated lower precision in the landmarks zygomaxillare and orbitale in the 3D method, and zygomaticotemporal suture in the 2D method. The unpaired landmarks (mainly located at the midsagittal plane) and the landmarks frontomalar temporale and frontomalar orbitale had the best results of precision. Regarding the influence of NSD and asymmetries in the nasomaxillary complex, our main results showed that no statistically significant differences were observed between the Procrustes and Mahalanobis distances (fluctuating asymmetry) of the nasomaxilar complex between the groups (P>0.05). However, with the results of the multivariate regression, related to the more specific aspects of asymmetry (asymmetry component), there was a positive correlation between the NSD angle and palatal regions (*P=0.035* and *P=0.047*, middle and posterior, respectively), and also with the shape of the NS and the anterior palatal region (*P=0.039*). Therefore, we

conclude that both the 2D and 3D methods of positioning craniofacial landmarks in the nasomaxillary complex and the lateral facial region showed high reliability, however, the 2D method showed higher precision values in most of the landmarks evaluated. Furthermore, all landmarks evaluated in this study are are reasonably considered acceptable for clinical purposes. Regarding the study of the nasal septum and nasomaxillary complex, all groups evaluated presented significant levels of fluctuating asymmetry. However, no significant differences were observed in the fluctuating asymmetry of the nasomaxillary complex in the groups with mild NSD compared to the groups with moderate to severe NSD, in both stages of skeletal maturation. Finally, a positive correlation was observed between the NSD angle and the asymmetry component in the middle and posterior palatine regions and between the shape of the nasal septum and the anterior palatine region asymmetry component. There were no significant correlations with the nasal and lateral regions of the nasomaxillary complex.

LISTA DE SIGLAS

CG	Crista galli.
CVA	*Canonical Variable Analysis.*
CVM	*Cervical Vertebral Maturation.*
DSN	Desvio de septo nasal.
ENA	*External nasal angle.*
FDF	*Fisher's Discriminant Function.*
FNP	Forame nasopalatino.
GPA	*Generalized Procrustes Analysis.*
MPR	*Multiplanar reconstruction.*
NPF	*Nasopalatine foramen.*
NS	*Nasal septum.*
NSD	*Nasal septum deviation.*
OP	*Occlusal plane.*
PNS	*Posterior nasal spine.*
SPT	Sutura palatina transversa.
TPS	*Transverse palatine suture.*

LISTA DE FIGURAS

DELINEAMENTO DA PESQUISA Página

Figura 1 **A,** Corte sagital de TCFC representando estágio de maturação esquelética antes do surto de crescimento. **B,** Corte sagital de TCFC representando estágio de maturação esquelética após o surto de crescimento. **C,** Corte coronal de TCFC representando desvio de intensidade leve (<10º). **D,** Corte coronal de TCFC representando desvio de intensidade moderada a severa (>10º). Todos os cortes foram selecionados no programa CS 3D Imaging 9

Figura 2 Ferramenta de reformatação para orientação da cabeça no programa CS 3D Imaging. **A**, Corte sagital: plano axial (linha amarela) paralelo ao plano palatal. **B,** Corte coronal: plano axial (linha amarela) tangente ao assoalho nasal em seu nível mais inferior, onde ambas as raízes palatinas dos primeiros molares superiores são vistas. **C,** Corte axial: plano sagital mediano (linha verde) ao longo da sutura palatina mediana..... 10

Figura 3 Reconstrução 3D de TCFC ilustrando a segmentação do crânio e demarcação dos pontos craniofaciais utilizados no estudo. **A,** 1- násio, 2- rhinion, 3- espinha nasal anterior, 4-ponto A, 5- próstio, 6,7- suturas zigomaticomaxilares, 8,9- orbitários e 10 a 15- pontos na região lateral da face. **B,** 16 a 25- pontos na região da rafe, junção dos processos alveolares e palatinos e espinha nasal posterior..... 13

Figura 4 Representação de corte coronal de TCFC no programa ImageJ®. **A,** mensuração do ângulo DSN (º). **B,** medição da área de desvio (mm^2) com a ferramenta "*Polygon*"..... 14

Figura 5 Corte coronal de TCFC ilustrando a representação dos pontos marcados no corte coronal de maior DSN, no programa TpsDIG2. **1,** Topo da crista galli. **2,** Ponto mais inferior do septo nasal. **3,** 15

Ponto de maior desvio do lado direito. **4,** Ponto de maior desvio do lado esquerdo. **5,** Segundo ponto de maior desvio.....

Figura 6 Cortes multiplanares de TCFC ilustrando a representação 2D dos pontos nasais internos utilizados para avaliar assimetrias na região nasal. **A,** corte sagital ilustrando as duas regiões avaliadas na cavidade nasal. **ENP,** Espinha Nasal Posterior. **CG,** crista galli. **B,** Pontos demarcados no corte localizado na CG. **1,** Topo da CG. **2 e 3,** Pontos bilaterais localizados no aspecto mais lateral da cavidade nasal. **4 e 5,** Pontos bilaterais localizados no aspecto mais lateral do assoalho nasal. **C**, Pontos demarcados no corte localizado na ENP. **6,** aspecto superior do septo nasal ao nível da ENP. **7 e 8,** Pontos bilaterais localizados no aspecto mais lateral da cavidade nasal..... 17

Figura 7 Corte coronal de TCFC ilustrando a representação bidimensional dos pontos bilaterais na região lateral da face. **9 e 10,** Sutura zigomaticomaxilar. **11 e 12,** ponto orbitário..... 17

Figura 8 Cortes multiplanares de TCFC ilustrando a representação 2D dos pontos da região palatina. **A,** Corte sagital ilustrando as três regiões utilizadas para determinação dos cortes coronais. **SPT,** sutura palatina transversa. **FNP,** forame nasopalatino. **50%,** metade da distância entre SPT e FNP**. B,** Pontos no corte FNP: **13 e 15,** pontos bilaterais localizados na junção do processo alveolar/palatino. **14,** sutura palatina mediana. **C,** Pontos no corte SPT: **16 e 18,** pontos bilaterais localizados na junção do processo alveolar/palatino. **17,** sutura palatina mediana. **D,** Pontos no corte 50%: **19 e 21,** pontos bilaterais localizados na junção do processo alveolar/palatino. **20,** sutura palatina mediana. **22 e 23,** pontos bilaterais localizados no ponto mais lateral do processo alveolar vestibular..... 18

Figura 9 Cortes multiplanares de TCFC ilustrando a mensuração do ângulo nasal externo. **A,** Posicionamento dos planos coronal e axial no corte sagital. **B,** Mensuração do ângulo nasal externo no corte axial..... 19

Figura 10 Cortes coronais de TCFC ilustrando a mensuração do plano oclusal. **A,** Determinação do plano oclusal no programa CS 3D Imaging. **B,** Mensuração do ângulo obtido no programa ImageJ®..... 20

Página

DESENVOLVIMENTO DA PESQUISA

ARTIGO 1

Figure 1 3D CBCT reconstruction illustrating skull segmentation and demarcation of craniofacial landmarks used in the study. **A,** 1- nasion, 2- rhinion, 3- anterior nasal spine, 4-point A, 5- prostium, 6,7- zygomaxillare, 8,9- orbitals and 10 to 15- landmarks in the lateral region of the face. **B,** 16 to 25 - landmarks in the region of the intermaxillary suture, junction of the alveolar and palatine processes and posterior nasal spine…….. 37

Figure 2 Bland-Altman plots expressing intra-examiner agreement for the landmark left zygomaxillare. **A,** in X coordinate, in the 2D method, we can observe the points closer to the mean and more homogeneous distribution, indicating good reproducibility. **B,** in X coordinate, in the 3D method, we observed spread points (heterogeneous distribution) and some distant from the mean, indicating lower reproducibility. **C and D,** in Y coordinate, in both methods, we have good reproducibility, with 2D a little better. **E,** Z coordinate in 3D method, good reproducibility..... 38

Figure 3 Bland-Altman plots expressing intra-examiner agreement for the landmark right orbitale. **A,** in X coordinate, in the 2D method, we can observe the points closer to the mean and more homogeneous distribution, indicating good reproducibility. **B,** in X coordinate, in the 3D method, we observed spread points (heterogeneous distribution) and some distant from the mean, indicating lower reproducibility. **C,** Y coordinate, 2D method, good reproducibility. **D,** Y coordinate, 3D method, good reproducibility, but lower. **E,** Z coordinate, 3D method, good reproducibility..... 39

Figure 4 Bland-Altman plots expressing intra-examiner agreement for the landmark superior zigomaticotemporal suture (left). **A,** X coordinate, 2D method, good reproducibility. **B,** X coordinate, 3D method, great reproducibility, a little better than 2D. **C,** Y coordinate, 2D method, we observed spread points (heterogeneous distribution) and some distant from the mean, indicating lower reproducibility. **D,** Y coordinate, 2D method, we can observe the points closer to the mean and more homogeneous distribution, indicating good reproducibility. **E,** Z coordinate, 3D method, good reproducibility..... 40

Figure 5 Bland-Altman plots expressing intra-examiner agreement for the landmark prosthion. **A,** X coordinate, 2D method, great reproducibility. **B,** x coordinate, 3D method, great reproducibility. **C,** Y coordinate, 2D method, good reproducibility. **D,** Y coordinate, 3D method, good reproducibility. **E,** Z coordinate, 3D method, good reproducibility…… 41

Figure 6 Bland-Altman plots expressing intra-examiner agreement for the landmark right frontomalare orbitale. **A,** x coordinate, 2D method, great reproducibility. **B,** x coordinate, 3D method, great 42

reproducibility. **C,** y coordinate, 2D method, good reproducibility, but with more scattered points. **D,** y coordinate, 3D method, good reproducibility. **E,** z coordinate, 3D method, good reproducibility…

Figure 7 Bland-Altman plots expressing intra-examiner agreement for the landmark left frontomalare temporale. **A,** X coordinate, 2D method, great reproducibility. **B,** X coordinate, 3D method, great reproducibility. **C,** Y coordinate, 2D method, good reproducibility, but with more scattered points. **D,** Y coordinate, 3D method, good reproducibility. **E,** Z coordinate, 3D method, good reproducibility.. 43

ARTIGO 2

Figure 1 **A,** NSD angle measurement and **B**, deviation area measurement (mm²), both in ImageJ® software. C, representation of the landmarks in the TpsDIG2 software, used for morphometric analysis. In the same coronal section, five landmarks were used, namely: **1,** top of the crista galli. **2,** lowest point of the nasal septum. **3,** point of greatest deviation on the right side. **4,** point of greatest deviation on left side. **5,** second point of greatest deviation.……..... 65

.

Figure 2 Two-dimensional representations of the landmarks in all regions. **A,** in nasal region, landmarks were collected from two internal planes: the first plane was located on top of the crista galli and the second plane was at posterior nasal spine. **B,** the first plane, indicating the landmarks: 1, top of the crista galli; 2/3, bilateral landmarks located at the most lateral aspect of the nasal cavity; 4/5, bilateral landmarks located at the most lateral aspect of the nasal floor. **C,** the second plane, indicating the landmarks: 6, upper aspect of the nasal septum; 7/8, bilateral landmarks located at the most lateral aspect of the nasal cavity. **D**, in lateral regions, the landmarks used was: 9/10, zygomaticomaxillary sutures; 11/12, orbitals. **E,** in palatal regions, landmarks were collected from three internal planes: NF = nasopalatine foramen, TPS = transverse palatal suture and 50% = halfway distance between NF and TPS. **F,** landmarks in the first plane: 13/15, bilateral landmarks located at the alveolar/palatal process junction at the level of the posterior margin of the NF; 14, intermaxillary suture at NF. **G,** landmarks in the second plane: 16/18, bilateral landmarks located at the alveolar/palatal process junction at TPS; 17, intermaxillary suture at TPS. **H,** landmarks in the third plane: 19/21, bilateral landmarks located at the alveolar/palatal process junction at 50%; 20, intermaxillary suture at 50%; 22/23, bilateral landmarks located at the most lateral point of the buccal alveolar process at 50%..... 66

Figure 3 **A**, To select the external nasal angle, the coronal slice must be in the transverse palatal suture (purple line) and the axial slice perpendicular to it, at the junction of the perpendicular blade of 67

the ethmoid with the vomer; **B,** in the axial slice, the angle is made between the middle of the nose and the line representing the midpalatal suture (the lower point should be halfway along the length of the nasal septum).…….

Figure 4 **A,** Representation of the coronal section used in which it is possible to visualize the tips of the buccal cusps of the maxillary first molars and their relationship with the axial plane of the image (*yellow*); **B**, View of the angle obtained in ImageJ® software……. 67

Figure 5 Analysis of Canonical Variables representing the slice of the greatest NSD. It is possible to observe that groups MD BG and MD AG (mild deviation) have a similar format (they are on the right side of the graph), and groups MSD BG and MSD AG (moderate/severe deviation) also have a similar format (right side of the graph) …….. 68

Figure 6 Thin-plate splines showing the shape of the nasal septum at slice of the greatest NSD. The colors indicate that the closer to blue, the greater the contraction region, while the closer to red, the greater the expansion region. **A,** in control groups (mild deviation), we can observe that the septum has a narrower shape in general, with an expansion region in the central part of the septum. **B,** in experimental groups (moderate/severe deviation), we observed a wider shape, and an expansion region in the central part of the septum……. 69

Figure 7 Scatter plot of our multivariate regression. **A,** correlating the asymmetry component of variation of palatal region 2 (transverse palatine suture) against nasal septal deviation angle. **B,** asymmetry component of variation of palatal region 3 (halfway distance between nasopalatine foramen and transverse palatine suture) against nasal septal deviation angle. **C,** asymmetry component of variation of palatal region 1 (nasopalatine foramen) against nasal septum shape……. 70

LISTA DE TABELAS

	DELINEAMENTO DA PESQUISA	Página
Quadro 1	Descrição dos grupos do estudo de acordo com o desvio de septo nasal e maturação esquelética.....	8
Quadro 2	Definição dos pontos craniofaciais utilizados no estudo de validação. **Nota.** Quadro adaptado do artigo de HARTMAN *et al*., 2016.....	12
Quadro 3	Pontos de referência usados para avaliar a morfologia do complexo nasomaxilar. **Nota.** Quadro adaptado do artigo de HARTMAN *et al*., 2016.....	16

	DESENVOLVIMENTO DA PESQUISA	Página
	ARTIGO 1	
Table 1	Definition of Landmarks.....	35
Table 2	Mean differences and standard deviation between measurements trials and results of Dahlberg's formula for the coordinates of the 2D and 3D methods…….	36
	ARTIGO 2	
Table 1	Nasomaxillary complex landmark's number and description according to the nasal, lateral, and palatal regions of the face……	61
Table 2	Descriptive statistics of NSD angle, NSD area, ENA and OP variables according to the study groups…….	61
Table 3	P values of Procrustes (PC) and Mahalanobis (MH) distances (fluctuating asymmetry) of nasomaxillary complex nasal, lateral and palatal regions according to the study groups……..	62

Table 4	Spearman's correlation test (and P values) for nasal septum and nasomaxillary complex variables (n = 60)….	62
Table 5	Multivariate regression for nasal septum and nasomaxillary complex variables (n = 60) ……	63
Supplementary Table 1	Procrustes ANOVA results for the nasal regions……	63
Supplementary Table 2	Procrustes ANOVA for the lateral region.....	64
Supplementary Table 3	Procrustes ANOVA for the palatal regions……....	64

ÍNDICE

Página

1 INTRODUÇÃO..... 1

2 PROPOSIÇÃO..... 5

3 DELINEAMENTO DA PESQUISA..... 6

3.1 DESENHO DO ESTUDO E ASPECTOS ÉTICOS..... 6

3.2 CASUÍSTICA 6

3.3 SELEÇÃO E CARACTERIZAÇÃO DA AMOSTRA..... 6

3.4 ORIENTAÇÃO DA CABEÇA..... 9

3.5 VALIDAÇÃO DA DEMARCAÇÃO DOS PONTOS CRANIOFACIAIS 10

3.6 ANÁLISE DO SEPTO NASAL..... 13

3.7 ANÁLISE DO COMPLEXO NASOMAXILAR..... 15

3.8 AVALIAÇÃO DO ÂNGULO NASAL EXTERNO..... 18

3.9 AVALIAÇÃO DO PLANO OCLUSAL..... 19

4.0 ANÁLISE ESTATÍSTICA..... 20

4 DESENVOLVIMENTO DA PESQUISA..... 24

4.1 ARTIGO 1: DE PAULA, S.B.S.; RUELLAS, A.C.O.; CASTRO, A.C.R. **Reliability and precision of two-dimensional and three-dimensional craniofacial landmarks in CBCT exams.** A ser submetido ao periódico The Angle Orthodontist..... 25

4.2 ARTIGO 2: DE PAULA, S.B.S.; NUNES, L.A.; RUELLAS, A.C.O.; CASTRO, A.C.R. **Nasal septum deviation and fluctuating asymmetries of the nasomaxillary complex according to skeletal maturation: a cross-sectional study.** A ser submetido ao periódico The Journal of Craniofacial Surgery..... 44

5 CONCLUSÃO..... 71

6 RECOMENDAÇÕES..... 72

7 REFERÊNCIAS BIBLIOGRÁFICAS..... 73

8 ANEXOS..... 79

8.1 ANEXO 1 – PARECER DO COMITÊ DE ÉTICA EM PESQUISA..... 79

8.2 ANEXO 2 – UTILIZAÇÃO DO BANCO DE DADOS DA DISCIPLINA DE ORTODONTIA 80

1 INTRODUÇÃO

A análise da simetria facial é muito importante no diagnóstico e planejamento em diversas áreas biológicas. Entretanto, não é fácil determinar o limiar que define faces simétricas e assimétricas, sendo este frequentemente determinado pelo senso de equilíbrio dos clínicos e pela percepção de desequilíbrio dos pacientes (BISHARA; BURKEY; KHAROUF, 1994). Para a verificação de assimetrias, a tomografia computadorizada de feixe cônico (TCFC) vem sendo muito utilizada por ser uma ferramenta diagnóstica moderna, onde podemos visualizar com precisão a forma tridimensional do crânio (LIN; CHUANG; WENG; LO, 2015). Para fins de diagnóstico e estudos nessa área, a marcação de pontos craniofaciais é geralmente utilizada (LOU; LAGRAVERE; COMPTON; MAJOR *et al.*, 2007; NUR; ÇAKAN; ARUN, 2016).

A assimetria facial esquelética apresenta diversas etiologias, e, embora a causalidade não possa ser determinada, estudos anteriores relataram uma relação entre o desvio anatômico do septo nasal (SN) e assimetrias relacionadas ao desenvolvimento facial (HARTMAN; HOLTON; MILLER; YOKLEY *et al.*, 2016; HOLTON; YOKLEY; FIGUEROA, 2012; KANG; HUN; PARK; CHUNG *et al.*, 2015). O septo nasal consiste em uma parede mediana que divide a cavidade nasal em fossas nasais direita e esquerda. A porção anterior é formada pela cartilagem do septo e pela lâmina perpendicular do osso etmoide, e a porção

posterior é formada pelo osso vômer (FEHRENBACH; MJ; HERRING; SW, 2005). O desvio do septo nasal (DSN) consiste em um desalinhamento do septo em relação à linha média facial, podendo envolver as partes óssea e cartilaginosa isoladamente, ou de forma combinada (BAYRAK; USTAOĞLU; DEMIRALP; KURŞUN ÇAKMAK, 2018), e é encontrado com uma prevalência razoável na população em geral, mas principalmente em adultos (ROBLIN; ECCLES, 2002). Visto que as estruturas anatômicas do complexo nasomaxilar apresentam íntima relação durante sua formação, é possível que o crescimento alterado do septo nasal possa influenciar a morfologia do complexo nasomaxilar.

Existem duas teorias principais que discorrem sobre o crescimento e desenvolvimento pré e pós-natal da região central da face. A primeira teoria, que pode ser chamada de “teoria do septo nasal”, sugere que a cartilagem do septo nasal é um centro primário de crescimento, deslocando os ossos centrais da face para frente e para baixo (SCOTT, 1953). Latham, em uma modificação desta teoria, propôs que o septo nasal atua como um mecanismo iniciador, deslocando a pré-maxila e maxila para frente através dos ligamentos septo-premaxilares (LATHAM, 1970). A função da cartilagem septal como um “centro de crescimento” é certamente possível, pois as suturas da maxila responderiam ao crescimento da cartilagem nasal formando novo osso quando estas fossem afastadas pelas forças do crescimento da cartilagem septal (PROFFIT; FIELDS; SARVER, 2012).

A segunda teoria considerou a cartilagem septal como uma estrutura da cavidade nasal sem papel morfogenético primário, na qual, MOSS propôs a hipótese de que, em conformidade com a teoria da matriz funcional, o crescimento do septo nasal é secundário e compensatório à expansão da

cavidade nasal (MOSS; BROMBERG; SONG; EISENMAN, 1968). Sendo assim, nesse ponto de vista conceitual, os tecidos moles crescem, e o osso juntamente com a cartilagem, reagem a esse controle epigenético (PROFFIT; FIELDS; SARVER, 2012).

Estudos prévios conduzidos em animais demonstraram que o septo nasal desempenha um papel importante nos padrões normais e anormais do crescimento facial, uma vez que a ressecção cirúrgica de todo ou parte do septo nasal resultou em deficiência nas dimensões anteroposteriores da maxila e pré-maxila (LATHAM; TG; CT, 1975; SARNAT; WEXLER, 1966; WEXLER; SARNAT, 1961). Pressupõe-se que mecanismo semelhante ocorra em humanos, e que portanto, o crescimento desviado do septo nasal possa ter alguma contribuição para o desenvolvimento de assimetrias faciais (HARTMAN; HOLTON; MILLER; YOKLEY *et al.*, 2016).

A anatomia do septo nasal é amplamente estudada na área de Otorrinolaringologia, enfatizando a importância do diagnóstico na tomada de decisões clínicas. De acordo com D'Ascanio et al., a indicação de septoplastia pediátrica pode ser considerada, já que de foi relatado que crianças respiradoras bucais com DSN não corrigido demonstraram anomalias faciais e dentais em comparação às crianças com respiração nasal (controles) (D'ASCANIO; LANCIONE; POMPA; REBUFFINI *et al.*, 2010). Além disso, o estudo prévio de literatura de Lawrence, indicou que a opção por não realizar ou retardar a septoplastia quando indicada pode afetar o crescimento nasal e facial (LAWRENCE, 2012).

Ambas as teorias propostas sobre o papel da cartilagem septal no crescimento e desenvolvimento da face têm fundamentos, porém nenhuma

destas esclarece a questão de forma absoluta. Ainda não se sabe ao certo se, durante a fase de crescimento e desenvolvimento do indivíduo, o desvio septal apresenta relação com crescimento assimétrico da face, mais precisamente do complexo nasomaxilar. Um estudo recente indicou que existe associação entre o DSN e o crescimento anormal do complexo nasomaxilar, sendo observadas dimensões reduzidas de largura e área da maxila e cavidade nasal nos grupos de indivíduos com maior DSN (ABOU SLEIMAN; SAADÉ, 2021). Alguns estudos prévios, abrangendo adolescentes e adultos entre 14 e 71 anos, observaram associação entre o desvio do septo nasal com assimetrias faciais por meio de análises fotográficas (HAFEZI; NAGHIBZADEH; NOUHI; YAVARI, 2010; KIM; RHA; WEISSMAN; HWANG *et al.*, 2011), e outros estudos utilizando tomografia computadorizada (HARTMAN; HOLTON; MILLER; YOKLEY *et al.*, 2016; HOLTON; YOKLEY; FIGUEROA, 2012; KANG; HUN; PARK; CHUNG *et al.*, 2015). Sendo assim, faz-se necessário o estudo da influência do desvio do septo nasal na morfologia do complexo nasomaxilar em diferentes estágios do desenvolvimento humano.

2 PROPOSIÇÃO

Investigar a influência do desvio do septo nasal na morfologia do complexo nasomaxilar, quanto a:

2.1 Analisar a confiabilidade e precisão na marcação de pontos craniofaciais bidimensionais e tridimensionais nas regiões nasal, palatina e facial lateral em imagens de TCFC;

2.2 Investigar a influência do desvio do septo nasal na morfologia do complexo nasomaxilar, quanto ao grau de assimetria em indivíduos com estágios de maturação esquelética distintos; bem como, verificar a relação entre o grau de severidade do desvio do septo nasal e assimetria do complexo nasomaxilar.

.

3 DELINEAMENTO DA PESQUISA

3.1 DESENHO DO ESTUDO E ASPECTOS ÉTICOS

Trata-se de um estudo observacional retrospectivo, de corte transversal, que foi aprovado pelo Comitê de Ética em Pesquisa do Hospital Universitário Clementino Fraga Filho (CEP-HUCFF/UFRJ) sob o parecer número 3.888.756 (Anexo I, página 79).

3.2 CASUÍSTICA

A casuística do presente estudo foi composta por 35 homens e 25 mulheres, de 9 a 30 anos de idade. Os critérios de elegibilidade do estudo incluíram a disponibilidade de arquivos de TCFC em formato DICOM (*Digital Imaging and Communications in Medicine*), incluindo a quarta vértebra cervical de indivíduos saudáveis, ausência de síndromes craniofaciais, deformidades faciais, processos patológicos ósseos extensos, trauma craniofacial, bem como intervenções cirúrgicas na região facial, incluindo septoplastia e cirurgia ortognática prévias, e ausência de tratamento ortodôntico.

3.3 SELEÇÃO E CARACTERIZAÇÃO DA AMOSTRA

A amostra do presente estudo foi composta por exames de TCFC, selecionados aleatoriamente do acervo da Clínica de Ortodontia do Programa de Pós-graduação em Odontologia da Faculdade de Odontologia da Universidade Federal do Rio de Janeiro (PPGO FO-UFRJ). Uma vez que os exames de TCFC são parte integrante da documentação ortodôntica solicitada para fins de tratamento e/ou acompanhamento ortodôntico, o acesso e uso de banco de dados obedeceu aos princípios éticos legais regulamentados pela resolução CNS 466/2012 e a Declaração de Responsabilidade foi devidamente assinada (Anexo II, página 80).

Os exames de TCFC foram realizados no tomógrafo Kodak 9500 Cone Beam 3D System (Carestream Health, Rochester, NY, EUA), seguindo as especificações de 90 KV, 10 mA, FOV (*field of view*) 18,4 x 20,6 cm, voxel de 0,3 mm e tempo de escaneamento de 24s.

A partir da análise de 120 exames de TCFC, 60 exames atenderam aos critérios de elegibilidade, foram incluídos na amostra do estudo e alocados em quatro grupos (n=15) de acordo com o estágio de maturação esquelética e grau de desvio do septo nasal (Quadro 1, página 8).

O estágio de maturação esquelética foi avaliado de acordo com o método de Maturação Vertebral Cervical, descrito por BACCETTI em 2005 (BACCETTI; FRANCHI; JR, 2005) nos cortes sagitais das imagens de TCFC, obtidos no programa CS 3D Imaging (Figura 1 A e B, página 9). De acordo com o método proposto, o pico do surto de crescimento ocorre entre os estágios CS3 e CS4. Considerando uma margem para variabilidade individual e visto que, que no estágio CS4 o paciente ainda pode apresentar crescimento considerável, consideramos, para fins de melhor abrangência do presente estudo, o grupo

antes do surto de crescimento (AS) compreendendo os estágios CS1 a CS4, e após o surto de crescimento (DS), os estágios CS5 e CS6.

Em seguida, a intensidade do desvio de septo foi classificada de acordo com o valor do ângulo DSN, descrito no item 3.6 (Páginas 12 e 13), sendo considerado como desvio de intensidade leve (DL) (DSN<10º), e intensidade moderada a severa (DMS) (DSN>10º), considerando que a partir dos valores de intensidade moderada o desvio de septo nasal é considerado clinicamente significativo (GREGURIĆ; BAUDOIN; TOMLJENOVIĆ; GRGIĆ *et al.*, 2016; SERIFOGLU; OZ; DAMAR; BUYUKUYSAL *et al.*, 2017) (Figura 1 C e D, página 9).

Grupos (n=15)	**Desvio de septo nasal**	**Maturação esquelética**
DL-AS	Grau leve (<10º)	Antes do surto
DMS-AS	Grau moderado a severo (>10º)	Antes do surto
DL-DS	Grau leve (<10º)	Depois do surto
DMS-DS	Grau moderado a severo (>10º)	Depois do surto

Quadro 1. Descrição dos grupos do estudo de acordo com o desvio de septo nasal e maturação esquelética. **DL-AS**, desvio leve antes do surto. **DMS-AS**, desvio moderado a severo antes do surto. **DL-DS**, desvio leve depois do surto. **DMS-DS**, desvio moderado a severo depois do surto.

Figura 1. A, Corte sagital de TCFC representando estágio de maturação esquelética antes do surto de crescimento. **B,** Corte sagital de TCFC representando estágio de maturação esquelética após o surto de crescimento. **C,** Corte coronal de TCFC representando desvio de intensidade leve (<10º). **D,** Corte coronal de TCFC representando desvio de intensidade moderada a severa (>10º). Todos os cortes foram selecionados no programa CS 3D Imaging.

3.4 ORIENTAÇÃO DA CABEÇA

Previamente à análise das imagens de TCFC, foi realizada a orientação da cabeça nos planos axial, coronal e sagital no programa CS 3D Imaging

(Carestream Dental LLC Atlanta, GA, EUA) (Figura 2, página 10), adaptada de Lin et al., (LIN; AHN; KIM; MOON *et al.*, 2015) de acordo com os seguintes critérios: no corte sagital, o plano axial paralelo ao plano palatal (Espinha Nasal Anterior – Espinha Nasal Posterior); no corte coronal, o plano axial tangente ao assoalho nasal em seu nível mais inferior, onde ambas as raízes palatinas dos primeiros molares superiores são vistas; e, no corte axial, o plano sagital mediano ao longo da sutura palatina mediana. A orientação no corte coronal só foi alterada quando o indivíduo apresentava o assoalho nasal muito assimétrico, onde, nesses casos, foi feita uma média entre os lados direito e esquerdo, sempre visualizando o efeito na posição natural da cabeça.

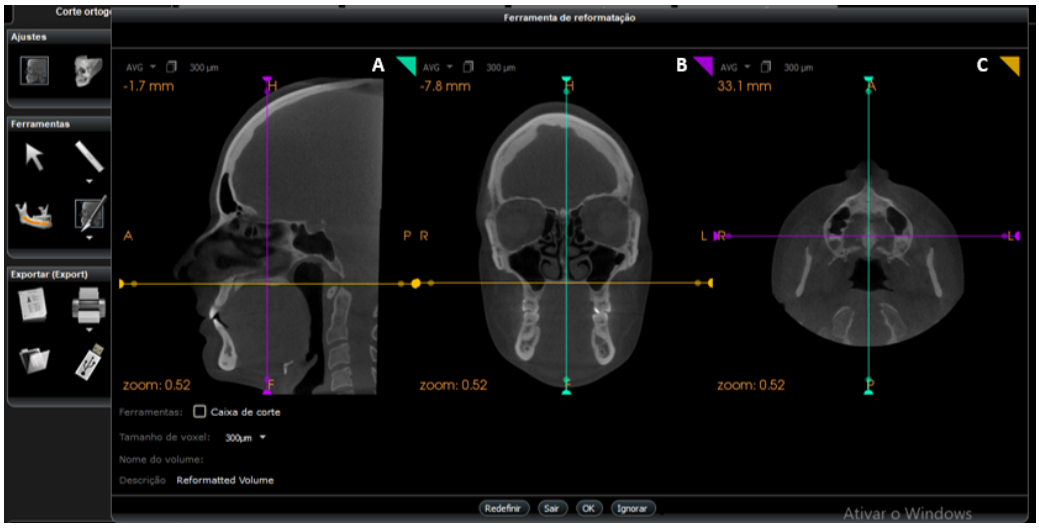

Figura 2 Ferramenta de reformatação para orientação da cabeça no programa CS 3D Imaging. **A**, Corte sagital: plano axial (linha amarela) paralelo ao plano palatal. **B,** Corte coronal: plano axial (linha amarela) tangente ao assoalho nasal em seu nível mais inferior, onde ambas as raízes palatinas dos primeiros molares superiores são vistas. **C,** Corte axial: plano sagital mediano (linha verde) ao longo da sutura palatina mediana.

3.5 VALIDAÇÃO DA DEMARCAÇÃO DOS PONTOS CRANIOFACIAIS

A análise de validação da demarcação dos pontos craniofaciais foi realizada em 30 exames de TCFC, correspondendo a 50% da amostra total do estudo.

Vinte e cinco pontos craniofaciais, descritos no Quadro 2 (página 12), foram demarcados pelo mesmo examinador (S.B.S.P.) em um intervalo de duas semanas. Estes pontos foram alocados em três grupos conforme as regiões correspondentes, sendo elas região nasal, palatina e facial lateral (adaptado de HARTMAN; HOLTON; MILLER; YOKLEY *et al.*, 2016). A região nasal foi representada pelos pontos násio, rhinion e espinha nasal anterior. A região palatina foi representada por pontos de referência unilaterais e bilaterais posicionados na rafe, na junção dos processos alveolares e palatinos e na espinha nasal posterior. Os pontos demarcados na abóbada palatina foram coletados ao longo de quatro cortes coronais selecionados ao longo do comprimento do palato. O primeiro corte foi posicionado na margem posterior do forame nasopalatino; o segundo corte foi posicionado na sutura palatina transversa; o terceiro corte foi posicionado no ponto médio entre a margem posterior do forame nasopalatino e a sutura palatina transversa; e o quarto corte foi posicionado na espinha nasal posterior. Por fim, a região facial lateral foi representada por marcos bilaterais ao longo da superfície lateral dos ossos zigomáticos e no assoalho das órbitas.

A demarcação dos pontos foi realizada de forma bidimensional (2D) e tridimensional (3D), como segue:

- método 2D, por meio de cortes multiplanares de TCFC no programa CS 3D Imaging. Este programa foi utilizado apenas para a obtenção das imagens

2D, em seguida, a marcação dos pontos e obtenção das coordenadas (X, Y) foram realizadas no programa TpsDIG2 (Rohlf, F. J. 2004); e

- método 3D, por meio de segmentação semiautomática 3D do crânio realizada no programa ITK Snap (Pensilvânia, Utah, EUA) (Figura 3, página 12) com visualização simultânea dos cortes multiplanares da TCFC. As coordenadas (X, Y, Z) dos pontos demarcados foram obtidas no programa 3D Slicer (The Slicer Community).

Número	Nome/descrição do ponto	Região
1	Násio	Nasal
2	Rhinion	Nasal
3	Espinha nasal anterior	Nasal/palatal
4	Ponto A	Palatal
5	Próstio	Palatal
6/7	Ponto mais inferior da sutura zigomaticomaxilar (direito/esquerdo)	Facial lateral
8/9	Orbitário (direito/esquerdo)	Facial lateral
10/11	Sutura frontozigomatico-orbital (direito/esquerdo)	Facial lateral
12/13	Sutura frontozigomatico-temporal (direito/esquerdo)	Facial lateral
14/15	Ponto mais superior da sutura zigomaticotemporal (direito/esquerdo)	Facial lateral
16/18	Junção do processo alveolar/palatal à nível da margem posterior do forame nasopalatino (direito/esquerdo)	Palatal
17	Sutura intermaxilar à nível da margem posterior do forame nasopalatino	Palatal
19/21	Junção do processo alveolar/palatal à nível da sutura palatina transversa (direito/esquerdo)	Palatal
20	Sutura intermaxilar à nível da sutura palatina transversa	Palatal
22/24	Junção do processo alveolar/palatal na metade da distância entre margem posterior do forame nasopalatino e sutura palatina transversa (direito/esquerdo)	Palatal
23	Sutura intermaxilar na metade da distância entre margem posterior do forame nasopalatino e sutura palatina transversa	Palatal
25	Espinha nasal posterior	Palatal

Quadro 2 Definição dos pontos craniofaciais utilizados no estudo de validação de pontos craniofaciais. **Nota.** Quadro adaptado do artigo de HARTMAN *et al*., 2016.

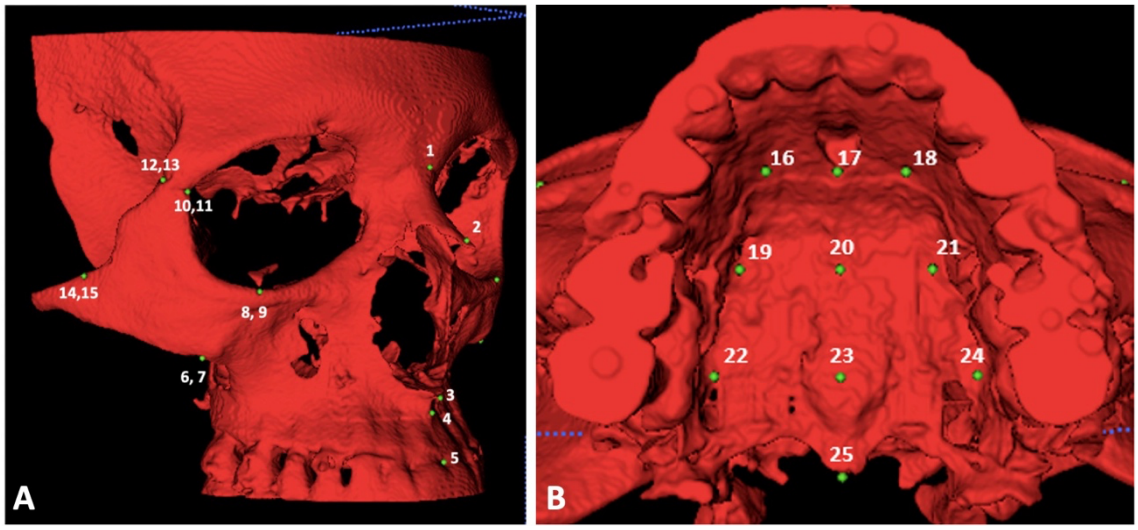

Figura 3 Reconstrução 3D de TCFC feita no programa ITK Snap, ilustrando a segmentação do crânio e demarcação dos pontos craniofaciais utilizados no estudo. **A,** 1- násio, 2- rhinion, 3- espinha nasal anterior, 4-ponto A, 5- próstio, 6,7- suturas zigomaticomaxilares, 8,9- orbitários e 10 a 15- pontos na região lateral da face. **B,** 16 a 25- pontos na região da rafe, junção dos processos alveolares e palatinos e espinha nasal posterior.

3.6 ANÁLISE DO SEPTO NASAL

A análise do septo nasal foi realizada no programa CS 3D Imaging, no qual foram percorridos os cortes coronais da TCFC, seguindo um eixo anteroposterior, até a identificação do corte com maior DSN. Apenas a região óssea do septo foi considerada na análise, para fins de evitar interferência da cartilagem nasal na mensuração do desvio. Após a seleção desse corte, o ângulo DSN (º) e a área DSN (mm²) foram mensurados no programa ImageJ® (National Institutes of Health, Bethesda, Maryland, EUA).

A mensuração do ângulo DSN utilizou os seguintes pontos de referência: crista galli (interseção do plano sagital mediano ao nível da crista galli); espinha nasal anterior (interseção do plano sagital mediano ao nível da espinha nasal anterior) e ponto de maior desvio do septo nasal (ponto hiperdenso mais proeminente ao longo do septo nasal (AKOĞLU; KARAZINCIR; BALCI;

OKUYUCU *et al.*, 2007; BAYRAK; USTAOĞLU; DEMIRALP; KURŞUN ÇAKMAK, 2018; CODARI; ZAGO; GUIDUGLI; PUCCIARELLI *et al.*, 2016; ORHAN; AYDIN; ORMECI; YILMAZ, 2014; SERIFOGLU; OZ; DAMAR; BUYUKUYSAL *et al.*, 2017) (Figura 4 A, página 14). A mensuração da área DSN compreendeu o ponto de maior desvio do septo nasal até o plano sagital mediano, adaptado de LIN; WHEATLEY; HANDWERKER; HARRIS *et al.*, 2014 (Figura 4 B, página 14). A mensuração da área e a conversão de pixels para mm^2 foram realizadas com as ferramentas "*Polygon*" e "*Set scale*" do programa ImageJ®, respectivamente.

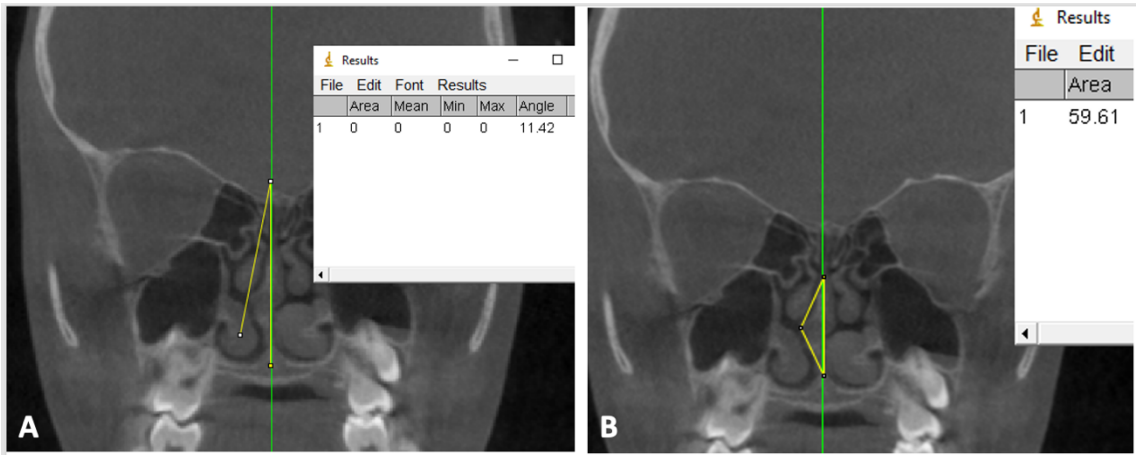

Figura 4. Representação de corte coronal de TCFC no programa ImageJ®. **A,** mensuração do ângulo DSN (°). **B,** medição da área de desvio (mm^2) com a ferramenta "*Polygon*".

Em seguida, o corte coronal com maior DSN foi utilizado para a marcação de 5 pontos bidimensionais no software TpsDIG2, sendo estes: 1, ponto mais alto (topo) da crista galli; 2, ponto mais inferior do septo nasal; 3, ponto de maior desvio do lado direito; 4, ponto de maior desvio do lado esquerdo; 5, segundo ponto de maior desvio (lado direito ou esquerdo, dependendo de cada indivíduo) em relação ao plano sagital mediano (Figura 5, página 15). A morfologia do septo nasal foi avaliada por meio de abordagem de geometria morfométrica, na qual

as coordenadas dos pontos de referência foram submetidas à análise de Procrustes (do inglês, *Generalized Procrustes Analysis - GPA*), no programa MorphoJ (Versão 2.0, Klingenberg lab, The University of Manchester, Inglaterra).

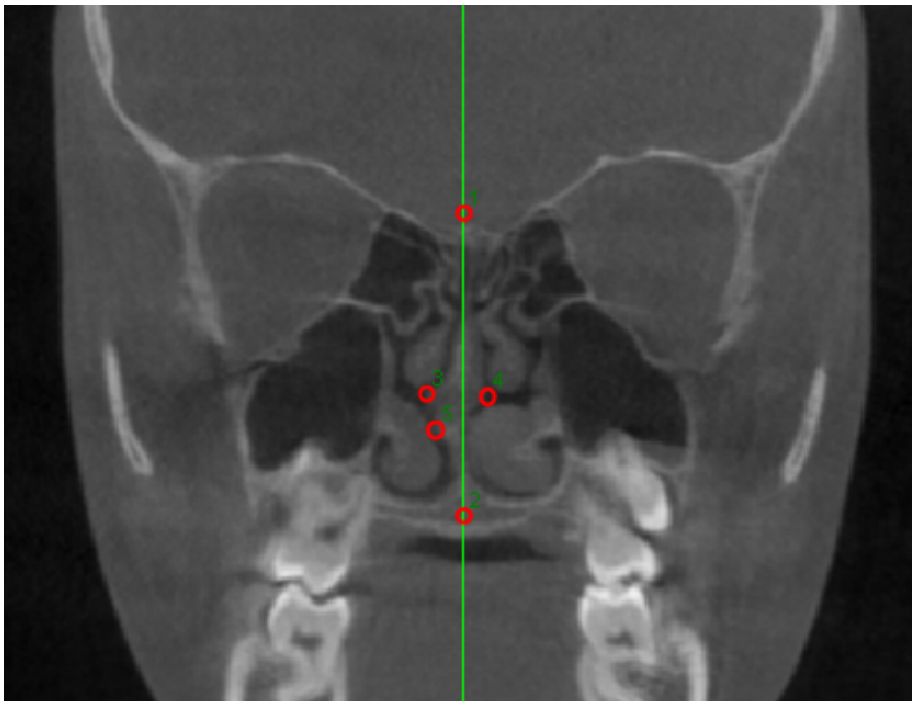

Figura 5 Corte coronal de TCFC ilustrando a representação dos pontos marcados no corte coronal de maior DSN, no programa TpsDIG2. **1,** Topo da crista galli. **2,** Ponto mais inferior do septo nasal. **3,** Ponto de maior desvio do lado direito. **4,** Ponto de maior desvio do lado esquerdo. **5,** Segundo ponto de maior desvio.

3.7 ANÁLISE DO COMPLEXO NASOMAXILAR

A morfologia do complexo nasomaxilar foi avaliada por meio da coleta de 23 pontos de referência bidimensionais do esqueleto facial (HARTMAN; HOLTON; MILLER; YOKLEY *et al.*, 2016) (Quadro 3, página 16). A análise dos cortes multiplanares foi realizada no programa CS 3D Imaging, e os pontos bidimensionais foram demarcados e suas respectivas coordenadas 2D (X, Y) geradas no programa TpsDIG2. Os pontos de referência foram agrupados em

três regiões faciais, sendo elas a região nasal, facial lateral e palatina (Figuras 6, 7 e 8, respectivamente).

A região nasal foi representada pela cavidade nasal interna (Figura 6), onde os pontos de referência foram coletados ao longo de dois cortes coronais. O primeiro corte (Figura 6 A e B, página 17) localizou-se na direção do topo da crista galli, aproximadamente na metade do comprimento do assoalho nasal, e o segundo corte (Figura 6 A e C, página 17) localizou-se na espinha nasal posterior, ou seja, 100% do comprimento do assoalho nasal. A região lateral da face foi representada por pontos de referência bilaterais localizados na sutura zigomaticomaxilar e no assoalho das órbitas, avaliados em corte coronal (Figura 7, página 17).

A região palatina foi representada por pontos de referência unilaterais e bilaterais localizados na junção dos processos alveolares e palatinos, coletados ao longo de três cortes coronais selecionados em relação ao comprimento do palato (Figura 8 A, página 18). O primeiro corte foi posicionado na margem posterior do forame nasopalatino (Figura 8 B, página 18), o segundo corte foi posicionado na sutura palatina transversa (Figura 8 C, página 18) e o terceiro corte foi posicionado no ponto médio entre a margem posterior do forame nasopalatino e a sutura palatina transversa (Figura 8 D, página 18).

Número	Nome/Descrição	Região
1	Topo da crista galli	Nasal
2/3	Pontos de referência bilaterais localizados no aspecto mais lateral da cavidade nasal ao nível da crista galli	Nasal
4/5	Pontos de referência bilaterais localizados no aspecto mais lateral do assoalho nasal ao nível da crista galli	Nasal
6	Aspecto superior do septo nasal ao nível da espinha nasal posterior	Nasal
7/8	Pontos de referência bilaterais localizados no aspecto mais lateral da cavidade nasal ao nível da espinha nasal posterior	Nasal
9/10	Pontos de referência bilaterais localizados no ponto mais inferior da sutura zigomaticomaxilar	Facial Lateral
11/12	Pontos de referência bilaterais localizados no ponto mais inferior da órbita	Facial Lateral
13/15	Pontos de referência bilaterais localizados na junção do processo alveolar/palatal ao nível da margem posterior do forame nasopalatino	Palatal
14	Sutura palatina mediana ao nível da margem posterior do forame nasopalatino	Palatal

16/18	Pontos de referência bilaterais localizados na junção do processo alveolar/palatal ao nível da sutura palatina transversa	Palatal
17	Sutura palatina mediana ao nível da sutura palatina transversa	Palatal
19/21	Pontos de referência bilaterais localizados na junção do processo alveolar/palatal na metade da distância entre margem posterior do forame nasopalatino e sutura palatina transversa	Palatal
20	Sutura palatina mediana na metade da distância entre margem posterior do forame nasopalatino e sutura palatina transversa	Palatal
22/23	Pontos de referência bilaterais localizados no ponto mais lateral do processo alveolar vestibular no corte da metade da distância entre margem posterior do forame nasopalatino e sutura palatina transversa	Palatal

Quadro 3 Pontos de referência usados para avaliar a morfologia do complexo nasomaxilar. **Nota.** Quadro adaptado do artigo de HARTMAN *et al*., 2016.

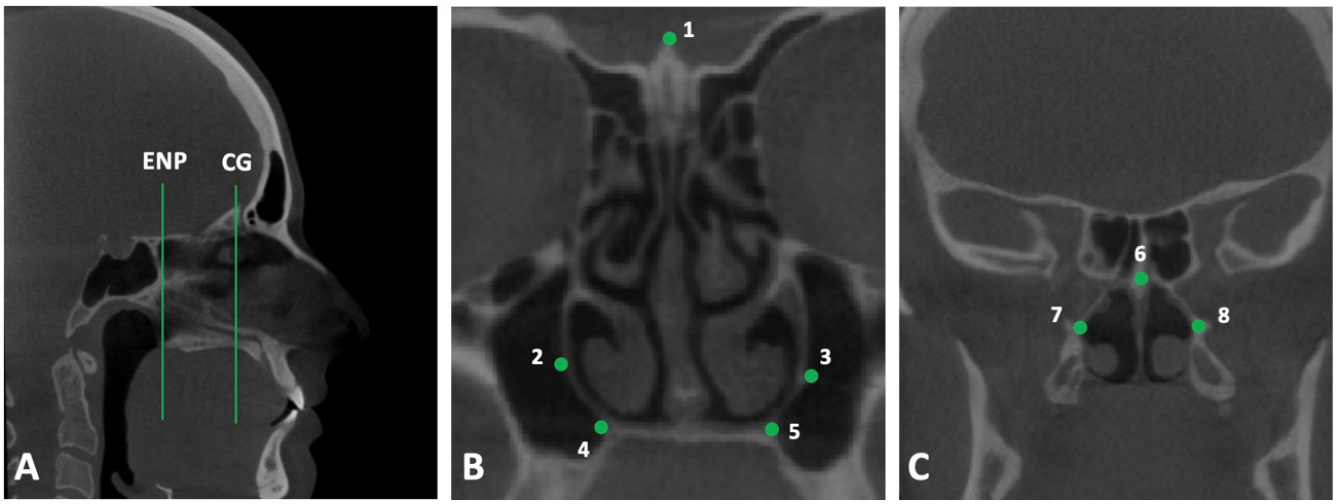

Figura 6 Cortes multiplanares de TCFC ilustrando a representação 2D dos pontos nasais internos utilizados para avaliar assimetrias na região nasal. **A,** corte sagital ilustrando as duas regiões avaliadas na cavidade nasal. **ENP,** Espinha Nasal Posterior. **CG,** crista galli. **B,** Pontos demarcados no corte localizado na CG. **1,** Topo da CG. **2 e 3,** Pontos bilaterais localizados no aspecto mais lateral da cavidade nasal. **4 e 5,** Pontos bilaterais localizados no aspecto mais lateral do assoalho nasal. **C**, Pontos demarcados no corte localizado na ENP. **6,** aspecto superior do septo nasal ao nível da ENP. **7 e 8,** Pontos bilaterais localizados no aspecto mais lateral da cavidade nasal.

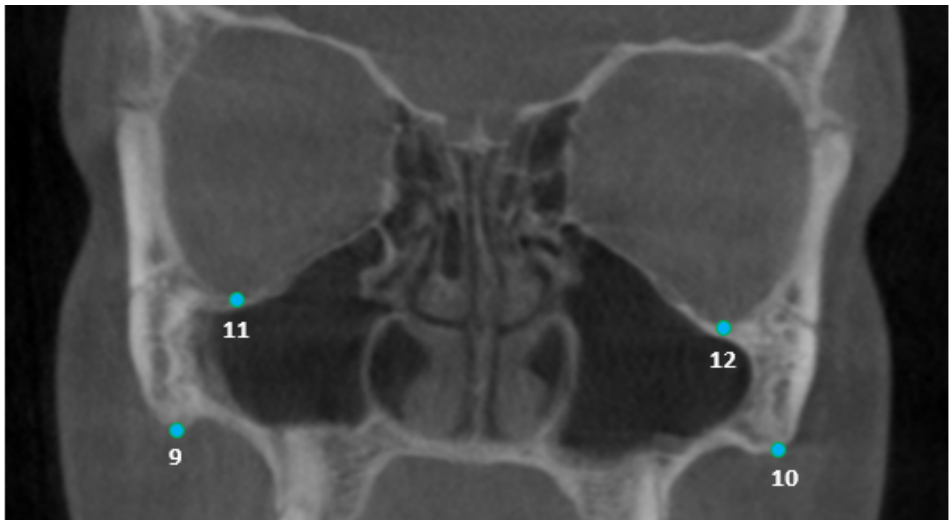

Figura 7 Corte coronal de TCFC ilustrando a representação bidimensional dos pontos bilaterais na região lateral da face. **9 e 10,** Sutura zigomaticomaxilar. **11 e 12,** ponto orbitário.

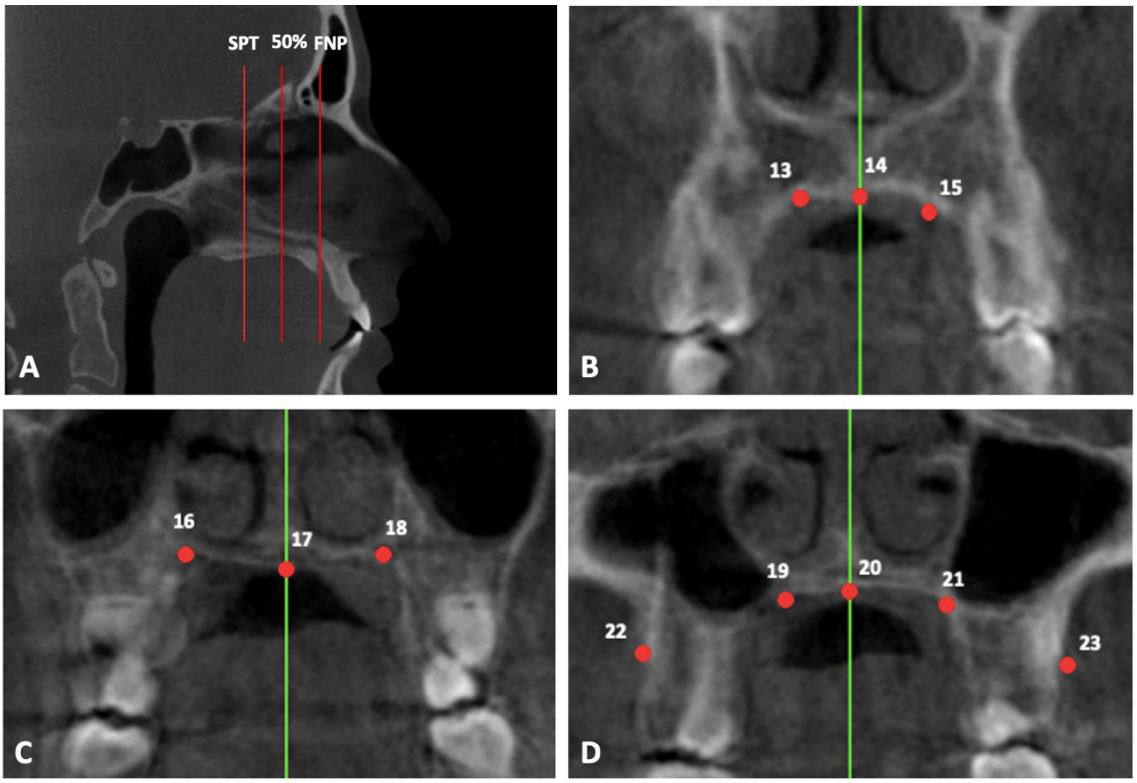

Figura 8 Cortes multiplanares de TCFC ilustrando a representação 2D dos pontos da região palatina. **A,** Corte sagital ilustrando as três regiões utilizadas para determinação dos cortes coronais. **SPT,** sutura palatina transversa. **FNP,** forame nasopalatino. **50%,** metade da distância entre SPT e FNP**. B,** Pontos no corte FNP: **13 e 15,** pontos bilaterais localizados na junção do processo alveolar/palatino. **14,** sutura palatina mediana. **C,** Pontos no corte SPT: **16 e 18,** pontos bilaterais localizados na junção do processo alveolar/palatino. **17,** sutura palatina mediana. **D,** Pontos no corte 50%: **19 e 21,** pontos bilaterais localizados na junção do processo alveolar/palatino. **20,** sutura palatina mediana. **22 e 23,** pontos bilaterais localizados no ponto mais lateral do processo alveolar vestibular.

Em seguida, foi realizada a Análise de Procrustes Generalizada para avaliação da simetria do complexo nasomaxilar por meio do programa MorphoJ (KLINGENBERG, 2011).

3.8 AVALIAÇÃO DO ÂNGULO NASAL EXTERNO

O ângulo nasal externo (º) foi avaliado no programa CS 3D Imaging. A partir da visualização do corte sagital determinado pelo plano sagital mediano, o plano coronal foi posicionado ao nível da sutura palatina transversa e o plano axial perpendicular a esta, na altura da junção da lâmina perpendicular do etmoide com o vômer (Figura 9 A). Em seguida, o ângulo nasal externo foi mensurado no corte axial, entre o plano sagital mediano e a ponta do nariz na vista axial (Figura 9 B).

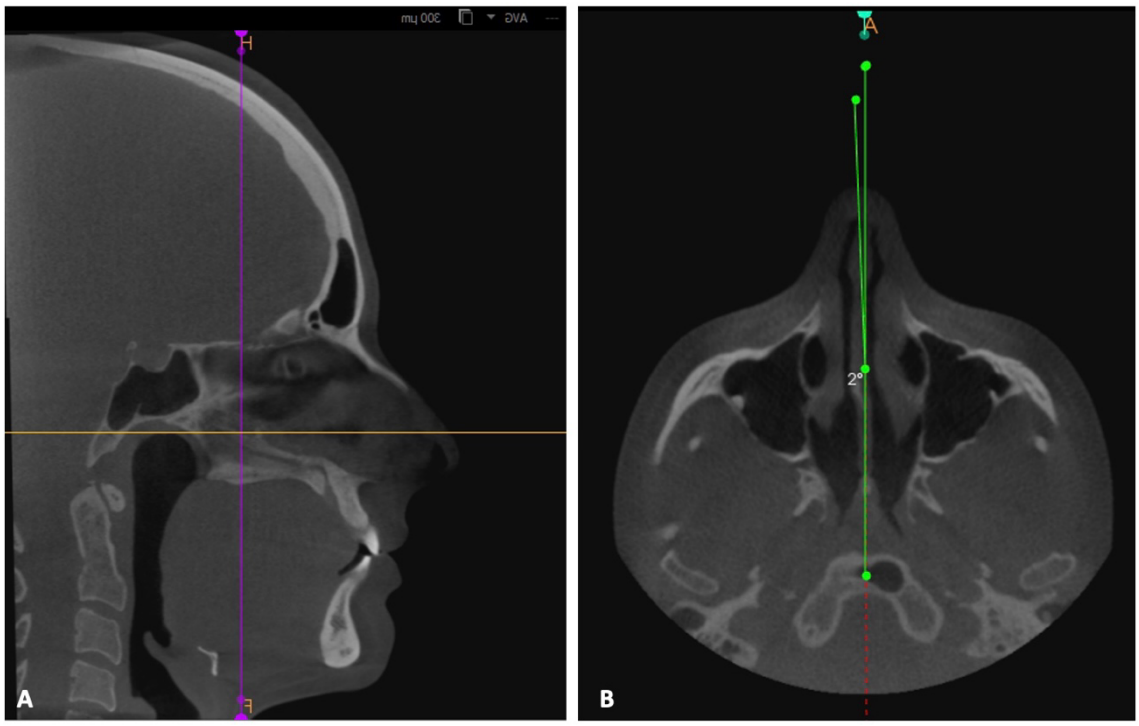

Figura 9 Cortes multiplanares de TCFC ilustrando a mensuração do ângulo nasal externo. **A,** Posicionamento dos planos coronal e axial no corte sagital. **B,** Mensuração do ângulo nasal externo no corte axial.

3.9 AVALIAÇÃO DO PLANO OCLUSAL

O plano oclusal (º) foi avaliado em corte coronal de TCFC, por meio da determinação do plano formado pelas pontas das cúspides vestibulares dos primeiros molares superiores direito e esquerdo (SYGOUROS; MOTRO; UGURLU; ACAR, 2014), no programa CS 3D Imaging. O grau de assimetria foi

determinado pela quantificação, em graus, da diferença entre o plano oclusal obtido e o respectivo plano axial da imagem, no programa ImageJ® (Figura 10, página 20).

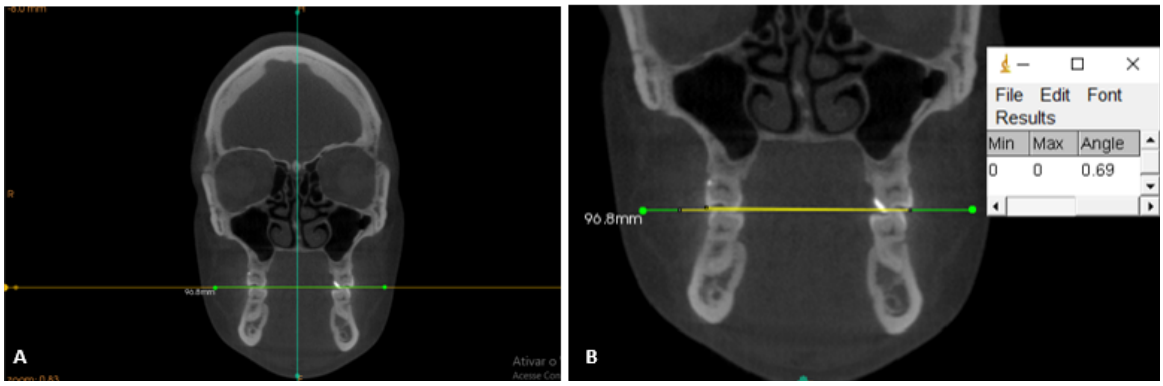

Figura 10 Cortes coronais de TCFC ilustrando a mensuração do plano oclusal. **A,** Determinação do plano oclusal no programa CS 3D Imaging. **B,** Mensuração do ângulo obtido no programa ImageJ®.

4.0 ANÁLISE ESTATÍSTICA

O cálculo do poder do estudo foi realizado, *a posteriori*, no software G * Power (Faul, Erdfelder, Lang, & Buchner, 2007), a partir dos dados obtidos do universo amostral de 15 exames de TCFC por grupo, e indicou tamanho do efeito de 2,67 e 2,09 e poder de 0,99 para os dados apresentados pelos grupos antes (DL-AS e DMS-AS) e após (DL-DS e DMS-DS) o surto de crescimento puberal, respectivamente.

A confiabilidade e precisão das coordenadas dos pontos em ambos os métodos foram avaliadas por meio do Coeficiente de Correlação Intraclasse (ICC) no programa SPSS versão 20 (Statistical Package of Social Sciences, SPSS Inc., Chicago, IL, EUA), diferenças das médias obtidas entre as duas medições, fórmula de Dalhberg e gráficos de Bland-Altman obtidos no programa

MEDCALC (MedCalc statistical package v. 14.10.2; MedCalc Software, Ostend, Bélgica).

A avaliação da normalidade dos dados e comparações intergrupos das variáveis de desvio do septo nasal (ângulo DSN, área DSN), ângulo nasal externo, plano oclusal e variáveis morfométricas (distâncias de Procrustes e Mahalanobis), de acordo com o estágio de maturação esquelética (DL-AS x DMS-AS e DL-DS x DMS-DS), foram realizados com os testes Shapiro-Wilk e Mann-Whitney U, respectivamente, no programa SPSS versão 20.

Os pontos de referência das coordenadas 2D da morfologia do septo nasal foram avaliados por meio da análise de Procrustes, que permite centralizar, dimensionar e girar cada configuração, removendo toda variação morfológica que não é devida à forma (GOWER, 1975). Em seguida, foram utilizadas Função Discriminante de Fisher com validação cruzada, Análise das Variáveis Canônicas e grades de deformação, a fim de visualizar a similaridade entre os sujeitos de cada grupo, e indicar se os grupos poderiam ser distinguidos de forma confiável (KLINGENBERG, 2011). As grades de deformação foram usadas para construir imagens correspondentes às mudanças na forma, de modo que, características de forma que são compartilhadas por diferentes indivíduos puderam ser descritas (KLINGENBERG, 2011; ROHLF; LOY; CORTI, 1996).

Previamente a análise de assimetria, as medições dos pontos do complexo nasomaxilar foram repetidas em 100% da amostra (n=60) e avaliadas com o teste de Procrustes ANOVA (PALMER, 1999), a fim de garantir que o efeito de assimetria flutuante não fosse decorrente do erro de medição. Além disso, uma análise de regressão foi realizada para verificar o efeito da alometria

(forma x tamanho), devido às diferentes idades dos indivíduos do estudo. Como o crânio apresenta simetria de objeto, as configurações dos pontos foram distinguidas em um componente de variação simétrica e um componente de variação assimétrica, onde o componente simétrico é determinado pela média das configurações de pontos reais e espelhados para cada indivíduo, e o componente assimétrico da variação é calculado como o desvio entre a configuração do ponto original para cada indivíduo e sua configuração simétrica simulada (KLINGENBERG; BARLUENGA; MEYER, 2002; MARDIA KV; BOOKSTEIN FL; IJ, 2000; SAVRIAMA; KLINGENBERG, 2011).

O teste de Procrustes ANOVA foi aplicado para avaliar o nível de assimetria nos grupos do estudo, testando os efeitos da assimetria direcional (lado) e flutuante ("indivíduo x lado") (KLINGENBERG; BARLUENGA; MEYER, 2002). A assimetria direcional é uma tendência para um traço a ser desenvolvido em maneiras diferentes nos lados direito e esquerdo (KLINGENBERG, 2015), e indicaria uma diferença consistente na forma entre os lados esquerdo e direito do indivíduo (isto é, um desvio não aleatório da simetria). A assimetria flutuante denota pequenas diferenças entre os lados esquerdo e direito devido a imprecisões aleatórias nos processos de desenvolvimento, ou seja, desvios aleatórios da simetria entre os indivíduos (KLINGENBERG, 2015; KLINGENBERG; BARLUENGA; MEYER, 2002; KLINGENBERG; MCINTYRE, 1998).

A relação entre as variáveis do SN (ângulo DSN, área DSN, tamanho do centróide e forma do SN), ângulo nasal externo, plano oclusal e as variáveis morfométricas do complexo nasomaxilar (distâncias de Procrustes e Mahalanobis, tamanho do centróide e formato das regiões nasal, lateral e

palatinas), foi avaliada por meio do teste de Correlação de Spearman no programa SPSS versão 20. O grau do coeficiente de correlação (r) foi classificado nas seguintes categorias: correlação positiva (negativa) muito alta 0,9 a 1,0 (-0,9 a -1,0); correlação positiva (negativa) alta 0,7 a 0,9 (-0,7 a -0,9); correlação positiva (negativa) moderada 0,5 a 0,7 (-0,5 a -0,7); correlação positiva (negativa) baixa 0,3 a 0,5 (-0,3 a -0,5); e pouca ou nenhuma correlação 0,0 a 0,3 (0,0 a -0,3). Além disso, foi realizada uma regressão multivariada a fim de determinar se havia uma relação significativa entre as variáveis do septo nasal (ângulo DSN, área DSN, tamanho do centróide e forma do septo nasal) (independentes) com componentes de assimetria das regiões nasal, palatina e lateral da face (variáveis dependentes). Nas análises de geometria morfométrica, de simetria e regressão multivariada, foi utilizado o programa MorphoJ. O nível de significância de 0,05 foi adotado em todas as análises.

4 DESENVOLVIMENTO DA PESQUISA

4.1 ARTIGO 1

DE PAULA, S.B.S.; RUELLAS, A.C.O.; CASTRO, A.C.R. **Reliability and accuracy of marking two-dimensional and three-dimensional craniofacial landmarks in CBCT exams.** A ser submetido ao periódico The Angle Orthodontist.

4.2 ARTIGO 2

DE PAULA, S.B.S.; NUNES, L.A.; RUELLAS, A.C.O; CASTRO, A.C.R. **Nasal septum deviation and fluctuating asymmetries of the nasomaxillary complex according to skeletal maturation: a cross-sectional study.** A ser submetido ao periódico The Journal of Craniofacial Surgery.

4.1 ARTIGO 1

RELIABILITY AND PRECISION OF TWO-DIMENSIONAL AND THREE-DIMENSIONAL CRANIOFACIAL LANDMARKS IN CBCT EXAMS.

Sarah Braga Sayão de Paula[a], Antônio Carlos de Oliveira Ruellas[b], Amanda Cunha Regal de Castro[c]

[a]MS student, Departamento de Odontopediatria e Ortodontia, Faculdade de Odontologia, Universidade Federal do Rio de Janeiro (UFRJ), Rua Professor Rodolpho Paulo Rocco, 325, Cidade Universitária, Zip code 21941-617, Rio de Janeiro, RJ, Brazil. E-mail: sarah.sayao@gmail.com. Phone: + 55 (21) 982339857.

[b]Professor, Departamento de Odontopediatria e Ortodontia, Faculdade de Odontologia, Universidade Federal do Rio de Janeiro (UFRJ), Rua Professor Rodolpho Paulo Rocco, 325, Cidade Universitária, Zip code 21941-617, Rio de Janeiro, RJ, Brazil. E-mail: antonioruellas@yahoo.com.br. Phone: + 55 (35) 988743484.

[c]Professor, Departamento de Odontopediatria e Ortodontia, Faculdade de Odontologia, Universidade Federal do Rio de Janeiro (UFRJ), Rua Professor Rodolpho Paulo Rocco, 325, Cidade Universitária, Zip code 21941-617, Rio de Janeiro, RJ, Brazil. E-mail: amandacunha@ortodontia.ufrj.br. Phone: + 55 (21) 982875189.

Corresponding author: Amanda Cunha Regal de Castro, Departamento de Odontopediatria e Ortodontia, Faculdade de Odontologia, Universidade Federal do Rio de Janeiro (UFRJ), Brazil. Avenida Professor Rodolpho Rocco, 325, Ilha do Fundão, Rio de Janeiro, RJ, Brazil, 21941-617. Phone Number: +55 21 3938-2014 / +55 21 3938-2015. Email: amandacunha@ortodontia.ufrj.br.

ABSTRACT

Objective: To evaluate the reliability and precision of two-dimensional (2D) and three-dimensional (3D) craniofacial landmarks in cone beam computed tomography (CBCT) images, for the evaluation of the nasomaxillary complex and lateral facial region.

Material and Methods: 30 CBCT exams were randomly selected. The marking of 25 craniofacial landmarks was performed using two different methods: 2D, in CBCT multiplanar sections (MPR) in CS 3D Imaging Software (Carestream Dental LLC Atlanta, GA, EUA); and 3D, from the 3D segmentation of the skull in the ITK Snap software (Pennsylvania/Utah, USA), together with MPR views. Landmarks were selected by the same examiner at a 2-week interval. Data from 2D (X, Y) and 3D (X, Y, Z) coordinates were analyzed using the Intraclass Correlation Coefficient (ICC) (a = 0.05), Dalhberg's formula, Bland-Altman plots and mean differences between measurements.

Results: ICC values ranged from 0.95 to 1.0 in the 2D method and were greater than or equal to 0.99 in the 3D method, indicating that both methods are highly reliable. Dahlberg's formula and Bland-Altman plots indicated less precision in the left zygomaxillare (D=1.80 mm) and right orbitale (D=1.82 mm) landmarks in the 3D method (in the X coordinate) and in the left zygomaticotemporal suture (D=1.95 mm) in the 2D method (in the Y coordinate). The unpaired landmarks (mainly located at the midsagittal plane) and the right frontomalare orbital (D=0.22 mm) and left frontomalare temporale (D=0.22 mm) sutures (in the X coordinate) had the best results with higher precision.

Conclusions: Both methods had excellent reliability, but generally, the 2D landmarks were slightly more precise than the 3D landmarks. All landmarks evaluated in this study recorded mean differences around 1 mm, and therefore, are reasonably considered acceptable for clinical purposes.

KEY WORDS: Cone-beam computed tomography; Anatomic Landmarks; Orthodontics

INTRODUCTION

Cone beam computed tomography (CBCT) is a diagnostic tool that enables the visualization of the three-dimensional (3D) shape of the skull, including soft and hard tissues[1], and provides clinicians to investigate human anatomy slice by slice[2]. Craniofacial landmarks in CBCT images have been widely used for many diagnostic and study purposes in the area of Maxillofacial Surgery and Orthodontics, such as to verify asymmetries, for example. [3,4] As interest in facial esthetics increases, complaints of asymmetry are likely to increase, and an accurate diagnosis to address its etiology is important.[4]

CBCT allows the evaluation of several craniofacial asymmetry measurements as distances, angles, as well as surface area and volume, enabling a more realistically visualization of the craniofacial morphology.[5] Most studies include landmarks on the mandible to analyze asymmetry, and mandibular anatomical landmarks have been extensively evaluated[6-8] since facial asymmetry is more frequently identified in the lower third of the face.[5,9] However, there may also be great levels of asymmetry in the midface[9], which includes the nasomaxillary complex, and this has been a region less studied in the literature for the assessment of asymmetries.

Anatomical structures are better located on CBCT than on conventional two-dimensional (2D) radiographs[2]. Many previous studies have seen the reproducibility and precision of 3D craniofacial landmarks, but mainly related to cephalometry[10-15] In this study, we focused on evaluating craniofacial landmarks of the nasomaxillary complex and lateral region of the face.

It is suggested that there are differences in the landmark's localization depending on the method used[14], and it is unclear if there is a difference in the reproducibility of craniofacial landmarks when demarcated exclusively in CBCT multiplanar sections (MPR) or when combined with a 3D segmentation of the areas of interest.

Therefore, this study aimed to assess the reliability and precision of the identification of anatomical landmarks in CBCT images using a 2D method with only MPR visualization, and a 3D method, which comprised a MPR with a 3D segmentation visualization for the evaluation of the nasomaxillary complex and lateral facial region.

MATERIAL AND METHODS

This study was approved by the Research Ethics Committee of the Hospital Universitário Clementino Fraga Filho (CEP-HUCFF/UFRJ) under protocol number 3.888,756.

The sample consisted of 30 CBCT of randomly selected patients (13 male and 17 female; ages, 9 - 30 years) from the Orthodontics Clinics of the Graduate course in Dentistry of the Universidade Federal do Rio de Janeiro. These records were available due to previous acquisition for orthodontic diagnosis and treatment planning purposes.

Eligibility criteria comprised availability of CBCT DICOM files of healthy subjects, without craniofacial syndromes, facial deformities, extensive bone pathological processes, craniofacial trauma, as well as surgical interventions in the facial region, like orthognathic surgery, and no history of orthodontic treatment.

CBCT scans were performed on a Kodak 9500 digital tomograph (Carestream Health, Rochester, NY, USA) under the acquisition parameters: 90 kVp, 10 mA, field of view (FOV) of 18.4 x 20.6 cm, 0.3 mm isotropic voxel size, and scanning time of 24 s.

CBCT analysis

The CBCT images were oriented in the axial, coronal and sagittal planes, using the CS 3D Imaging Software program (Carestream Dental LLC Atlanta, GA, USA), addapted from Lin, et al.[16]. Sagittal section: axial plane parallel to palatal plane; Coronal section: axial plane tangent to nasal floor; Axial section: midsagittal plane parallel to midpalatal suture.

Nasomaxillary complex and lateral facial region analysis comprised the identification of 25 craniofacial landmarks (described in Table 1). The nasomaxillary anatomical landmarks were located in three regions, which were nasal, palatal and lateral region of the face (adapted from Hartman et al.[17]). The nasal region was represented by the landmarks nasion, rhinion and anterior nasal spine. The palatal region was represented by unilateral and bilateral landmarks representing anterior midline (i.e., subnasal region), roof of the palate and posterior nasal spine. Palatal landmarks on the roof of the palate were collected

along three coronally oriented planes selected relative to the length of the palate. The first plane was located at the posterior margin of the nasopalatine foramen, the second plane was located at the transverse palatine suture, and the third plane was located at the midpoint (between the posterior margin of the nasopalatine foramen and the transverse palatine suture). The lateral facial region was represented by bilateral landmarks along the lateral surface of the zygomatic bones and floor of the orbits.

Two different methods of landmark identification were applied: a 2D, performed in CBCT MPR visualization using CS 3D Imaging Software (Carestream Dental LLC Atlanta, GA, USA); and a 3D, comprised of CBCT MPR visualization with a semi-automatic 3D segmentation of the skull in the ITK Snap software (Pennsylvania/Utah, USA) (Figure 1). The coordinates (X, Y) of the 2D method were obtained in the TpsDIG2 software (Rohlf, F. J. 2004. tpsDig, digitize landmarks and outlines, version 2.0. Department of Ecology and Evolution, State University of New York at Stony Brook), while the coordinates (X, Y, Z) of the 3D method were obtained in the 3D Slicer software.

STATISTICAL ANALYSIS

All craniofacial landmarks were performed by the same observer (S.B.S.P.) and repeated after a 2-week interval. Reliability of all landmarks coordinates was verified through the Intraclass Correlation Coefficient (ICC) (α=0.05) in the SPSS software version 20 (Statistical Package of Social Sciences, SPSS Inc., Chicago, IL, USA), and was graded as follows: excellent when it was above 0.90; good, when it was between 0.75 and 0.90; moderate, when it was between 0.50 and 0.75; and poor when it was below 0.50.[18]

Precision was verified through mean differences between the first and second measurements, Dalhberg's formula, and Bland-Altman plots (MedCalc statistical package v. 14.10.2; MedCalc Software, Ostend, Belgium), a statistical approach based on the quantification of the agreement between two quantitative measurements by studying the difference against their mean and estimating the limits of agreement (LoA).[19]

RESULTS

The ICC values ranged from 0.95 to 1.0 in X and Y coordinates of all landmarks in the 2D method, and were greater than 0.99 in X, Y and Z coordinates of all landmarks in the 3D method.

Mean differences between the first and second measurements were generally less than 1.0 mm in both of the methods, except from the X coordinate of the left zygomaxillare (1.03 mm) and left orbitale (1.06 mm) 3D measurements (Table 2).

According to the Dahlberg's formula, in the 2D method, 4 landmarks recorded values above 1.0 mm, and were specifically in the Y coordinate (rZigT, D=1.17 mm; lZigT, D=1.95 mm; rNPF, D=1.31 mm; lNPF, D=1.18 mm). In the 3D method, 9 out of the 25 landmarks recorded values above 1.0 mm (X coordinate: rZigM, D=1.69 mm; lZigM, D=1.80 mm; rOr, D=1.82 mm; lOr, D=1.18 mm; rNPF, D=1.01 mm; lNPF, D=1.01 mm; Y coordinate: rTPS, D=1.40 mm; lSTPS, D=1.46 mm; lTPS, D=1.44 mm; and Z coordinate: rNPF, D=1.19 mm; lNPF, D=1.23 mm). Therefore, the less precise landmarks (above 1.5 mm) were: the Y coordinate of the left zygomaticotemporal suture (D=1.95 mm) in 2D method; and the X coordinate of the right zygomaxillare (D=1.69 mm), left zygomaxillare (D=1.80 mm) and right orbitale (D=1.82 mm) in the 3D method (Table 2, in bold).

Figures 2, 3 and 4 illustrates the Bland-Altman plots of the landmarks with the lowest intra-examiner agreement in 2D and 3D methods. For the left zygomaxillare and right orbitale (X coordinate), the width of LoA of the 2D method was narrower (T0-T1: -1.12 and +1.08; T0-T1: -1.6 and + 1.3, respectively) than the 3D method (T0-T1: -3.6 and +5.7; T0-T1: -3.9 and + 5.7, respectively). However, the width of LoA of the Y coordinate of the left zygomaticotemporal suture, in the 3D method was narrower (T0-T1: -2.5 and +2.2) than the 2D method (T0-T1: -5.2 and +5.8). Figures 5, 6 and 7 show the Bland-Altman plots of the landmarks with the highest intra-examiner agreement in 2D and 3D methods. For the prosthion (X coordinate), the width of LoA of the 2D method was narrower (T0-T1: -0.6 and +0.3) than the 3D method (T0-T1: -0.82 and +0.63). For the landmarks right frontomalare orbitale and left frontomalare temporale (X coordinate), the width of LoA of the 3D method was narrower (T0-T1: -0.64 and +0.62; T0-T1: -0.48 and +0.7, respectively) than the 2D method (T0-T1: -1.11 and +0.67; T0-T1: -0.97 and +0.72, respectively).

DISCUSSION

Several studies evaluated the reproducibility and precision of 3D craniofacial landmarks, mainly related to cephalometry,[10-15] and to facial asymmetry.[6,7] However, there is no previous data comparing two different methodologies (2D and 3D) in relation to the nasomaxillary complex, including nasal, lateral facial and palatal region, which may be of interest to professionals in the field of maxillofacial surgery and orthodontists, especially.

In addition, in this study, the 3D methodology was not performed with the software's 3D rendering, but with a semi-automatic segmentation method, which can improve the reliability of the measurements. The 2-week interval period between the first and second measurements was chosen since it is important that the observer do not memorize the landmarks position,[14] so that it does not compromise the veracity of the results.

In the present study, ICC values were > 0.90 for all coordinates in 2D and 3D methods, indicating that they both have a high reliability. However, when we observe the results of the mean differences between the first and second measurements and Dahlberg's formula, we can observe that, in general, the 2D landmarks was slightly more precise than the 3D landmarks.

The unpaired landmarks (N, Rhi, ANS, A, Pr, PNS) and the frontomalare orbitale and frontomalare temporale were the landmarks that had the best reproducibility and precision considering all coordinates in both of the methods. This is probably because they are easier to visualize in anatomic regions that are better demarcated in the CBCT. In the 2D method, at the Y coordinate, the landmark zygomaticotemporal suture was less precise. This result indicates that this suture is very difficult to visualize only in MPR views, especially the determination of the landmark height in the 2D image (Y-axis), requiring a 3D segmentation of this region to better visualize and for a more reliable marking. In the 3D method, at the X coordinate, the landmarks zygomaxillare and orbitale were less reproducible. This indicates a greater difficulty found in marking these landmarks lateral position (right-left). Orbital landmarks, in other studies, were better visualized with 3D reconstruction[10,14], which contrasted with the present study results. This can be possibly attributed to the fact that as the image with 3D

segmentation can be rotated and seen from different angles, it can easliy confuse the observer in the landmark position.

According to Lagravere et al.[20], it is reasonable that mean differences less than 1 mm are considered clinically acceptable, and that mean differences between 1 and 2 mm are useful in most analyses. All landmarks used in this study had small mean differences, and only two landmarks above 1.0 mm, that were the X-coordinate of the left zygomaxillare (1.03 mm) and left orbitale (1.06 mm) in 3D method. However, even so, those differences were very close to 1.0 mm, indicating that these landmarks might be considered under clinically acceptable differences.

It is important to note that, with the results of the present study, the 3D segmentation might induce the observer to inaccuracy, mainly because it is an image with three dimensions and can be visualized from different angles. Therefore, as much as the segmentation is one more tool that can be used to landmarks identification, it must be used with great care and caution, as any small deviation can lead to a greater measurement error. However, depending on the anatomical region, the 3D segmentation can quite help in the landmark visualization.

CONCLUSIONS

- Both methods had excellent reliability (ICC > 0.90) in nasomaxillary complex and lateral facial region measurements.
- The unpaired landmarks, the frontomalare orbitale and frontomalare temporale recorded a higher precision in both of the methods, while the 3D landmarks zygomaxillare and orbitale, and the 2D landmark superior zygomaticotemporal suture were less precise. Generally, the 2D landmarks were slightly more precise than the 3D landmarks.
- All landmarks evaluated in this study recorded mean differences around 1 mm, and therefore, are reasonably considered acceptable for clinical purposes.

ACKNOWLEDGEMENTS

This study was supported in part by the Coordenação de Aperfeiçoamento de Pessoal de Nível Superior – Brazil – (CAPES), Finance Code 001.

REFERENCES

1. Lin HH, Chuang YF, Weng JL, Lo LJ. Comparative validity and reproducibility study of various landmark-oriented reference planes in 3-dimensional computed tomographic analysis for patients receiving orthognathic surgery. *PLoS One*. 2015;10(2):e0117604.
2. Lou L, Lagravere MO, Compton S, Major PW, Flores-Mir C. Accuracy of measurements and reliability of landmark identification with computed tomography (CT) techniques in the maxillofacial area: a systematic review. *Oral Surg Oral Med Oral Pathol Oral Radiol Endod*. Sep 2007;104(3):402-11.
3. Moro A, Correra P, Boniello R, Gasparini G, Pelo S. Three-dimensional analysis in facial asymmetry: comparison with model analysis and conventional two-dimensional analysis. *J Craniofac Surg*. Mar 2009;20(2):417-22.
4. Baek C, Paeng JY, Lee JS, Hong J. Morphologic evaluation and classification of facial asymmetry using 3-dimensional computed tomography. *J Oral Maxillofac Surg*. May 2012;70(5):1161-9.
5. Nur RB, Çakan DG, Arun T. Evaluation of facial hard and soft tissue asymmetry using cone-beam computed tomography. *Am J Orthod Dentofacial Orthop*. Feb 2016;149(2):225-37.
6. Yáñez-Vico RM, Iglesias-Linares A, Torres-Lagares D, Gutiérrez-Pérez JL, Solano-Reina E. Three-dimensional evaluation of craniofacial asymmetry: an analysis using computed tomography. *Clin Oral Investig*. Oct 2011;15(5):729-36.
7. de Moraes ME, Hollender LG, Chen CS, Moraes LC, Balducci I. Evaluating craniofacial asymmetry with digital cephalometric images and cone-beam computed tomography. *Am J Orthod Dentofacial Orthop*. Jun 2011;139(6):e523-31.
8. Porto OC, de Freitas JC, de Alencar AH, Estrela C. The use of three-dimensional cephalometric references in dentoskeletal symmetry diagnosis. *Dental Press J Orthod*. 2014 Nov-Dec 2014;19(6):78-85.
9. Severt TR, Proffit WR. The prevalence of facial asymmetry in the dentofacial deformities population at the University of North Carolina. *Int J Adult Orthodon Orthognath Surg*. 1997;12(3):171-6.
10. de Oliveira AE, Cevidanes LH, Phillips C, Motta A, Burke B, Tyndall D. Observer reliability of three-dimensional cephalometric landmark identification on cone-beam computerized tomography. *Oral Surg Oral Med Oral Pathol Oral Radiol Endod*. Feb 2009;107(2):256-65.
11. Schlicher W, Nielsen I, Huang JC, Maki K, Hatcher DC, Miller AJ. Consistency and precision of landmark identification in three-dimensional cone beam computed tomography scans. *Eur J Orthod*. Jun 2012;34(3):263-75.
12. Hassan B, Nijkamp P, Verheij H, et al. Precision of identifying cephalometric landmarks with cone beam computed tomography in vivo. *Eur J Orthod*. Feb 2013;35(1):38-44.
13. Naji P, Alsufyani NA, Lagravère MO. Reliability of anatomic structures as landmarks in three-dimensional cephalometric analysis using CBCT. *Angle Orthod*. Sep 2014;84(5):762-72.

14. Neiva MB, Soares Á, Lisboa CeO, Vilella OeV, Motta AT. Evaluation of cephalometric landmark identification on CBCT multiplanar and 3D reconstructions. *Angle Orthod*. Jan 2015;85(1):11-7.
15. Ludlow JB, Gubler M, Cevidanes L, Mol A. Precision of cephalometric landmark identification: cone-beam computed tomography vs conventional cephalometric views. *Am J Orthod Dentofacial Orthop*. Sep 2009;136(3):312.e1-10; discussion 312-3.
16. Lin L, Ahn HW, Kim SJ, Moon SC, Kim SH, Nelson G. Tooth-borne vs bone-borne rapid maxillary expanders in late adolescence. *Angle Orthod*. Mar 2015;85(2):253-62.
17. Hartman C, Holton N, Miller S, et al. Nasal Septal Deviation and Facial Skeletal Asymmetries. *Anat Rec (Hoboken)*. Mar 2016;299(3):295-306.
18. Mattos CT, Cruz CV, da Matta TC, et al. Reliability of upper airway linear, area, and volumetric measurements in cone-beam computed tomography. *Am J Orthod Dentofacial Orthop*. Feb 2014;145(2):188-97.
19. Bland JM, Altman DG. Statistical methods for assessing agreement between two methods of clinical measurement. *Lancet*. Feb 08 1986;1(8476):307-10.
20. Lagravère MO, Low C, Flores-Mir C, et al. Intraexaminer and interexaminer reliabilities of landmark identification on digitized lateral cephalograms and formatted 3-dimensional cone-beam computerized tomography images. *Am J Orthod Dentofacial Orthop*. May 2010;137(5):598-604.

TABLES

Table 1 Definition of Landmarks.

Number	Landmark name/description	Abreviattion	Region
1	Nasion: most anterior point of the frontonasal suture in the median plane	N	Nasal
2	Rhinion: midpoint, in the internasal suture, in its lowest and most anterior part	Rhi	Nasal
3	Anterior nasal spine: tip of the anterior nasal spine	ANS	Nasal/palatal
4	A point: point at the deepest midline concavity on the maxilla between ANS and prosthion	A	Palatal
5	Prosthion: most anterior point on the alveolar ridge, between the maxillary central incisors	Pr	Palatal
6/7	Right/Left zygomaxillare: lowest point of the zygomaticomaxillary suture)	rZigM/ lZigM	Lateral facial
8/9	Right/Left orbitale: lowest point in the inferior margin of the orbit	rOr/ lOr	Lateral facial
10/11	Right/Left frontomalare orbitale: most anterior point of the frontomalar suture, where it cuts the orbital edge	rFMO/ lFMO	Lateral facial
12/13	Right/Left frontomalare temporale: most posterior and lateral point of the frontomalar suture, in the temporal region	rFMT/ lFMT	Lateral facial
14/15	Right/Left superior point of the zygomaticotemporal suture	rZigT/ lZigT	Lateral facial
16/18	Right/Left alveolar/palatal process junction at nasopalatine foramen	rNPF/ lNPF	Palatal
17	Intermaxillary suture at nasopalatine foramen	ISNPF	Palatal
19/21	Right/Left alveolar/palatal process junction at transverse palatal suture	rTPS/ lTPS	Palatal
20	Intermaxillary suture at transverse palatal suture	ISTPS	Palatal
22/24	Right/Left alveolar/palatal process junction at 50% of the distance between NF and TPS	r50%/ l50%	Palatal
23	Intermaxillary suture at 50% of the distance between NF and TPS	IS50%	Palatal
25	Posterior nasal spine: tip of the posterior nasal spine	PNS	Palatal

Table 2 Mean differences and standard deviation between the first and second measurements and results of Dahlberg's formula for the coordinates of the 2D and 3D methods.

Landmark abreviattion	2D Method						3D Method								
	X			Y			X			Y			Z		
	Mean	*SD*	*D*	*Mean*	*SD*	*D*	*Mean*	*SD*	*D*	*Mean*	*SD*	*D*	*Mean*	*SD*	*D*
N	0.03	0.30	0.21	0.19	0.57	0.43	0.04	0.63	0.44	0.09	0.31	0.23	0.10	1.22	0.85
Rhi	0.10	0.42	0.30	0.23	0.41	0.33	0.12	0.34	0.25	0.01	0.71	0.49	0.02	0.82	0.57
ANS	0.15	0.59	0.43	0.06	0.30	0.21	0.08	0.37	0.26	0.03	0.69	0.48	0.06	0.61	0.43
A	0.02	0.33	0.23	0.34	0.64	0.51	0.14	0.37	0.27	0.06	0.46	0.32	0.16	0.90	0.63
Pr	0.13	0.24	0.19	0.39	0.54	0.47	0.09	0.36	0.26	0.13	0.65	0.46	0.36	0.79	0.61
rZigM	0.16	1.20	0.86	0.24	0.76	0.56	0.98	2.23	**1.69**	0.47	1.09	0.83	0.19	0.93	0.66
lZigM	0.02	0.55	0.38	0.23	0.40	0.32	1.03	2.36	**1.80**	0.18	0.77	0.55	0.19	1.06	0.75
rOr	0.16	0.72	0.52	0.10	0.37	0.27	0.93	2.44	**1.82**	0.36	1.25	0.90	0.03	0.60	0.42
lOr	0.21	0.77	0.56	0.07	0.36	0.26	1.06	1.32	1.18	0.35	0.79	0.60	0.04	0.54	0.38
rFMO	0.22	0.44	0.35	0.28	0.83	0.62	0.01	0.32	0.22	0.02	0.50	0.35	0.11	0.71	0.50
lFMO	0.02	0.46	0.32	0.14	0.84	0.60	0.21	0.73	0.53	0.13	0.48	0.35	0.21	0.85	0.61
rFMT	0.14	0.33	0.25	0.03	0.60	0.42	0.13	0.33	0.25	0.24	0.84	0.61	0.09	0.70	0.49
lFMT	0.12	0.42	0.31	0.09	0.63	0.45	0.10	0.30	0.22	0.12	0.64	0.45	0.03	0.51	0.35
rZigT	0.23	0.62	0.47	0.33	1.62	1.17	0.30	0.62	0.48	0.15	1.25	0.88	0.12	0.45	0.32
lZigT	0.17	0.85	0.61	0.30	2.73	**1.95**	0.11	0.55	0.39	0.13	1.21	0.84	0.13	0.59	0.42
rNPF	0.77	0.79	0.78	0.25	1.84	1.31	0.43	1.38	1.01	0.16	1.40	0.98	0.33	1.68	1.19
lSNPF	0.15	0.31	0.24	0.03	1.17	0.83	0.10	0.45	0.32	0.10	1.33	0.93	0.13	1.10	0.77
lNPF	0.67	0.83	0.75	0.36	1.63	1.18	0.17	1.45	1.01	0.22	1.39	0.98	0.39	1.72	1.23
rTPS	0.40	0.99	0.75	0.15	0.44	0.33	0.34	0.95	0.70	0.43	1.97	1.40	0.14	0.83	0.59
lSTPS	0.16	0.32	0.25	0.12	0.35	0.26	0.08	0.36	0.26	0.58	2.02	1.46	0.20	0.73	0.53
lTPS	0.29	0.81	0.61	0.07	0.55	0.39	0.22	1.04	0.74	0.50	2.00	1.44	0.11	0.76	0.53
r50%	0.48	0.83	0.68	0.15	0.50	0.36	0.23	0.94	0.67	0.36	1.21	0.88	0.27	0.72	0.53
lS50%	0.16	0.31	0.25	0.19	0.66	0.49	0.09	0.49	0.35	0.30	1.25	0.89	0.18	0.48	0.36
l50%	0.15	0.67	0.49	0.00	0.60	0.42	0.01	0.85	0.59	0.34	1.26	0.91	0.16	0.65	0.47
PNS	0.17	0.40	0.31	0.14	0.36	0.27	0.00	0.57	0.39	0.20	1.04	0.73	0.07	0.61	0.42

Note. *SD*= standard deviation. *D*= Dahlberg's formula.

FIGURES

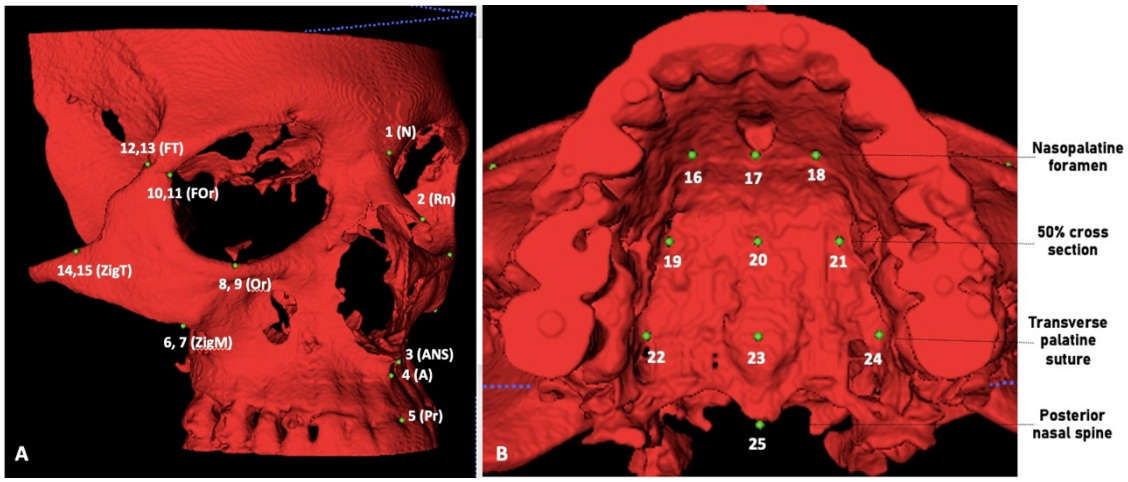

Figure 1 3D CBCT reconstruction illustrating skull segmentation and demarcation of craniofacial landmarks used in the study. **A,** 1- nasion, 2- rhinion, 3- anterior nasal spine, 4-point A, 5- prosthion, 6,7- zigomaxillares, 8,9- orbitales and 10 to 15- landmarks in the lateral region of the face. **B,** 16 to 25 - landmarks in the region of the intermaxillary suture, junction of the alveolar and palatine processes and posterior nasal spine.

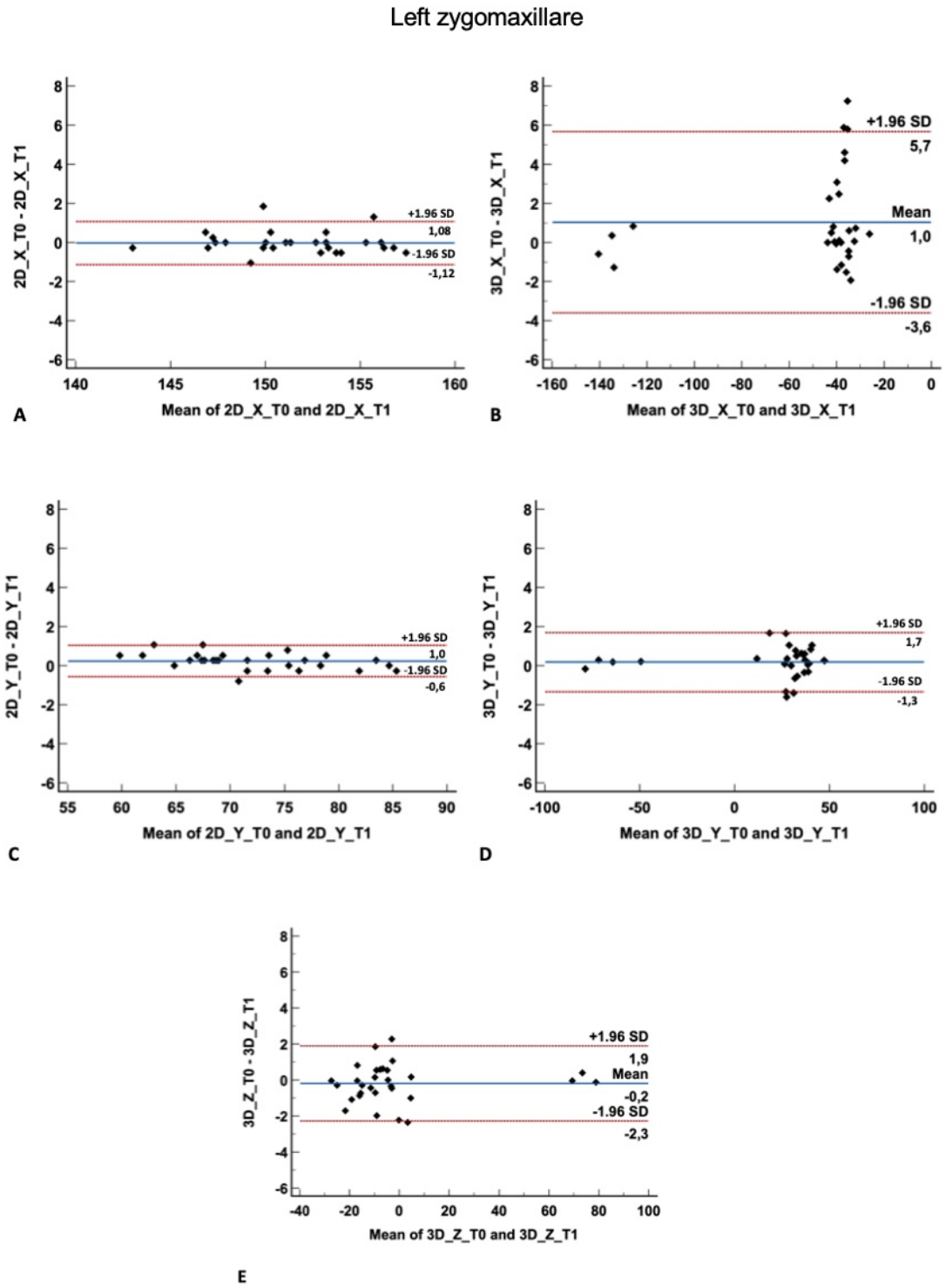

Figure 2 Bland-Altman plots expressing intra-examiner agreement for the landmark left zygomaxillare. **A,** in X coordinate, in the 2D method, we can observe the points closer to the mean and more homogeneous distribution, indicating good reproducibility. **B,** in X coordinate, in the 3D method, we observed spread points (heterogeneous distribution) and some distant from the mean, indicating lower reproducibility. **C and D,** in Y coordinate, in both methods, we have good reproducibility, with 2D a little better. **E,** Z coordinate in 3D method, good reproducibility.

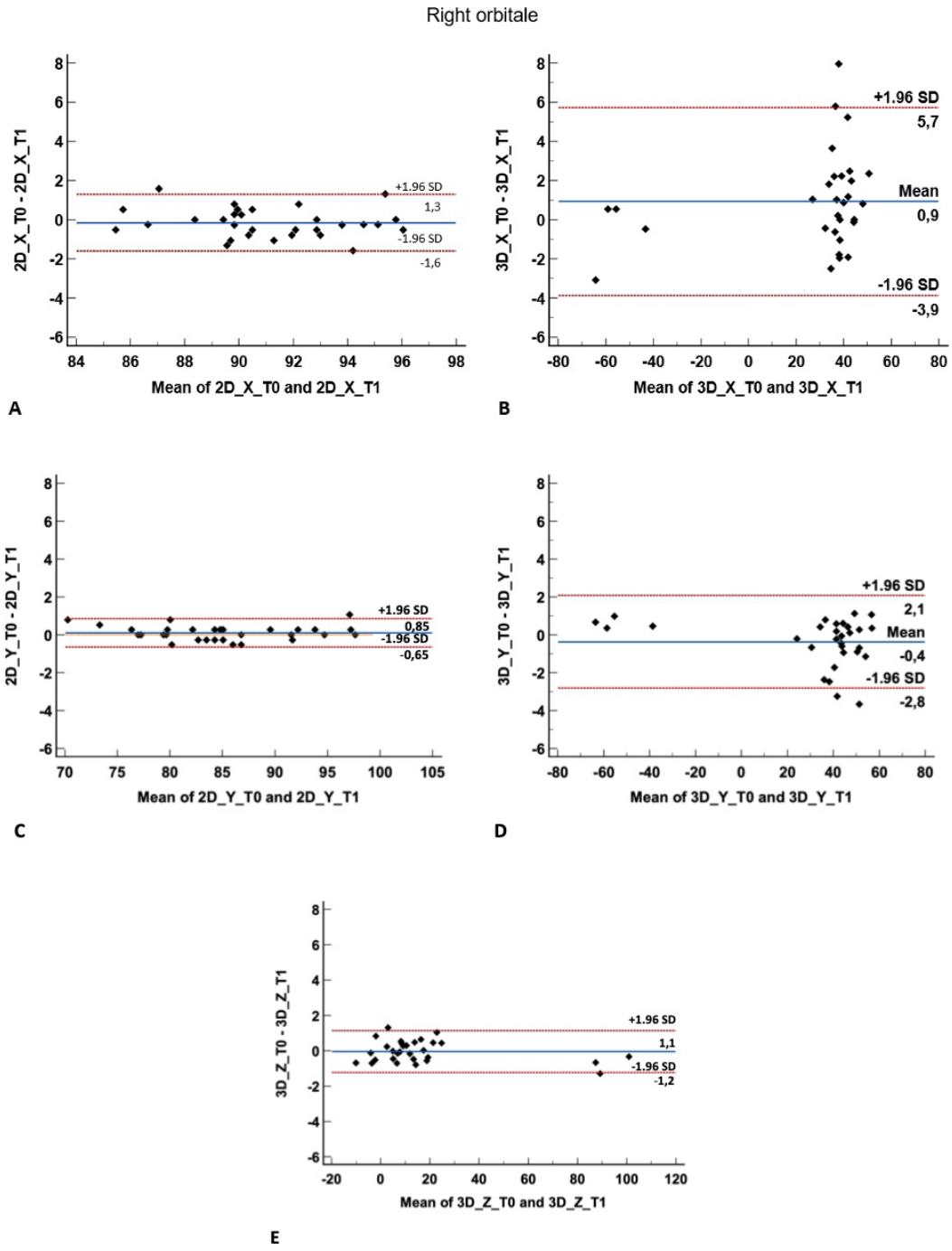

Figure 3 Bland-Altman plots expressing intra-examiner agreement for the landmark right orbitale. **A,** in X coordinate, in the 2D method, we can observe the points closer to the mean and more homogeneous distribution, indicating good reproducibility. **B,** in X coordinate, in the 3D method, we observed spread points (heterogeneous distribution) and some distant from the mean, indicating lower reproducibility. **C,** Y coordinate, 2D method, good reproducibility. **D,** Y coordinate, 3D method, good reproducibility, but lower. **E,** Z coordinate, 3D method, good reproducibility.

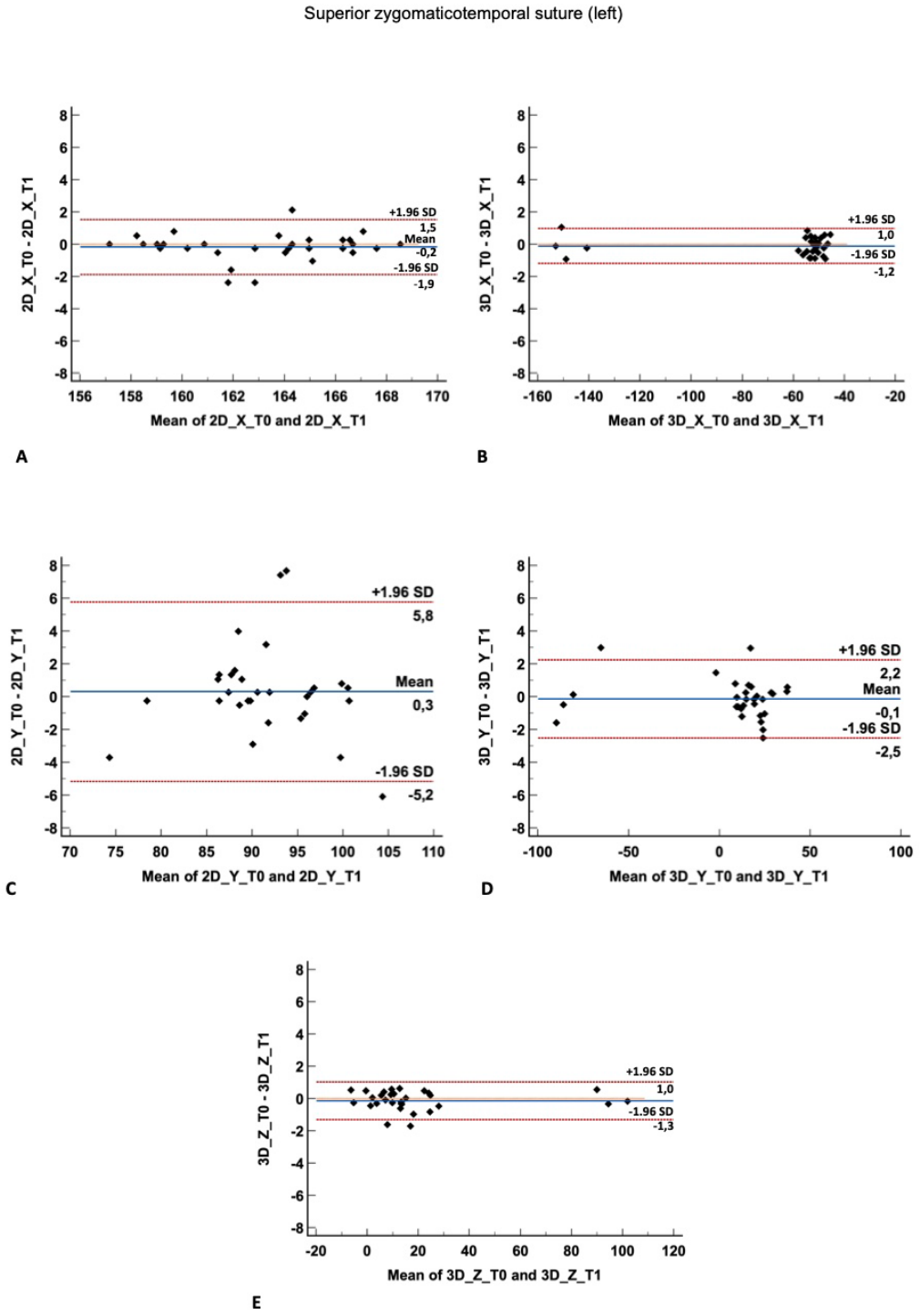

Figure 4 Bland-Altman plots expressing intra-examiner agreement for the landmark superior zigomaticotemporal suture (left). **A,** X coordinate, 2D method, good reproducibility. **B,** X coordinate, 3D method, good reproducibility, a little better than 2D. **C,** Y coordinate, 2D method, we observed spread points (heterogeneous distribution) and some distant from the mean, indicating less reproducibility. **D,** Y coordinate, 2D method, we can observe the points closer to the mean and more homogeneous distribution, indicating good reproducibility. **E,** Z coordinate, 3D method, good reproducibility.

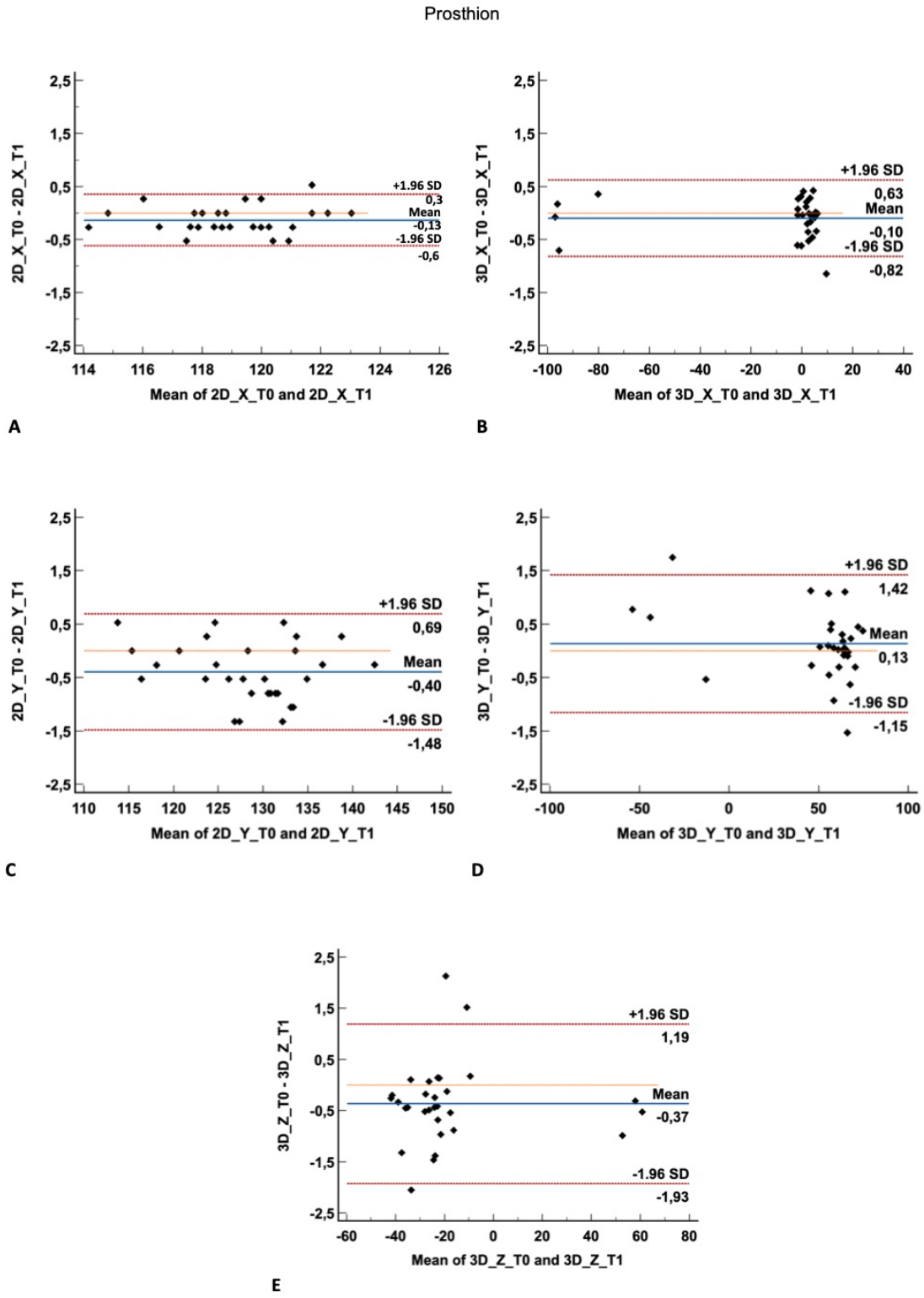

Figure 5 Bland-Altman plots expressing intra-examiner agreement for the landmark prosthion. **A,** X coordinate, 2D method, good reproducibility. **B,** Xcoordinate, 3D method, good reproducibility. **C,** Y coordinate, 2D method, good reproducibility. **D,** Y coordinate, 3D method, good reproducibility. **E,** Z coordinate, 3D method, good reproducibility.

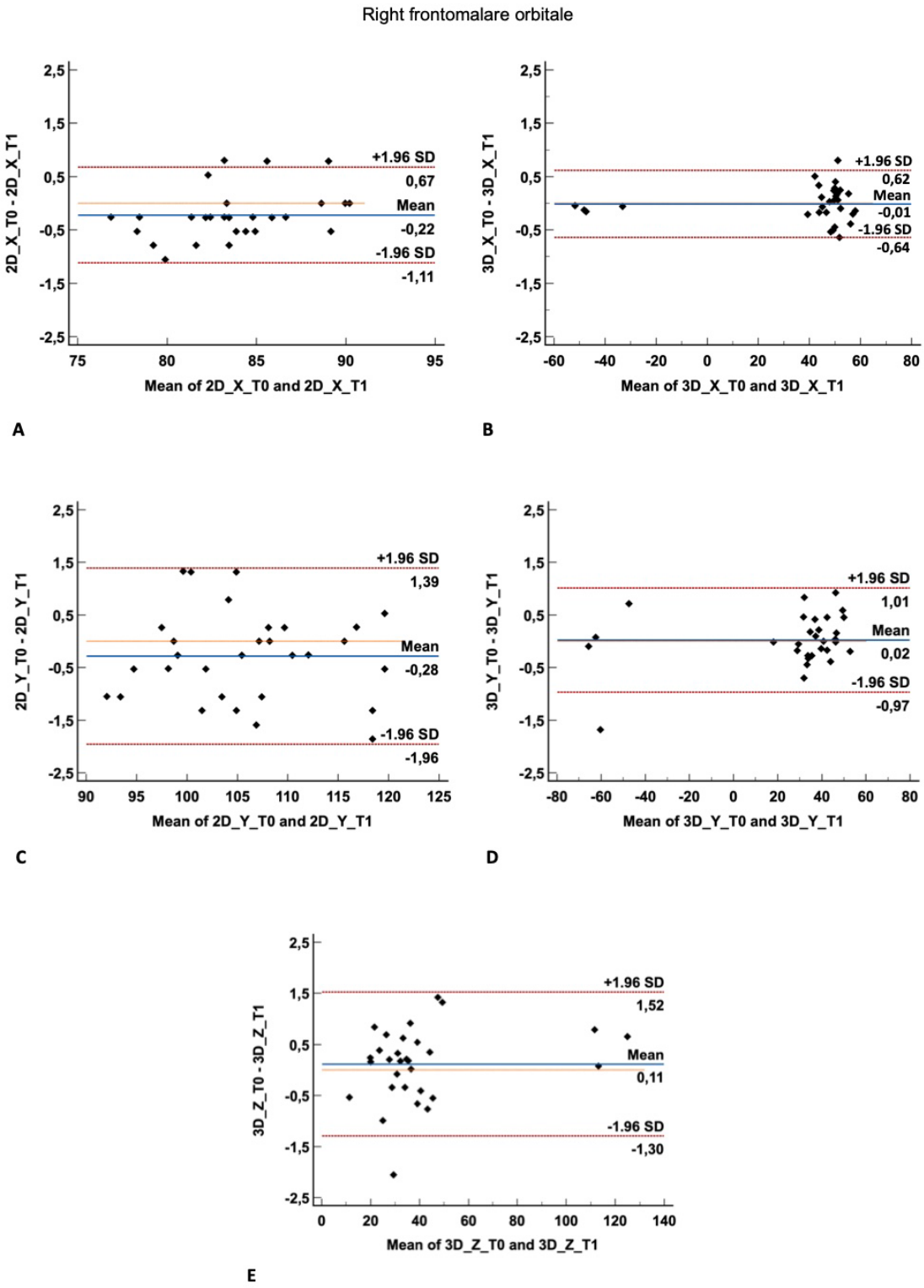

Figure 6 Bland-Altman plots expressing intra-examiner agreement for the landmark right frontomalare orbitale. **A,** X coordinate, 2D method, great reproducibility. **B,** X coordinate, 3D method, great reproducibility. **C,** Y coordinate, 2D method, good reproducibility, but with more scattered points. **D,** Y coordinate, 3D method, good reproducibility. **E,** Z coordinate, 3D method, good reproducibility.

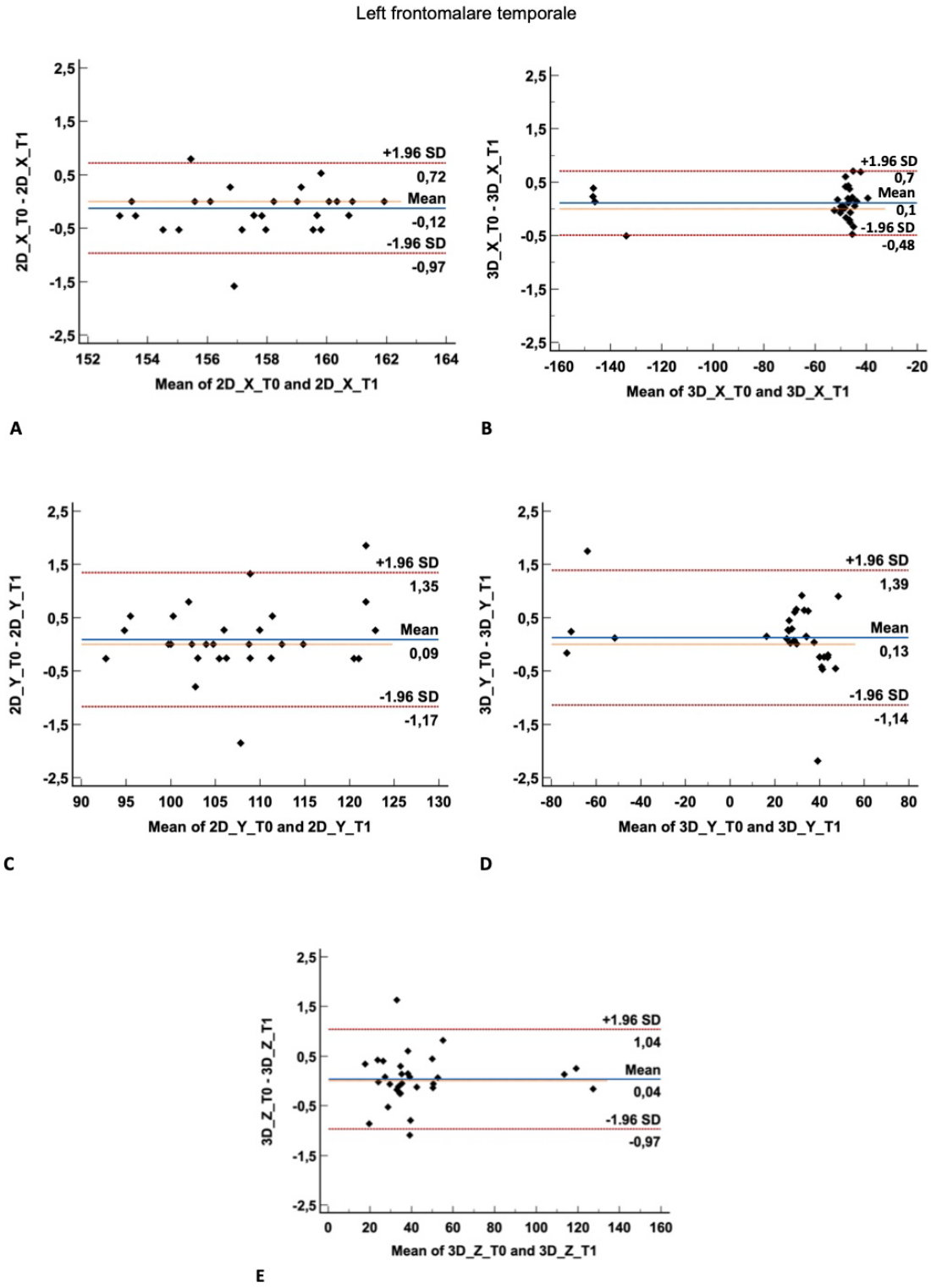

Figure 7 Bland-Altman plots expressing intra-examiner agreement for the landmark left frontomalare temporale. **A,** X coordinate, 2D method, good reproducibility. **B,** X coordinate, 3D method, good reproducibility. **C,** Y coordinate, 2D method, good reproducibility, but with more scattered points. **D,** Y coordinate, 3D method, good reproducibility. **E,** Z coordinate, 3D method, good reproducibility.

4.2 ARTIGO 2

NASAL SEPTUM DEVIATION AND FLUCTUATING ASYMMETRIES OF THE NASOMAXILLARY COMPLEX ACCORDING TO SKELETAL MATURATION: A CROSS-SECTIONAL STUDY.

Sarah Braga Sayão de Paula[a], Lorena Andrade Nunes[b], Antônio Carlos de Oliveira Ruellas[c], Amanda Cunha Regal de Castro[d]

[a]MS student, Departamento de Odontopediatria e Ortodontia, Faculdade de Odontologia, Universidade Federal do Rio de Janeiro (UFRJ), Rua Professor Rodolpho Paulo Rocco, 325, Cidade Universitária, Zip code 21941-617, Rio de Janeiro, RJ, Brazil. E-mail: sarah.sayao@gmail.com. Phone: + 55 (21) 982339857.

[b] Professor, Colegiado de Nutrição, Centro Universitário UniFTC, Avenida Adolfo Ribeiro, 357, São Judas, Zip code 46204-068, Jequié, Bahia, Brazil. E-mail: lorenunes2@gmail.com. Phone: +55 (73) 988385883.

[c]Professor, Departamento de Odontopediatria e Ortodontia, Faculdade de Odontologia, Universidade Federal do Rio de Janeiro (UFRJ), Rua Professor Rodolpho Paulo Rocco, 325, Cidade Universitária, Zip code 21941-617, Rio de Janeiro, RJ, Brazil. E-mail: antonioruellas@yahoo.com.br. Phone: + 55 (35) 988743484.

[d]Professor, Departamento de Odontopediatria e Ortodontia, Faculdade de Odontologia, Universidade Federal do Rio de Janeiro (UFRJ), Rua Professor Rodolpho Paulo Rocco, 325, Cidade Universitária, Zip code 21941-617, Rio de Janeiro, RJ, Brazil. E-mail: amandacunha@ortodontia.ufrj.br. Phone: + 55 (21) 982875189.

Corresponding author: Amanda Cunha Regal de Castro, Departamento de Odontopediatria e Ortodontia, Faculdade de Odontologia, Universidade Federal do Rio de Janeiro (UFRJ), Brazil. Avenida Professor Rodolpho Rocco, 325, Ilha do Fundão, Rio de Janeiro, RJ, Brazil, 21941-617. Phone Number: +55 21 3938-2014 / +55 21 3938-2015. Email: amandacunha@ortodontia.ufrj.br.

ABSTRACT

INTRODUCTION: The aim of the present study was to investigate the influence of nasal septum deviation on nasomaxillary complex fluctuating asymmetries at different stages of skeletal maturation, and if there is an association between the degree of severity of the septal deviation and the degree of asymmetry of the nasomaxillary complex.

METHODS: This was a retrospective, cross-sectional observational study, which sample consisted of 60 selected CBCT scans and divided into four groups (n = 15), according to the degree of septal deviation and skeletal maturation, being mild deviation (MD) <10°, moderate to severe deviation (MSD) (≥10°), before spurt (BS) and after spurt (AS). The angle of greatest nasal septal deviation (NSD) was measured, as well as the area of deviation. A Geometric Morphometrics approach was performed to evaluate the nasal septum (NS). The morphology of the nasomaxillary complex and presence of fluctuating asymmetries was evaluated by 23 two-dimensional landmarks on the nasomaxillary complex (nasal, lateral and palatal regions) and by making Procrustes ANOVA and Mann-Whitney test. In addition, we used Spearman's correlation and multivariate regression to correlate nasal septum deviation with asymmetries in these regions.

RESULTS: No significant differences were observed in the Procrustes and Mahalanobis distances (fluctuating asymmetry) of the nasomaxillary complex between the groups MD-BS x MSD-BS and MD-AS x MSD-AS (*P<0.05*) However, with the results of our multivariate regression, we saw that regarding the more specific aspects of asymmetry (asymmetry component), there was a positive correlation between the NSD angle and the palatal regions (*P=0.035 and P=0.047*, middle and posterior, respectively), and also between nasal septum shape and anterior palatal region (*P=0.039*). The nasal and lateral regions were not correlated with the NSD angle in our multivariate regression *(P>0.05).*

CONCLUSION: The groups with mild NSD did not show significant differences in the fluctuating asymmetry of the nasomaxillary complex in relation to the groups with moderate to severe NSD, both before and after the growth spurts stages. However, a positive correlation was observed between the nasal septum deviation angle and asymmetry component in the middle and posterior palatal

regions, and between nasal septum shape and anterior palatal region asymmetry component. No significant relationships were observed with the nasal and lateral regions of the nasomaxillary complex.

KEY WORDS: Nasal septum, Facial Asymmetry, Cone-beam computed tomography

INTRODUCTION

Facial symmetry is an important parameter for diagnosis analysis and treatment planning of different biological areas. However, it is not simple to determine the threshold that defines symmetrical and asymmetrical faces, which is often determined by the clinicians' sense of balance and the patients' perception of imbalance.[1] Several etiological factors have been attributed to skeletal facial asymmetry, and despite causality cannot be determined, previous studies reported a relationship between anatomical deviation of the nasal septum (NS) and facial development.[2-4]

Nasal septum deviation (NSD) consists of a misalignment of the septum in relation to the facial midline, which may involve the bony or cartilaginous parts isolated, or in combination[5], and is found with a reasonable prevalence in the general population, but mainly in adults.[6] The "nasal septum theory" suggests that the nasal septum cartilage is a primary growth center, displacing the central bones of the face forward and downward.[7] Latham proposed that the nasal septum acts as an initiating mechanism moving the premaxilla and maxilla forward through the septum-premaxillary ligaments.[8] The function of the septal cartilage as a “growth center” is certainly possible, as the maxillary sutures would respond to the growth of nasal cartilage forming new bone when they were pushed aside by the forces of septal cartilage growth.[9] Besides, a surgical resection of all or part of the nasal septum, in a variety of animal models, resulted in a deficiency in the anteroposterior dimensions of the maxilla and premaxilla.[10-12] Therefore, it is hypothesized that the deviated growth of a nasal septum may have some contribution to the development of facial asymmetries.[2]

Previous studies, comprising adolescents and adult subjects aged from 14 to 71 years, observed an association between nasal septum deviation and facial asymmetries, through photographic analysis, [13,14] and also with facial asymmetries, evaluated by computed tomography (CT) [2-4].

Regarding patients in growing stages, diagnosis is critical, and the indication of pediatric septoplasty can be considered, since a previous study by D’Ascanio et al. reported that mouth-breathing children with uncorreted NSD in comparison to nose-breathing children demonstrate facial and dental anomalies.[15] Furthermore, not performing or delaying septoplasty when indicated

may affect nasal e facial growth.[16] A recent study indicated that there is an association between NSD and the abnormal growth of the nasomaxillary complex, with reduced dimensions of width and area of the maxilla and nasal cavity being observed in the groups of individuals with greater NSD[17].

Therefore, the aim of the present study was to investigate the influence of nasal septum deviation on nasomaxillary complex fluctuating asymmetries at different stages of skeletal maturation, and if there is an association between the degree of severity of the septal deviation and the degree of asymmetry of the nasomaxillary complex.

MATERIAL AND METHODS

Study design

This was a retrospective, cross-sectional observational study[18], approved by the Research Ethics Committee of the Hospital Universitário Clementino Fraga Filho (CEP-HUCFF/UFRJ) under the protocol number 3.888,756.

The sample consisted of cone-beam computed tomography (CBCT) exams of 60 randomly selected patients (25 male and 35 female; ages, 9 - 30 years) from the Orthodontics Clinics of the Graduate course in Dentistry of the Universidade Federal do Rio de Janeiro. These records were available due to previous acquisition for orthodontic diagnosis and treatment planning purposes.

Eligibility criteria comprised availability of CBCT DICOM files, including full fourth cervical vertebra of healthy subjects, without craniofacial syndromes, facial deformities, extensive bone pathological processes, craniofacial trauma, as well as surgical interventions in the facial region, including septoplasty and previous orthognathic surgery, and no history of orthodontic treatment.

CBCT scans were performed on a Kodak 9500 digital tomograph (Carestream Health, Rochester, NY, USA) under the acquisition parameters: 90 kVp, 10 mA, field of view (FOV) of 18.4 x 20.6 cm, 0.3 mm isotropic voxel size, and scanning time of 24 s. CBCT exams were allocated into four groups (n = 15) according to the skeletal maturity stage and nasal septum deviation. The skeletal maturity stage was identified by the Cervical Vertebral Maturation (CVM) method described by BACCETTI in 2005[19]. Exams were assigned to the group before growth spurt (BG) from stage CS1 to CS4, and after growth spurt (AG), for stages

CS5 and CS6. According to the angle of the nasal septum deviation, CBCTs images were further assigned to group MD, with mild deviation (<10°), and group MSD, with moderate to severe deviation (≥10°)[20].

CBCT analysis

The CBCT images were oriented using the CS 3D Imaging software (Carestream Dental LLC Atlanta, GA, USA), adapted from LIN et, al. [21] Sagittal section: axial plane parallel to palatal plane; Coronal section: axial plane tangent to nasal floor; Axial section: midsagittal plane parallel to midpalatal suture. In cases where the patient had an extensive nasal floor asymmetry, observed in the coronal section, an average between the right and left sides of the nasal floor was used, always considering the effect of the movement on the head and its proximity to its natural position.

Nasal septum

Nasal septum analysis was performed using the CS 3D Imaging software, in the slice with the greatest nasal septum deviation, and, for this, the CBCT coronal slices were covered, following an anterior to posterior axis of the nasal septum, until this point was visible. This slice was selected in the bone region of the septum, from the Crista Galli (CG) to the most posterior region, so that the cartilage area would not compromise the measurement.

Once the coronal slice with the greatest nasal septum deviation was selected, ImageJ® software was used to measure the NSD angle (º) and NSD area (mm²). NSD angle (º) was measured, following the reference points: superior intersection of the NS at the level of CG; inferior intersection of the NS at the level of the anterior nasal spine; and the most prominent hyperdense point along the NS (Figure 1A).[5,22-25] NSD angle degree was considered as mild (<10°), and moderate to severe (≥10°)[20], and determined the MD and MSD groups allocation, respectively. NSD area (mm²) was measured from the point of greatest NSD to the midsagittal plane (Figure 1B).

Nasal septum morphology was assessed by Generalized Procrustes Analysis (GPA) performed in the MorphoJ software[26] (Klingenberg, 2011), by identifying two-dimensional (2D) landmarks in the previously selected coronal slice, with the TpsDIG2 software[27] (Rohlf, F. J. 2004. tpsDig, digitize landmarks

and outlines, version 2.0. Department of Ecology and Evolution, State University of New York at Stony Brook). For this, five landmarks were used: top of the CG, lowest point of the NS, point of greatest deviation on the right side, point of greatest deviation on left side and second point of greatest deviation (right or left side – depending on each subject) (Figure 1C).

Nasomaxillary complex

The morphology of the nasomaxillary complex was assessed through 23 2D coordinate landmarks of the nasal, lateral and palatal regions of the face, adapted from Hartman et al., 2016[2], described in Table 1. The 2D images and respective coordinates of the nasomaxillary complex were obtained with the CS 3D Imaging and TpsDIG2 software. Then, a Generalized Procrustes Analysis (GPA) was performed for evaluating the nasomaxillary complex symmetry using the MorphoJ software.

The nasal region was represented by the internal nasal cavity, where unilateral and bilateral landmarks were collected along two coronally oriented planes (Figure 2A), located on top of the Crista Galli (nasal region 1) (Figure 2B) (corresponding to approximately 50% of nasal floor length), and at the posterior nasal spine (PNS) level (nasal region 2) (Figure 2C) (approximately 100% of nasal floor length). The lateral region of the face (Figure 2D) was represented by bilateral landmarks of the zygomaticomaxillary suture and the floor of the orbits, visualized in a coronally oriented plane.

The palatal region comprised unilateral and bilateral landmarks placed on the roof of the palate, which were collected along three coronally oriented planes selected in relation to the length of the palate (Figure 3E). The first plane was located at the posterior margin of the nasopalatine foramen (NPF) (palatal region 1) (Figure 2F), the second plane was located at the transverse palatine suture (TPS) (palatal region 2) (Figure 2G), and the third plane was located at the midpoint between the posterior margin of the NPF and the TPS (palatal region 3) (Figure 2H).

External nasal angle and occlusal plane

External nasal angle (ENA) and occlusal plane (OP) analysis were evaluated on axial and coronal slices images, respectively, provided by the CS 3D Imaging software.

In order to perform the external nasal angle (º) measurement, the coronal and axial planes were positioned parallel and perpendicular to the TPS, at the level of the junction of the perpendicular blade of the ethmoid with the vomer (Figure 3A). Then, the angle between the median sagittal plane and tip of the nose was measured in the axial view (Figure 3B).

The occlusal plane was determined in the coronal CBCT slice, by intercepting the buccal cusp tips of upper right and left first molars[28] (Figure 4A). Then, the angle between the determined occlusal plane and the respective axial plane of the image was measured using the ImageJ® software (Figure 4B).

Statistical analysis

A posteriori power analysis was performed in G*Power software[29] (Faul, Erdfelder, Lang, & Buchner, 2007) and indicated an effect size of 2.67 and 2.09, and achieved power of 0.99 for the groups before and after growth spurts, respectively.

Data normality assessment and intergroup comparisons of the NS deviation variables (NSD angle, NSD area), ENA, OP, and morphometric variables (Procrustes and Mahalanobis distances), according to skeletal maturation stage (MD-BG x MSD-BG and MD-AG x MSD-AG), were performed with Shapiro-Wilk and Mann-Whitney U tests, respectively, using the SPSS software version 20 (Statistical Package of Social Sciences, SPSS Inc., Chicago, IL, USA). All measurements were performed by the same observer (S.B.S.P.) and repeated after a 2-week. Reliability and precision were assessed for NSD angle, NSD area, ENA, OP and skeletal stage in 50% of the sample using the Intraclass Correlation Coefficient (ICC) (> 0.90) and Dahlberg's formula (0.02 – 0.78). Also, in order to ensure that the fluctuating asymmetry effect was not due to the measurement error, the 2D coordinate landmarks measurements of the nasomaxillary complex were carried out twice in the overall sample (n= 60) and assessed with the Procrustes ANOVA test.[30]

2D coordinate landmarks of NS morphology was assessed with a GPA, for purposes of superposition of these points, eliminating the effects of translation and rotation. In this way, the Procrustes superposition allows to centralize, scale and rotate each configuration, removing all morphological variation that is not due to the shape.[31] Then, we made Fisher's Discriminant Function (FDF) with cross validation, Canonical Variable Analysis (CVA) and thin-plate splines, in order to visualize the similarity between the subjects of each group, and to indicate whether the groups could be distinguished reliably.[26] The thin-plate spline function was used to construct images corresponding to changes in shape, thus, shape features shared by different subjects could be described.[26,32]

A regression analysis was performed to check the effect of allometry (shape vs. size), owing to the different ages of the subjects analyzed in the study. As the skull has object symmetry, landmarks configurations were distinguished into a component of symmetric variation and a component of asymmetric variation,[33,34] where the symmetric component was the average between the original configuration and reflected copy of each individual, and the asymmetric component was calculated as the differences between the original configurations and reflected copies.[33-35] The Procrustes ANOVA test was applied to compare the level of asymmetry among the study groups, by testing the effects of directional (side) and fluctuating asymmetry ("individual X side").[33] Directional asymmetry is a tendency for a trait to be developed in different ways on the right-left sides,[36] and would indicate a consistent difference in shape between the left and right sides (i.e., a non-random deviation from symmetry). Fluctuating asymmetry denotes small differences between the left and right sides due to random imprecisions in developmental processes, that is, random deviations from symmetry among individuals.[33,36,37]

The relationship between the NS variables (NSD angle, NSD area, NS centroid size and NS shape) and ENA, OP, and morphometric variables of the nasomaxillary complex (Procrustes and Mahalanobis distances, centroid size and shape of nasal, lateral and palatal regions), was assessed with the Spearman's Correlation test using the SPSS software version 20. The degree of the correlation coefficient (r) was classified into the following categories: very high positive (negative) correlation 0.9 to 1.0 (-0.9 to -1.0); high positive (negative) correlation 0.7 to 0.9 (-0.7 to -0.9); moderate positive (negative) correlation 0.5 to

0.7 (-0.5 to -0.7); low positive (negative) correlation 0.3 to 0.5 (-0.3 to -0.5); little if any correlation 0.0 to 0.3 (0.0 to -0.3).[38] Also, a multivariate regression was performed in the MorphoJ software in order to determine whether there was a significant relationship between the NS variables (NSD angle, NSD area, NS centroid size and NS shape), as independent variables, with asymmetry component of the nasal, palatal, and lateral facial regions, as dependent variables. For morphometric, symmetry and regression analyses, the MorphoJ software was used. The significance level of 0.05 was adopted in all analyzes.

RESULTS

Descriptive statistics of NSD angle, NSD area, ENA and OP variables are presented in Table 2. Statistically significant increased values of NSD angle and NSD area were observed in the groups with moderate to severe deviation before (MD-BG: 7.99 (2.26)º and 55.2 (31.0) mm^2/ MSD-BG: 13.03 (3.04)º and 117.0 (34.8) mm^2) and after growth spurt stages (MD-AG: 7.65 (2.62)º and 56.7 (23.1) mm^2/ MSD-AG: 14.04 (3.44)º and 95.5 (100.1) mm^2) (*P*<.001). ENA and OP did not present a statistically significant difference between the evaluated groups (MD-BG x MSD-BG and MD-AG x MSD-AG) (Table 2).

The morphological analysis of the nasal septum by Fisher's Discriminant Function with cross-validation indicated that, in relation to shape, there was a statistically significant difference between the groups MD-BG x MSD-BG (*P<0.0001)* and MD-AG x MSD-AG *(P=0.006)*. Intergroup comparisons are presented in a CVA graph (Figure 5). In addition, Figure 6 illustrates the similarity in the shape of the groups through thin-plate splines, in which the groups with mild deviation had a narrower shape and those with moderate/severe deviation had a wider/expanded shape, especially in the nasal septum central region. The regression analysis for the allometry effect was not significant (*P>0.05*), indicating that individual size did not interfere with the shape morphology in our study groups.

Regarding the nasomaxillary complex analysis, Procrustes ANOVA results indicated that there are significant levels of fluctuating asymmetry (“Individual x Side”) in the nasal, lateral and palatal regions of all the study groups

(Supplementary Tables 1, 2 and 3). It is important to note that the measurement error value was smaller than the fluctuating asymmetry ("Individual X Side"), indicating that the asymmetry values were not due to a measurement error on the right and left sides. No intergroup differences (MD-BG x MSD-BG and MD-AG X MSD-AG) were observed in the Procrustes and Mahalanobis distances variables (fluctuating asymmetry) ($P<0.05$) (Table 3).

Spearman's Correlation results (Table 4) indicated that the NSD angle had a low positive correlation with centroid size of the palatal region 2 (r= 0.32; *P=0.010*) and with the shape of the palatal region 3 (r= 0.46; *P=0.0001*). NSD area presented little if any correlation with the centroid size in the nasal region 1 (r= 0.26; *P= 0.040*), and with Procrustes values (fluctuating asymmetry) in the nasal region 2 (r= 0.26; *P= 0.038*), but presented a low positive correlation with the shape of the palatal region 3 (r= 0.44; *P=0.0004*). NS Centroid size had a low positive correlation with centroid size of the nasal region 1 (r= 0.37; *P=0.002*). Finally, the variable NS shape had a low positive correlation with centroid size of the nasal region 2 (r= 0.31; *P=0.014*) and presented little correlation with the centroid size of the palatal region 1 (r= -0.26; *P=0.037*).

The results of multivariate regression are presented in Table 5. NSD angle was positively correlated with the asymmetry component on palatal regions 2 and 3 (*P=0.047* and *P=0.035*, respectively; Figure 7A and B), and there was no correlation with the other areas (nasal, lateral facial and palatal region 1). The other independent variables, NSD area and NS centroid size, did not correlate with the asymmetric component in any of the evaluated regions. And, finally, the NS shape independent variable was positively correlated with the asymmetry component of palatal region 1 (NPF) (*P=0.039*).

DISCUSSION

Small levels of facial asymmetry are common in most individuals, and since they are not perceptible by most people, they are considered to be within the normal range.[39-41] There are numerous factors that can cause facial asymmetry, such as genetic factors or malformations, environmental factors and functional deviations. [1,42] Nasal septum deviation has been widely studied in the

literature, but there is no consensus on its role in the growth of the face, and more specifically, of the nasomaxillary complex.

To further understanding about the influence of a deviated nasal septum in the asymmetries of the nasal, lateral and palatal regions of the face in individuals who are still growing and who have already gone through the growth spurt, the present study used a geometric morphometric approach in CBCT images like some previous studies[2,3], which contrasts with previous studies that used photographs analysis. [13,14]

When it comes to nasal septum morphological variation, Fisher's Discriminant Function with cross-validation indicated that the slice with the greatest NSD showed significant differences between the groups, which was expected, since this slice was used to separate the groups. Therefore, the FDF showed us that the division of the groups was done correctly. Through the CVA (Fig. 5) and thin-plate splines (Fig. 6), it was clear that, the groups with mild deviation have a narrower deviation region, while the groups with moderate to severe have a wider/expanded deviation region. So, we could observe that, despite the difference between the growth stages, the mild deviation groups have similar septal shapes, as well as the moderate to severe groups.

The results of our Procrustes ANOVA indicate that all three regions of the nasomaxillary complex (i.e., nasal, lateral and palatal regions) exhibited significant levels of fluctuating asymmetry. Fluctuating asymmetry distance values, represented by Procrustes and Mahalanobis distances, are measures of deviation from perfect symmetry, and a greater distance value corresponds to a greater magnitude of total asymmetry for the given region.[2] Although all of the groups presented fluctuating asymmetry levels, no statistical differences were observed between the groups with mild and moderate to severe septal deviation, before and after the growth spurt.

Corroborating this comparison test, no correlation was found between the NSD angle and the Procrustes and Mahalanobis distances (fluctuating asymmetry), as seen in the study by Hartman et, al.[2] Regarding the other correlations found in this study, although existing, they were low or null.

In the multivariate regression, we evaluated the relation of the asymmetric component of each region with independent variables: NSD angle, NSD area, NS centroid size and NS shape. Although there was a positive

correlation between NSD angle and nasal region 2, in the multivariate regression we were unable to observe this relationship (which contrasted with other studies), probably because, this correlation, despite existing, was little. Our sample consisted of individuals with mild, moderate and severe NSD, but, on average, our total sample has a small amount of deviation (mainly in degrees). In samples with less septal deviation on average, it has been suggested that the nasal airways and associated turbinates can act as an accommodation zone that dampens the development of nasal wall asymmetries.[2] In individuals with NSD, it is common for the inferior turbinate on the opposite side to the deviation to be hypertrophied, being a compensatory mechanism to protect the nasal cavity,[22,43,44] therefore, it is possible that the asymmetrical development of the turbinates can compensate for the asymmetry of the nasal cavity in individuals with less deviation.[2] This can also happen with asymmetries in the lateral facial region, as the maxillary sinuses can act as a cushion, compensating for the internal nasal shape,[45] thus avoiding greater asymmetries in this region. Our study, as well as Hartman et. al[2], did not find a relationship between NSD and asymmetries in the lateral region of the nasomaxillary complex. Regarding to NSD angle, the regression results showed that the asymmetry component was related to the increase in the deviation angle in palatal regions 2 and 3 (transverse palatine suture and middle region of the roof of the palate). This result shows us that even though our sample does not have a high septal deviation degree, on average, the regression was able to detect an increase in asymmetry in palatal regions, probably because of the close relationship in these regions. The independent variables NSD area and NS centroid size did not have a significant relationship with any of the regions in our multivariate regression. Regarding the independent variable of NS shape, the results showed that there was a positive correlation between the NS shape and the asymmetry component of the palatal region 1. The other regions did not present this relationship.

The ENA and OP did not show statistical differences between the study groups, indicating that these variables were not influenced by the degree of septum deviation. For the ENA, this result shows us that, even if the individual has a considerable degree of deviated septum, the tip of the nose is not necessarily affected by it and may not be deviated. And, for the OP, we observe

that, with the results we obtained, there was no relationship of this angle with any of the septum variables (NSD angle, NSD area, NS centroid size and NS shape).

The results of the present study indicate that there is an association between the nasal septum and asymmetries in the nasomaxillary complex, mainly by the results of our multivariate regression. Therefore, we believe that this influence exists, but that it is not possible to establish a determining causal factor, since several external factors can act. Despite our study covered individuals with different stages of growth, since it is not a longitudinal study, we were unable to assess whether the septum deviation increases with increasing age and cessation of growth.

CONCLUSIONS

The groups with mild nasal septum deviation did not show significant differences in the fluctuating asymmetry of the nasomaxillary complex in relation to the groups with moderate to severe nasal septum deviation, both before and after the growth spurts stages. However, a positive correlation was observed between the nasal septum deviation angle and asymmetry component in the middle and posterior palatal regions, and between nasal septum shape and anterior palatal region asymmetry component. No significant relationships were observed with the nasal and lateral regions of the nasomaxillary complex.

ACKNOWLEDGEMENTS

This study was supported in part by a scholarship from Coordenação de Aperfeiçoamento de Pessoal de Nível Superior – Brasil – (CAPES), Finance Code 001.

REFERENCES

1. Bishara S, Burkey P, Kharouf J. Dental and facial asymmetries: a review. The Angle Orthodontist: April 19941994. p. 89-98.
2. Hartman C, Holton N, Miller S, et al. Nasal Septal Deviation and Facial Skeletal Asymmetries. *Anat Rec (Hoboken)*. Mar 2016;299(3):295-306. doi:10.1002/ar.23303
3. Holton NE, Yokley TR, Figueroa A. Nasal septal and craniofacial form in European- and African-derived populations. *J Anat*. Sep 2012;221(3):263-74. doi:10.1111/j.1469-7580.2012.01533.x

4. Kang DH, Hun KD, Park KR, Chung KJ, Kim YH. The Relationship Between Facial Asymmetry and Nasal Septal Deviation. *J Craniofac Surg*. Jun 2015;26(4):1273-6. doi:10.1097/SCS.0000000000001549
5. Bayrak S, Ustaoğlu G, Demiralp K, Kurşun Çakmak E. Evaluation of the Characteristics and Association Between Schneiderian Membrane Thickness and Nasal Septum Deviation. *J Craniofac Surg*. May 2018;29(3):683-687. doi:10.1097/SCS.0000000000004254
6. Roblin DG, Eccles R. What, if any, is the value of septal surgery? *Clin Otolaryngol Allied Sci*. Apr 2002;27(2):77-80. doi:10.1046/j.1365-2273.2002.00531.x
7. SCOTT J. The cartilage of the nasal septum. Br Dent J1953. p. 37-43.
8. Latham R. Maxillary development and growth: the septopremaxillary ligament. J Anat1970. p. 471–478.
9. Proffit W, FIELDS H, SARVER D. *Ortodontia Contemporânea*. vol 5ª edição. 2012:754p.
10. Latham R, TG D, CT C. A question of the role of the vomer in the growth of the premaxilla
segment. Cleft Palate J1975. p. 351-355.
11. WEXLER MR, SARNAT BG. Rabbit snout growth. Effect of injury to septovomeral region. *Arch Otolaryngol*. Sep 1961;74:305-13.
12. Sarnat BG, Wexler MR. Growth of the face and jaws after resection of the septal cartilage in the rabbit. *Am J Anat*. May 1966;118(3):755-67. doi:10.1002/aja.1001180306
13. Hafezi F, Naghibzadeh B, Nouhi A, Yavari P. Asymmetric facial growth and deviated nose: a new concept. *Ann Plast Surg*. Jan 2010;64(1):47-51. doi:10.1097/SAP.0b013e31819ae02d
14. Kim YM, Rha KS, Weissman JD, Hwang PH, Most SP. Correlation of asymmetric facial growth with deviated nasal septum. *Laryngoscope*. Jun 2011;121(6):1144-8. doi:10.1002/lary.21785
15. D'Ascanio L, Lancione C, Pompa G, Rebuffini E, Mansi N, Manzini M. Craniofacial growth in children with nasal septum deviation: a cephalometric comparative study. *Int J Pediatr Otorhinolaryngol*. Oct 2010;74(10):1180-3. doi:10.1016/j.ijporl.2010.07.010
16. Lawrence R. Pediatric septoplasy: a review of the literature. *Int J Pediatr Otorhinolaryngol*. Aug 2012;76(8):1078-81. doi:10.1016/j.ijporl.2012.04.020
17. Abou Sleiman R, Saadé A. Effect of septal deviation on nasomaxillary shape: A geometric morphometric study. *J Anat*. 10 2021;239(4):788-800. doi:10.1111/joa.13479
18. von Elm E, Altman DG, Egger M, et al. [The Strengthening the Reporting of Observational Studies in Epidemiology (STROBE) statement: guidelines for reporting of observational studies]. *Internist (Berl)*. Jun 2008;49(6):688-93. doi:10.1007/s00108-008-2138-4
19. Baccetti T, Franchi L, Jr MJ. The Cervical Vertebral Maturation (CVM) method
for the assessment of optimal treatment timing in dentofacial orthopedics.: Semin Orthod; 2005. p. 119-129.
20. Gregurić T, Baudoin T, Tomljenović D, Grgić M, Štefanović M, Kalogjera L. Relationship between nasal septal deformity, symptoms and disease severity in chronic rhinosinusitis. *Eur Arch Otorhinolaryngol*. Mar 2016;273(3):671-7. doi:10.1007/s00405-015-3615-8

21. Lin L, Ahn HW, Kim SJ, Moon SC, Kim SH, Nelson G. Tooth-borne vs bone-borne rapid maxillary expanders in late adolescence. *Angle Orthod*. Mar 2015;85(2):253-62. doi:10.2319/030514-156.1
22. Akoğlu E, Karazincir S, Balci A, Okuyucu S, Sumbas H, Dağli AS. Evaluation of the turbinate hypertrophy by computed tomography in patients with deviated nasal septum. *Otolaryngol Head Neck Surg*. Mar 2007;136(3):380-4. doi:10.1016/j.otohns.2006.09.006
23. Codari M, Zago M, Guidugli GA, et al. The nasal septum deviation index (NSDI) based on CBCT data. *Dentomaxillofac Radiol*. 2016;45(2):20150327. doi:10.1259/dmfr.20150327
24. Orhan I, Aydın S, Ormeci T, Yılmaz F. A radiological analysis of inferior turbinate in patients with deviated nasal septum by using computed tomography. *Am J Rhinol Allergy*. 2014 Jan-Feb 2014;28(1):e68-72. doi:10.2500/ajra.2014.28.4007
25. Serifoglu I, Oz İ, Damar M, Buyukuysal MC, Tosun A, Tokgöz Ö. Relationship between the degree and direction of nasal septum deviation and nasal bone morphology. *Head Face Med*. Feb 2017;13(1):3. doi:10.1186/s13005-017-0136-2
26. Klingenberg CP. MorphoJ: an integrated software package for geometric morphometrics. *Mol Ecol Resour*. Mar 2011;11(2):353-7. doi:10.1111/j.1755-0998.2010.02924.x
27. Rohlf FJ. tpsDig, digitize landmarks and outlines, version 2.0. Department of Ecology and Evolution, State University of New York at Stony Brook2004.
28. Sygouros A, Motro M, Ugurlu F, Acar A. Surgically assisted rapid maxillary expansion: cone-beam computed tomography evaluation of different surgical techniques and their effects on the maxillary dentoskeletal complex. *Am J Orthod Dentofacial Orthop*. Dec 2014;146(6):748-57. doi:10.1016/j.ajodo.2014.08.013
29. Faul F, Erdfelder E, Lang AG, Buchner A. G*Power 3: a flexible statistical power analysis program for the social, behavioral, and biomedical sciences. *Behav Res Methods*. May 2007;39(2):175-91. doi:10.3758/bf03193146
30. Palmer AR. Detecting Publication Bias in Meta-analyses: A Case Study of Fluctuating Asymmetry and Sexual Selection. *Am Nat*. Aug 1999;154(2):220-233. doi:10.1086/303223
31. Gower J. Generalized procrustes analysis.: Psychometrika; 1975. p. 33-51.
32. Rohlf FJ, Loy A, Corti M. Morphometric analysis of Old World Talpidae (Mammalia, Insectivora) unsing partial-warp scores. Systematic Biology 1996. p. 344–362.
33. Klingenberg CP, Barluenga M, Meyer A. Shape analysis of symmetric structures: quantifying variation among individuals and asymmetry. *Evolution*. Oct 2002;56(10):1909-20.
34. Mardia KV, Bookstein FL, IJ M. Statistical assessment of bilateral symmetry of shapes. Biometrika 2000. p. 285-300.
35. Savriama Y, Klingenberg CP. Beyond bilateral symmetry: geometric morphometric methods for any type of symmetry. *BMC Evol Biol*. Sep 29 2011;11:280. doi:10.1186/1471-2148-11-280
36. Klingenberg CP. Analyzing Fluctuating Asymmetry with Geometric Morphometrics: Concepts, Methods, and Applications. *Symmetry*2015.

37. Klingenberg CP, McIntyre GS. GEOMETRIC MORPHOMETRICS OF DEVELOPMENTAL INSTABILITY: ANALYZING PATTERNS OF FLUCTUATING ASYMMETRY WITH PROCRUSTES METHODS. *Evolution*. Oct 1998;52(5):1363-1375. doi:10.1111/j.1558-5646.1998.tb02018.x
38. DE H, W W, SG J. Applied Statistics for the Behavioral Sciences. Boston: Houghton Mifflin.2003.
39. Baek C, Paeng JY, Lee JS, Hong J. Morphologic evaluation and classification of facial asymmetry using 3-dimensional computed tomography. *J Oral Maxillofac Surg*. May 2012;70(5):1161-9. doi:10.1016/j.joms.2011.02.135
40. Vig PS, Hewitt AB. Asymmetry of the human facial skeleton. *Angle Orthod*. Apr 1975;45(2):125-9. doi:10.1043/0003-3219(1975)0452.0.CO;2
41. Shah SM, Joshi MR. An assessment of asymmetry in the normal craniofacial complex. *Angle Orthod*. Apr 1978;48(2):141-8. doi:10.1043/0003-3219(1978)0482.0.CO;2
42. Burstone CJ. Diagnosis and treatment planning of patients with asymmetries. *Semin Orthod*. Sep 1998;4(3):153-64. doi:10.1016/s1073-8746(98)80017-0
43. Berger G, Hammel I, Berger R, Avraham S, Ophir D. Histopathology of the inferior turbinate with compensatory hypertrophy in patients with deviated nasal septum. *Laryngoscope*. Dec 2000;110(12):2100-5. doi:10.1097/00005537-200012000-00024
44. Egeli E, Demirci L, Yazýcý B, Harputluoglu U. Evaluation of the inferior turbinate in patients with deviated nasal septum by using computed tomography. *Laryngoscope*. Jan 2004;114(1):113-7. doi:10.1097/00005537-200401000-00020
45. Holton N, Yokley T, Butaric L. The morphological interaction between the nasal cavity and maxillary sinuses in living humans. *Anat Rec (Hoboken)*. Mar 2013;296(3):414-26. doi:10.1002/ar.22655

TABLES

Table 1 Nasomaxillary complex landmark's number and description according to the nasal, lateral, and palatal regions of the face.

Number	Landmark description	Region
1	Top of the crista galli	Nasal
2/3	Bilateral landmarks located at the most lateral aspect of the nasal cavity at the level of the crista galli	Nasal
4/5	Bilateral landmarks located at the most lateral aspect of the nasal floor at the level of the crista galli	Nasal
6	Upper aspect of the nasal septum at the level of the posterior nasal spine (PNS)	Nasal
7/8	Bilateral landmarks located at the most lateral aspect of the nasal cavity at the level of the posterior nasal spine	Nasal
9/10	Bilateral landmarks located at the most inferior point of the zygomaticomaxillary suture	Lateral
11/12	Bilateral landmarks located at the most inferior point of the orbit	Lateral
13/15	Bilateral landmarks located at the alveolar/palatal process junction at the level of the posterior margin of the nasopalatine foramen	Palatal
14	Intermaxillary suture at the level of the posterior margin of the nasopalatine foramen	Palatal
16/18	Bilateral landmarks located at the Alveolar/palatal process junction at transverse palatine suture	Palatal
17	Intermaxillary suture at transverse palatine suture	Palatal
19/21	Bilateral landmarks located at the alveolar/palatal process junction at half the distance between the posterior margin of the nasopalatine foramen and the transverse palatine suture	Palatal
20	Intermaxillary suture at half the distance between the posterior margin of the nasopalatine foramen and transverse palatine suture	Palatal
22/23	Bilateral landmarks located at the most lateral point of the buccal alveolar process in the slice of half the distance between the posterior margin of the nasopalatine foramen and the transverse palatine suture	Palatal

Note. Table adapted from HARTMAN et al., 2016(HARTMAN; HOLTON; MILLER; YOKLEY *et al.*, 2016)

Table 2 Descriptive statistics of NSD angle, NSD area, ENA and OP variables according to the study groups.

Groups	NSD angle (º)	NSD angle area (mm^2)	ENA (º)	OP (º)
MD - BG	7.99 (2.26)	55.2 (31.0)	2.0 (3.0)	1.2 (1.3)
MSD - BG	13.03 (3.04)	117.0 (34.8)	2.0 (3.0)	1.3 (1.3)
P-value	0.000**	0.000**	0.935	0.870
MD - AG	7.65 (2.62)	56.7 (23.1)	1.0 (3.0)	1.4 (0.5)
MSD - AG	14.04 (3.44)	95.5 (100.1)	2.0 (2.0)	1.8 (2.6)
P-value	0.000**	0.000**	0.305	0.281

Note. Descriptive statistics represented as median (interquartile range). **MD-BG,** mild deviation before growth. **MSD-BG,** mild to severe deviation before growth. **MD-AG,** mild deviation after growth. **MSD-AG,** mild to severe deviation after growth. **NSD,** nasal septum deviation; **ENA,** external nasal angle. **OP,** occlusal plane. Intergroup comparisons performed with the Mann-Whitney U test. *(P<0.05). ** (P<0.01).

Table 3 P values of Procrustes (PC) and Mahalanobis (MH) distances (fluctuating asymmetry) of nasomaxillary complex nasal, lateral and palatal regions according to the study groups.

Groups		Nasal region 1	Nasal region 2	Lateral region	Palatal region 1	Palatal region 2	Palatal region 3
MD-BG x MSD-BG	PC distances	0.486	0.436	0.539	0.187	0.174	0.935
	MH distances	0.935	0.595	0.775	0.653	0.202	0.870
MD-AG X MSD-AG	PC distances	0.744	0.367	0.775	0.389	0.217	0.624
	MH distances	0.653	0.624	0.713	0.967	0.389	0.595

Note. MD-BG, mild deviation before growth. **MSD-BG,** mild to severe deviation before growth. **MD-AG,** mild deviation after growth. **MSD-AG,** mild to severe deviation after growth. Intergroup comparisons performed with the Mann-Whitney U test.

Table 4 Spearman's correlation test (and P values) for nasal septum and nasomaxillary complex variables (n = 60).

	NSD angle	NSD angle area	NS Centroid size	NS Shape
	r (P value)	*r (P value)*	*r (P value)*	*r (P value)*
ENA	0.04 (0.706)	0.15 (0.228)	0.21 (0.100)	0.12 (0.333)
OP	0.08 (0.541)	0.02 (0.840)	-0.08 (0.498)	-0.07 (0.589)
PC_nasal region 1	0.10 (0.412)	0.09 (0.472)	-0.07 (0.587)	-0.02 (0.874)
MH_nasal region 1	0.03 (0.786)	0.08 (0.538)	0.06 (0.623)	0.03 (0.817)
Shape_nasal region 1	0.12 (0.354)	0.09 (0.491)	-0.04 (0.708)	-0.09 (0.470)
Centroid size_nasal region1	0.15 (0.244)	0.26 (0.040)*	0.37 (0.002)**	0.17 (0.173)
PC_nasal region 2	0.11 (0.381)	0.26 (0.038)*	0.04 (0.732)	0.06 (0.638)
MH_nasal region 2	-0.13 (0.319)	0.03 (0.784)	0.09 (0.483)	0.06 (0.612)
Shape_nasal region2	0.16 (0.205)	0.22 (0.078)	-0.10 (0.446)	0.10 (0.415)
Centroid size_nasal region2	0.03 (0.800)	0.13 (0.318)	0.13 (0.286)	0.31 (0.014)*
PC_lateral region	0.06 (0.631)	-0.01 (0.934)	0.17 (0.177)	-0.07 (0.581)
MH_ lateral region	-0.00 (0.984)	-0.05 (0.655)	0.15 (0.223)	-0.05 (0.663)
Shape_ lateral region	0.24 (0.061)	0.21 (0.091)	-0.06 (0.641)	-0.24 (0.055)
Centroid size_ lateral region	0.19 (0.143)	0.24 (0.061)	0.15 (0.244)	0.10 (0.405)
PC_palatal region1	0.17 (0.180)	0.17 (0.193)	-0.07 (0.545)	0.03 (0.775)
MH_palatal region1	0.18 (0.154)	0.18 (0.146)	-0.12 (0.359)	0.01 (0.918)
Shape_palatal region1	0.21 (0.103)	0.24 (0.060)	0.10 (0.444)	-0.02 (0.821)
Centroid size_palatal region1	0.19 (0.131)	0.12 (0.345)	-0.12 (0.352)	-0.26 (0.037)*
PC_palatal region2	0.17 (0.193)	0.09 (0.484)	0.01 (0.895)	0.01 (0.936)
MH_palatal region2	0.12 (0.328)	0.06 (0.630)	0.03 (0.817)	0.00 (0.976)
Shape_palatal region2	-0.03 (0.790)	-0.10 (0.428)	0.05 (0.649)	-0.24 (0.062)
Centroid size_palatal region2	0.32 (0.010)*	0.20 (0.122)	0.07 (0.574)	-0.08 (0.525)
Procrustes_palatal region 3	-0.03 (0.817)	-0.18 (0.153)	-0.01 (0.936)	-0.04 (0.761)
Mahalanobis_palatal region3	0.06 (0.645)	-0.02 (0.832)	0.03 (0.779)	0.00 (0.945)
Shape_palatal region3	0.46 (0.0001)**	0.44 (0.0004)**	-0.08 (0.534)	-0.14 (0.268)
Centroid size_palatal region3	0.22 (0.084)	0.15 (0.251)	-0.02 (0.874)	-0.08 (0.519)

Note. NSD, nasal septum deviation. **NS,** nasal septum. **ENA,** external nasal angle. **OP,** occlusal plane. **PC,** Procrustes. **MH,** Mahalanobis. *****(*P<0.05*). ** (*P<0.01*).

Table 5 Multivariate regression for nasal septum and nasomaxillary complex variables (n = 60).

	NSD angle	**NSD area**	**NS Centroid size**	**NS Shape**
	P-value	***P-value***	***P-value***	***P-value***
Nasal region 1	0.5313	0.9736	0.3225	0.6261
Nasal region 2	0.0972	0.7229	0.9001	0.0707
Lateral facial region	0.9443	0.9021	0.3411	0.6245
Palatal region 1	0.8371	0.9272	0.7596	0.0392*
Palatal region 2	0.0473*	0.3066	0.3314	0.9758
Palatal region 3	0.0346*	0.1066	0.6640	0.4561

Note. NSD, nasal septum deviation. **NS,** nasal septum. ***(*P<0.05*).

Supplementary Table 1 Procrustes ANOVA results for the nasal regions

Region		***Effect***	***SS***	***MS***	***df***	***F***	***P***
Nasal region (Crista galli)	MD-BG	Individual	0.26138190	0.0062233786	42	11.35	<.0001
		Side	0.00204000	0.0006800008	3	1.24	0.3073
		Ind*Side	0.02303331	0.0005484122	42	2.27	0.0006
		Error	0.02178623	0.0002420693	90		
	MSD-BG	Individual	0.33752062	0.0080362053	42	5.16	<.0001
		Side	0.00030087	0.0001002894	3	0.06	0.9784
		Ind*Side	0.06544212	0.0015581456	42	29.69	<.0001
		Error	0.00472290	0.0000524766	90		
	MD-AG	Individual	0.18632128	0.0044362209	42	9.42	<.0001
		Side	0.00036024	0.0001200810	3	0.25	0.8574
		Ind*Side	0.01978414	0.0004710510	42	4.52	<.0001
		Error	0.00938956	0.0001043284	90		
	MSD-AG	Individual	0.27869468	0.0066355877	42	14.86	<.0001
		Side	0.00102164	0.0003405474	3	0.76	0.5215
		Ind*Side	0.01875700	0.0004465951	42	7.79	<.0001
		Error	0.00515720	0.0000573022	90		
Nasal region (Posterior Nasal Spine)	MD-BG	Individual	0.84250872	0.0601791942	14	37.48	<.0001
		Side	0.00064350	0.0006434967	1	0.40	0.5369
		Ind*Side	0.02247705	0.0016055039	14	5.36	<.0001
		Error	0.00898829	0.0002996096	30		
	MSD-BG	Individual	0.52345645	0.0373897462	14	11.16	<.0001
		Side	0.03551168	0.0355116814	1	10.60	0.0057
		Ind*Side	0.04689461	0.0033496152	14	5.22	<.0001
		Error	0.01924588	0.0006415292	30		
	MD-AG	Individual	0.43592890	0.0311377783	14	37.62	<.0001
		Side	0.00169503	0.0016950298	1	2.05	0.1744
		Ind*Side	0.01158858	0.0008277555	14	6.65	<.0001
		Error	0.00373214	0.0001244048	30		
	MSD-AG	Individual	0.86926433	0.0620903095	14	21.03	<.0001
		Side	0.00682434	0.0068243409	1	2.31	0.1507
		Ind*Side	0.04132946	0.0029521044	14	24.92	<.0001
		Error	0.00355349	0.0001184495	30		

Supplementary Table 2 Procrustes ANOVA for the lateral facial region

Region		*Effect*	*SS*	*MS*	*df*	*F*	*P*
Lateral facial region	MD-BG	Individual	0.02281257	0.0008147345	28	3.82	0.0003
		Side	0.00018837	0.0000941869	2	0.44	0.6475
		Ind*Side	0.00597299	0.0002133211	28	6.95	<.0001
		Error	0.00184039	0.0000306732	60		
	MSD-BG	Individual	0.05370147	0.0019179096	28	6.21	<.0001
		Side	0.00122076	0.0006103813	2	1.98	0.1573
		Ind*Side	0.00864256	0.0003086630	28	16.34	<.0001
		Error	0.00113368	0.0000188946	60		
	MD-AG	Individual	0.04885393	0.0017447834	28	6.23	<.0001
		Side	0.00076047	0.0003802325	2	1.36	0.2738
		Ind*Side	0.00784443	0.0002801581	28	18.17	<.0001
		Error	0.00092514	0.0000154190	60		
	MSD-AG	Individual	0.05770155	0.0020607698	28	8.26	<.0001
		Side	0.00001355	0.0000067759	2	0.03	0.9732
		Ind*Side	0.00698887	0.0002496024	28	11.66	<.0001
		Error	0.00128407	0.0000214011	60		

Supplementary Table 3 Procrustes ANOVA for the palatal regions

Region		*Effect*	*SS*	*MS*	*df*	*F*	*P*
Palatal region (nasopalatine foramen)	MD-BG	Individual	0.23752344	0.0169659598	14	6.48	0.0006
		Side	0.00008213	0.0000821308	1	0.03	0.8619
		Ind*Side	0.03663565	0.0026168322	14	3.43	0.0023
		Error	0.02290949	0.0007636496	30		
	MSD-BG	Individual	0.18362342	0.0131159586	14	3.01	0.0240
		Side	0.01780111	0.0178011071	1	4.09	0.0628
		Ind*Side	0.06100068	0.0043571916	14	4.86	0.0001
		Error	0.02688631	0.0008962105	30		
	MD-AG	Individual	0.77984704	0.0557033597	14	6.85	0.0005
		Side	0.06127597	0.0612759686	1	7.54	0.0158
		Ind*Side	0.11376668	0.0081261916	14	10.09	<.0001
		Error	0.02416745	0.0008055817	30		
	MSD-AG	Individual	0.27834959	0.0198821136	14	4.54	0.0039
		Side	0.02558959	0.0255895865	1	5.84	0.0299
		Ind*Side	0.06130409	0.0043788632	14	6.85	<.0001
		Error	0.01916597	0.0006388657	30		
Palatal region (transverse palatal suture)	MD-BG	Individual	0.01239905	0.0008856465	14	0.34	0.9751
		Side	0.00182763	0.0018276272	1	0.69	0.4195
		Ind*Side	0.03697748	0.0026412484	14	13.12	<.0001
		Error	0.00603914	0.0002013046	30		
	MSD-BG	Individual	0.07390053	0.0052786090	14	1.73	0.1577
		Side	0.00591196	0.0059119563	1	1.94	0.1854
		Ind*Side	0.04265536	0.0030468113	14	8.53	<.0001
		Error	0.01071909	0.0003573031	30		
	MD-AG	Individual	0.04852798	0.0034662845	14	1.38	0.2776
		Side	0.00120981	0.0012098105	1	0.48	0.4991
		Ind*Side	0.03518003	0.0025128591	14	9.96	<.0001
		Error	0.00756985	0.0002523283	30		
	MSD-AG	Individual	0.04072837	0.0029091694	14	0.87	0.5996
		Side	0.06102127	0.0610212696	1	18.28	0.0008
		Ind*Side	0.04672325	0.0033373748	14	15.81	<.0001
		Error	0.00633174	0.0002110580	30		
Palatal region at 50% of the distance	MD-BG	Individual	0.13831244	0.0032931533	42	7.31	<.0001
		Side	0.00375850	0.0012528321	3	2.78	0.0526
		Ind*Side	0.01891070	0.0004502548	42	7.79	<.0001
		Error	0.00520225	0.0000578028	90		
	MSD-BG	Individual	0.21326153	0.0050776555	42	11.34	<.0001

between nasopalatine foramen and transverse palatal suture		Side	0.00929912	0.0030997076	3	6.93	0.0007
		Ind*Side	0.01879942	0.0004476053	42	2.83	<.0001
		Error	0.01422445	0.0001580494	90		
	MD-AG	Individual	0.14292500	0.0034029762	42	6.08	<.0001
		Side	0.00553033	0.0018434438	3	3.29	0.0296
		Ind*Side	0.02350254	0.0005595844	42	13.92	<.0001
		Error	0.00361741	0.0000401934	90		
	MSD-AG	Individual	0.26871215	0.0063979083	42	13.96	<.0001
		Side	0.01327017	0.0044233902	3	9.65	<.0001
		Ind*Side	0.01925292	0.0004584029	42	5.45	<.0001
		Error	0.00756704	0.0000840783	90		

FIGURES

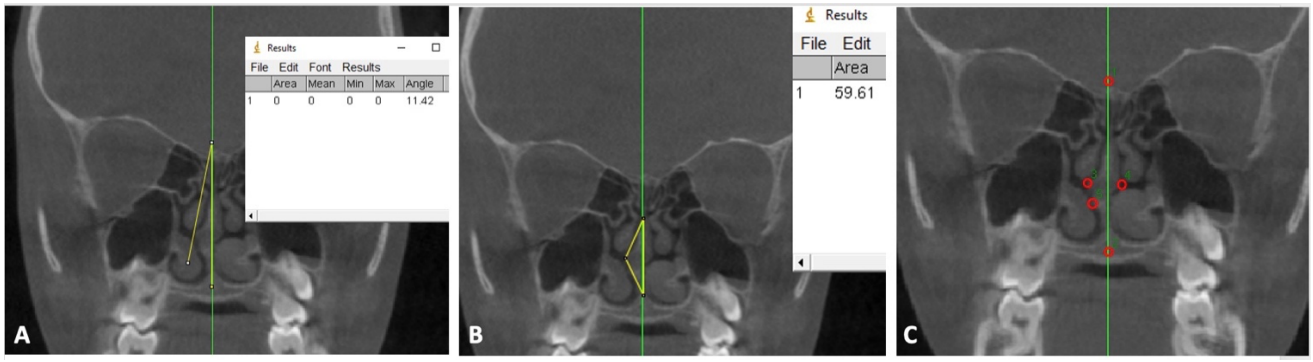

Figure 1 A, NSD angle measurement and **B**, deviation area measurement (mm²), both in ImageJ® software. C, representation of the landmarks in the TpsDIG2 software, used for morphometric analysis. In the same coronal section, five landmarks were used, namely: **1,** top of the crista galli. **2,** lowest point of the nasal septum. **3,** point of greatest deviation on the right side. **4,** point of greatest deviation on left side. **5,** second point of greatest deviation.

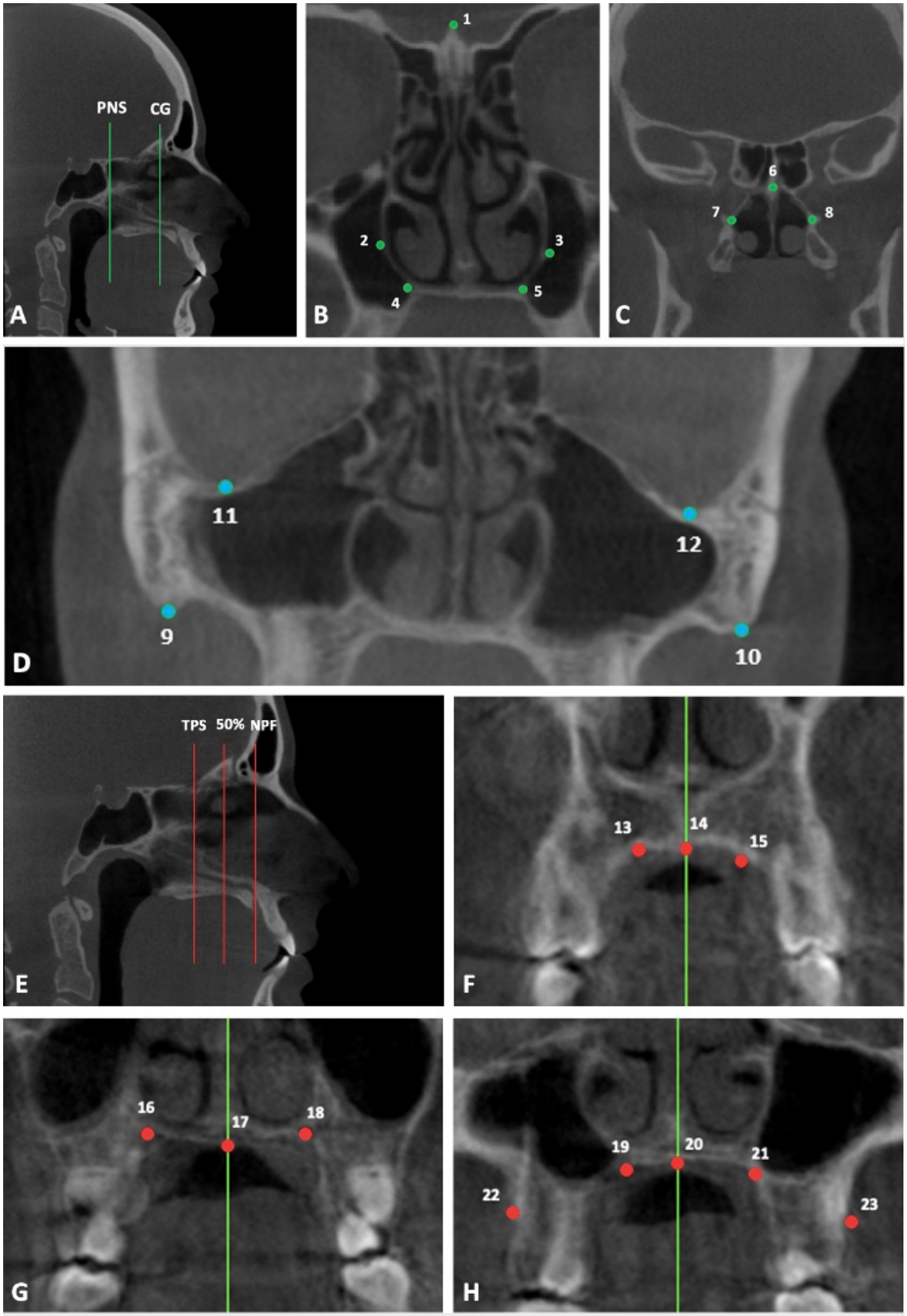

Figure 2 Two-dimensional representations of the landmarks in all regions. **A,** in nasal region, landmarks were collected from two internal planes: the first plane was located on top of the crista galli and the second plane was at posterior nasal spine. **B,** the first plane, indicating the landmarks: 1, top of the crista galli; 2/3, bilateral landmarks located at the most lateral aspect of the nasal cavity; 4/5, bilateral landmarks located at the most lateral aspect of the nasal floor. **C,** the second plane, indicating the landmarks: 6, upper aspect of the nasal septum; 7/8, bilateral

landmarks located at the most lateral aspect of the nasal cavity. **D**, in lateral regions, the landmarks used was: 9/10, zygomaticomaxillary sutures; 11/12, orbitals. **E,** in palatal regions, landmarks were collected from three internal planes: NF = nasopalatine foramen, TPS = transverse palatal suture and 50% = halfway distance between NF and TPS. **F,** landmarks in the first plane: 13/15, bilateral landmarks located at the alveolar/palatal process junction at the level of the posterior margin of the NF; 14, intermaxillary suture at NF. **G,** landmarks in the second plane: 16/18, bilateral landmarks located at the alveolar/palatal process junction at TPS; 17, intermaxillary suture at TPS. **H,** landmarks in the third plane: 19/21, bilateral landmarks located at the alveolar/palatal process junction at 50%; 20, intermaxillary suture at 50%; 22/23, bilateral landmarks located at the most lateral point of the buccal alveolar process at 50%.

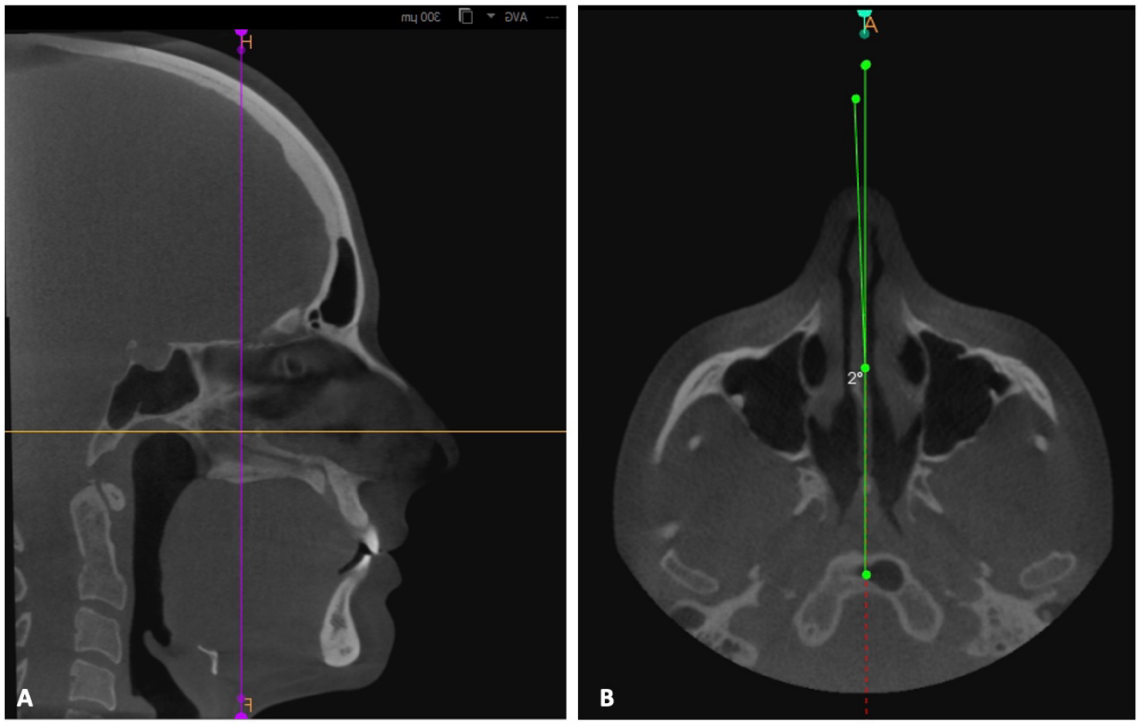

Figure 3 A, To select the external nasal angle, the coronal slice must be in the transverse palatal suture (purple line) and the axial slice perpendicular to it, at the junction of the perpendicular blade of the ethmoid with the vomer; **B,** in the axial slice, the angle is made between the middle of the nose and the line representing the midpalatal suture (the lower point should be halfway along the length of the nasal septum).

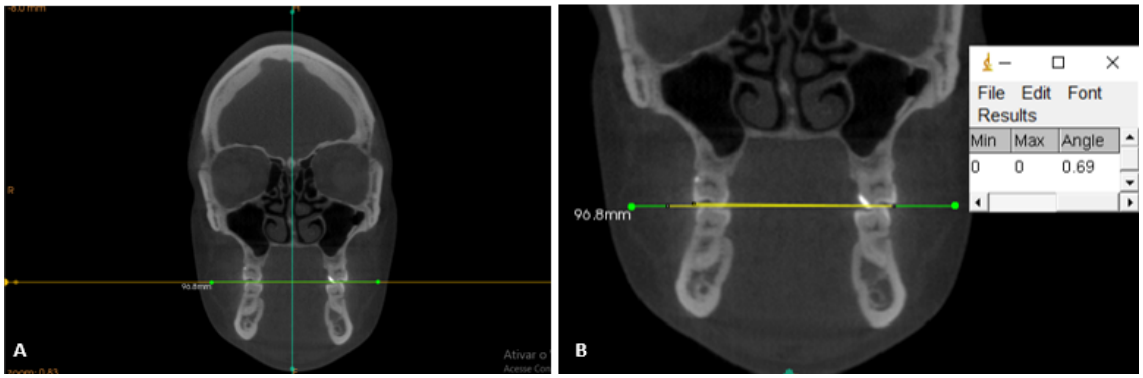

Figure 4 A, Representation of the coronal section used in which it is possible to visualize the tips of the buccal cusps of the maxillary first molars and their relationship with the axial plane of the image (*yellow*); **B**, View of the angle obtained in ImageJ® software.

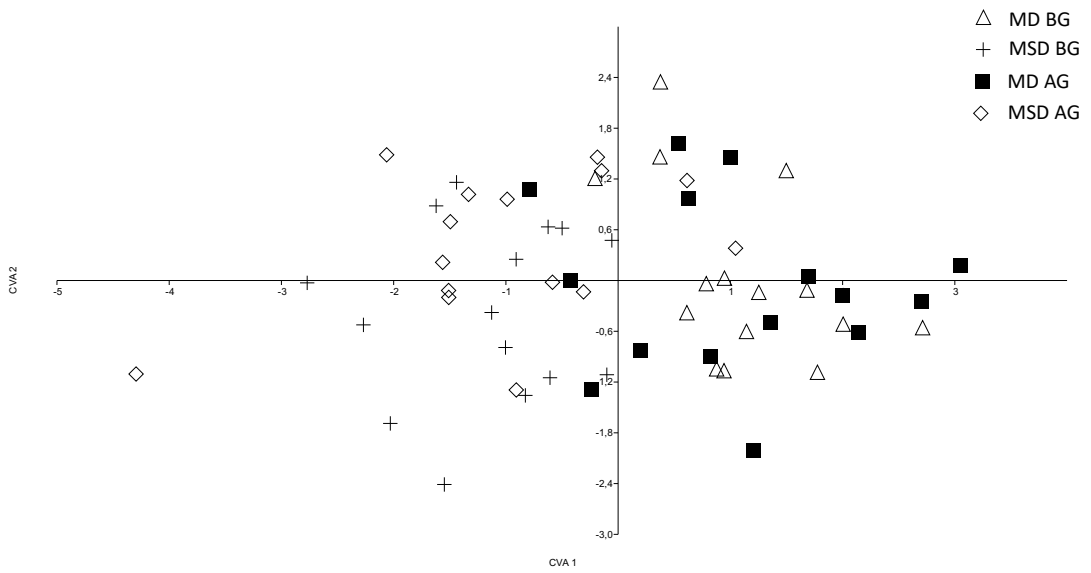

Figure 5 Analysis of Canonical Variables of nasal septum morphology. It is possible to observe that groups MD BG (mild deviation before growth) and MD AG (mild deviation after growth) have a similar format (right side of the graph), and groups MSD BG (moderate/severe deviation after growth) and MSD AG (moderate/severe deviation after growth) also present a similar format (right side of the graph).

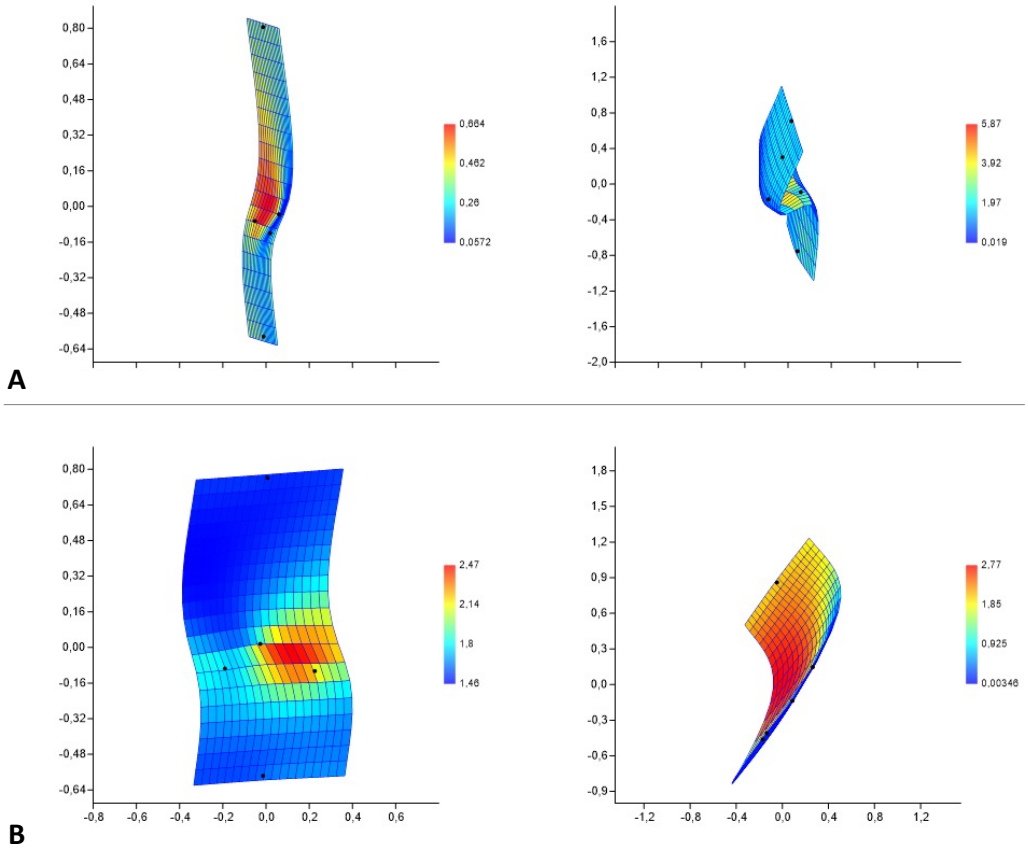

Figure 6 Thin-plate splines showing the shape of the nasal septum at slice of the NSD angle. The colors indicate that the closer to blue, the greater the contraction region, while the closer to red, the greater the expansion region. **A,** in control groups (mild deviation), we can observe that the septum has a narrower shape in general, with an expansion region in the central part of the septum. **B,** in experimental groups (moderate/severe deviation), we observed a wider shape, and an expansion region in the central part of the septum.

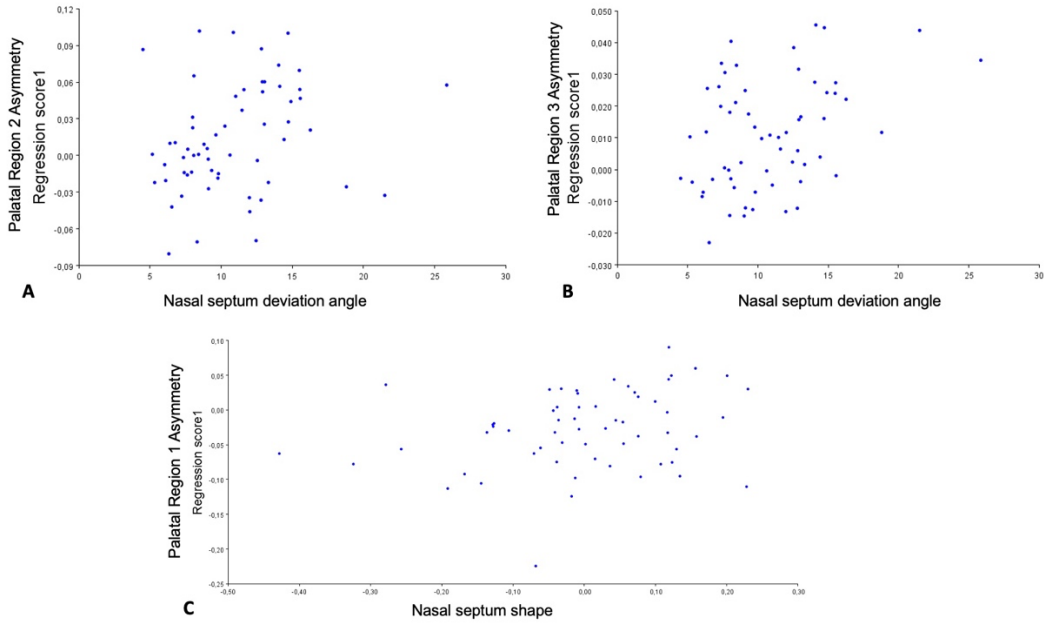

Figure 7 Scatter plot of our multivariate regression **A,** correlating the asymmetry component of variation of palatal region 2 (transverse palatine suture) against nasal septal deviation angle. **B,** asymmetry component of variation of palatal region 3 (halfway) against nasal septal deviation angle. C, asymmetry component of variation of palatal region 1 (nasopalatine foramen) against nasal septum shape.

5 CONCLUSÃO

A partir dos resultados do presente estudo observacional retrospectivo, pode-se concluir que:

5.1 ambos os métodos bidimensionais e tridimensionais de marcação de pontos craniofaciais no complexo nasomaxilar e facial lateral apresentaram alta confiabilidade, entretanto, o método bidimensional apresentou maiores valores de precisão na maioria dos pontos avaliados. Além disso, todos os pontos avaliados neste estudo são considerados clinicamente aceitáveis;

5.2 todos os grupos de indivíduos avaliados apresentaram níveis significativos de assimetria flutuante. Entretanto, não foram observadas diferenças significativas na assimetria flutuante do complexo nasomaxilar dos grupos com DSN leve em relação aos grupos com DSN moderado a severo, em ambos os estágios de maturação esquelética. Foi observada correlação positiva entre o ângulo DSN e o componente de assimetria nas regiões palatinas média e posterior e entre a forma do septo nasal e a região palatina anterior. Não foram observadas correlações significativas com as regiões nasal e lateral do complexo nasomaxilar.

6 RECOMENDAÇÕES

Para estudos futuros, sugere-se a condução de estudos longitudinais que avaliem os mesmos indivíduos ao longo do tempo, com desvio de septo severo e que não fizeram septoplastia comparando-os a indivíduos sem desvio de septo ou que foram submetidos à septoplastia. Assim, será possível avaliar de forma mais assertiva se o desvio do septo nasal pode ser considerado, de fato, um fator predisponente para assimetrias no complexo nasomaxilar.

7 REFERÊNCIAS

ABOU SLEIMAN, R.; SAADÉ, A. Effect of septal deviation on nasomaxillary shape: A geometric morphometric study. **J Anat**, 239, n. 4, p. 788-800, 10 2021.

AKOĞLU, E.; KARAZINCIR, S.; BALCI, A.; OKUYUCU, S. *et al.* Evaluation of the turbinate hypertrophy by computed tomography in patients with deviated nasal septum. **Otolaryngol Head Neck Surg**, 136, n. 3, p. 380-384, Mar 2007.

BACCETTI, T.; FRANCHI, L.; JR, M. J. The Cervical Vertebral Maturation (CVM) method
for the assessment of optimal treatment timing in dentofacial orthopedics.: Semin Orthod. 11**:** 119-129 p. 2005.

BAEK, C.; PAENG, J. Y.; LEE, J. S.; HONG, J. Morphologic evaluation and classification of facial asymmetry using 3-dimensional computed tomography. **J Oral Maxillofac Surg**, 70, n. 5, p. 1161-1169, May 2012.

BAYRAK, S.; USTAOĞLU, G.; DEMIRALP, K.; KURŞUN ÇAKMAK, E. Evaluation of the Characteristics and Association Between Schneiderian Membrane Thickness and Nasal Septum Deviation. **J Craniofac Surg**, 29, n. 3, p. 683-687, May 2018.

BERGER, G.; HAMMEL, I.; BERGER, R.; AVRAHAM, S. *et al.* Histopathology of the inferior turbinate with compensatory hypertrophy in patients with deviated nasal septum. **Laryngoscope**, 110, n. 12, p. 2100-2105, Dec 2000.

BISHARA, S.; BURKEY, P.; KHAROUF, J. Dental and facial asymmetries: a review. The Angle Orthodontist: April 1994. 64**:** 89-98 p. 1994.

BLAND, J. M.; ALTMAN, D. G. Statistical methods for assessing agreement between two methods of clinical measurement. **Lancet**, 1, n. 8476, p. 307-310, Feb 08 1986.

BURSTONE, C. J. Diagnosis and treatment planning of patients with asymmetries. **Semin Orthod**, 4, n. 3, p. 153-164, Sep 1998.

CODARI, M.; ZAGO, M.; GUIDUGLI, G. A.; PUCCIARELLI, V. *et al.* The nasal septum deviation index (NSDI) based on CBCT data. **Dentomaxillofac Radiol**, 45, n. 2, p. 20150327, 2016.

D'ASCANIO, L.; LANCIONE, C.; POMPA, G.; REBUFFINI, E. *et al.* Craniofacial growth in children with nasal septum deviation: a cephalometric comparative study. **Int J Pediatr Otorhinolaryngol**, 74, n. 10, p. 1180-1183, Oct 2010.

DE, H.; W, W.; SG, J. Applied Statistics for the Behavioral Sciences. Boston: Houghton Mifflin. 5th ed. Boston: 2003.

DE MORAES, M. E.; HOLLENDER, L. G.; CHEN, C. S.; MORAES, L. C. *et al.* Evaluating craniofacial asymmetry with digital cephalometric images and cone-beam computed tomography. **Am J Orthod Dentofacial Orthop**, 139, n. 6, p. e523-531, Jun 2011.

DE OLIVEIRA, A. E.; CEVIDANES, L. H.; PHILLIPS, C.; MOTTA, A. *et al.* Observer reliability of three-dimensional cephalometric landmark identification on cone-beam computerized tomography. **Oral Surg Oral Med Oral Pathol Oral Radiol Endod**, 107, n. 2, p. 256-265, Feb 2009.

EGELI, E.; DEMIRCI, L.; YAZÝCÝ, B.; HARPUTLUOGLU, U. Evaluation of the inferior turbinate in patients with deviated nasal septum by using computed tomography. **Laryngoscope**, 114, n. 1, p. 113-117, Jan 2004.

FAUL, F.; ERDFELDER, E.; LANG, A. G.; BUCHNER, A. G*Power 3: a flexible statistical power analysis program for the social, behavioral, and biomedical sciences. **Behav Res Methods**, 39, n. 2, p. 175-191, May 2007.

FEHRENBACH; MJ; HERRING; SW. **Anatomia Ilustrada da Cabeça e Pescoço**. São Paulo: Editora Manolev, 2005.

GOWER, J. Generalized procrustes analysis.: Psychometrika. 40(1)**:** 33-51 p. 1975.

GREGURIĆ, T.; BAUDOIN, T.; TOMLJENOVIĆ, D.; GRGIĆ, M. *et al.* Relationship between nasal septal deformity, symptoms and disease severity in chronic rhinosinusitis. **Eur Arch Otorhinolaryngol**, 273, n. 3, p. 671-677, Mar 2016.

HAFEZI, F.; NAGHIBZADEH, B.; NOUHI, A.; YAVARI, P. Asymmetric facial growth and deviated nose: a new concept. **Ann Plast Surg**, 64, n. 1, p. 47-51, Jan 2010.

HARTMAN, C.; HOLTON, N.; MILLER, S.; YOKLEY, T. *et al.* Nasal Septal Deviation and Facial Skeletal Asymmetries. **Anat Rec (Hoboken)**, 299, n. 3, p. 295-306, Mar 2016.

HASSAN, B.; NIJKAMP, P.; VERHEIJ, H.; TAIRIE, J. *et al.* Precision of identifying cephalometric landmarks with cone beam computed tomography in vivo. **Eur J Orthod**, 35, n. 1, p. 38-44, Feb 2013.

HOLTON, N.; YOKLEY, T.; BUTARIC, L. The morphological interaction between the nasal cavity and maxillary sinuses in living humans. **Anat Rec (Hoboken)**, 296, n. 3, p. 414-426, Mar 2013.

HOLTON, N. E.; YOKLEY, T. R.; FIGUEROA, A. Nasal septal and craniofacial form in European- and African-derived populations. **J Anat**, 221, n. 3, p. 263-274, Sep 2012.

KANG, D. H.; HUN, K. D.; PARK, K. R.; CHUNG, K. J. *et al.* The Relationship Between Facial Asymmetry and Nasal Septal Deviation. **J Craniofac Surg**, 26, n. 4, p. 1273-1276, Jun 2015.

KIM, Y. M.; RHA, K. S.; WEISSMAN, J. D.; HWANG, P. H. *et al.* Correlation of asymmetric facial growth with deviated nasal septum. **Laryngoscope**, 121, n. 6, p. 1144-1148, Jun 2011.

KLINGENBERG, C. P. MorphoJ: an integrated software package for geometric morphometrics. **Mol Ecol Resour**, 11, n. 2, p. 353-357, Mar 2011.

KLINGENBERG, C. P. Analyzing Fluctuating Asymmetry with Geometric Morphometrics: Concepts, Methods, and Applications. *Symmetry* 2015.

KLINGENBERG, C. P.; BARLUENGA, M.; MEYER, A. Shape analysis of symmetric structures: quantifying variation among individuals and asymmetry. **Evolution**, 56, n. 10, p. 1909-1920, Oct 2002.

KLINGENBERG, C. P.; MCINTYRE, G. S. GEOMETRIC MORPHOMETRICS OF DEVELOPMENTAL INSTABILITY: ANALYZING PATTERNS OF FLUCTUATING ASYMMETRY WITH PROCRUSTES METHODS. **Evolution**, 52, n. 5, p. 1363-1375, Oct 1998.

LAGRAVÈRE, M. O.; LOW, C.; FLORES-MIR, C.; CHUNG, R. *et al.* Intraexaminer and interexaminer reliabilities of landmark identification on digitized lateral cephalograms and formatted 3-dimensional cone-beam computerized tomography images. **Am J Orthod Dentofacial Orthop**, 137, n. 5, p. 598-604, May 2010.

LATHAM, R. Maxillary development and growth: the septopremaxillary ligament. J Anat. 107**:** 471–478 p. 1970.

LATHAM, R.; TG, D.; CT, C. A question of the role of the vomer in the growth of the premaxilla
segment. Cleft Palate J. 12**:** 351-355 p. 1975.

LAWRENCE, R. Pediatric septoplasy: a review of the literature. **Int J Pediatr Otorhinolaryngol**, 76, n. 8, p. 1078-1081, Aug 2012.

LIN, H. H.; CHUANG, Y. F.; WENG, J. L.; LO, L. J. Comparative validity and reproducibility study of various landmark-oriented reference planes in 3-

dimensional computed tomographic analysis for patients receiving orthognathic surgery. **PLoS One**, 10, n. 2, p. e0117604, 2015.

LIN, J. K.; WHEATLEY, F. C.; HANDWERKER, J.; HARRIS, N. J. *et al.* Analyzing nasal septal deviations to develop a new classification system: a computed tomography study using MATLAB and OsiriX. **JAMA Facial Plast Surg**, 16, n. 3, p. 183-187, 2014 May-Jun 2014.

LIN, L.; AHN, H. W.; KIM, S. J.; MOON, S. C. *et al.* Tooth-borne vs bone-borne rapid maxillary expanders in late adolescence. **Angle Orthod**, 85, n. 2, p. 253-262, Mar 2015.

LOU, L.; LAGRAVERE, M. O.; COMPTON, S.; MAJOR, P. W. *et al.* Accuracy of measurements and reliability of landmark identification with computed tomography (CT) techniques in the maxillofacial area: a systematic review. **Oral Surg Oral Med Oral Pathol Oral Radiol Endod**, 104, n. 3, p. 402-411, Sep 2007.

LUDLOW, J. B.; GUBLER, M.; CEVIDANES, L.; MOL, A. Precision of cephalometric landmark identification: cone-beam computed tomography vs conventional cephalometric views. **Am J Orthod Dentofacial Orthop**, 136, n. 3, p. 312.e311-310; discussion 312-313, Sep 2009.

MARDIA KV; BOOKSTEIN FL; IJ, M. Statistical assessment of bilateral symmetry of shapes. Biometrika 285-300 p. 2000.

MATTOS, C. T.; CRUZ, C. V.; DA MATTA, T. C.; PEREIRA, L. E. A. *et al.* Reliability of upper airway linear, area, and volumetric measurements in cone-beam computed tomography. **Am J Orthod Dentofacial Orthop**, 145, n. 2, p. 188-197, Feb 2014.

MORO, A.; CORRERA, P.; BONIELLO, R.; GASPARINI, G. *et al.* Three-dimensional analysis in facial asymmetry: comparison with model analysis and conventional two-dimensional analysis. **J Craniofac Surg**, 20, n. 2, p. 417-422, Mar 2009.

MOSS, M. L.; BROMBERG, B. E.; SONG, I. C.; EISENMAN, G. The passive role of nasal septal cartilage in mid-facial growth. **Plast Reconstr Surg**, 41, n. 6, p. 536-542, Jun 1968.

NAJI, P.; ALSUFYANI, N. A.; LAGRAVÈRE, M. O. Reliability of anatomic structures as landmarks in three-dimensional cephalometric analysis using CBCT. **Angle Orthod**, 84, n. 5, p. 762-772, Sep 2014.

NEIVA, M. B.; SOARES, Á.; LISBOA, C. E. O.; VILELLA, O. E. V. *et al.* Evaluation of cephalometric landmark identification on CBCT multiplanar and 3D reconstructions. **Angle Orthod**, 85, n. 1, p. 11-17, Jan 2015.

NUR, R. B.; ÇAKAN, D. G.; ARUN, T. Evaluation of facial hard and soft tissue asymmetry using cone-beam computed tomography. **Am J Orthod Dentofacial Orthop**, 149, n. 2, p. 225-237, Feb 2016.

ORHAN, I.; AYDIN, S.; ORMECI, T.; YILMAZ, F. A radiological analysis of inferior turbinate in patients with deviated nasal septum by using computed tomography. **Am J Rhinol Allergy**, 28, n. 1, p. e68-72, 2014 Jan-Feb 2014.

PALMER, A. R. Detecting Publication Bias in Meta-analyses: A Case Study of Fluctuating Asymmetry and Sexual Selection. **Am Nat**, 154, n. 2, p. 220-233, Aug 1999.

PORTO, O. C.; DE FREITAS, J. C.; DE ALENCAR, A. H.; ESTRELA, C. The use of three-dimensional cephalometric references in dentoskeletal symmetry diagnosis. **Dental Press J Orthod**, 19, n. 6, p. 78-85, 2014 Nov-Dec 2014.

PROFFIT, W.; FIELDS, H.; SARVER, D. **Ortodontia Contemporânea**. Mosby Elsevier, Rio de Janeiro: 2012. 754p p.

ROBLIN, D. G.; ECCLES, R. What, if any, is the value of septal surgery? **Clin Otolaryngol Allied Sci**, 27, n. 2, p. 77-80, Apr 2002.

ROHLF, F. J. tpsDig, digitize landmarks and outlines, version 2.0. Department of Ecology and Evolution, State University of New York at Stony Brook 2004.

ROHLF, F. J.; LOY, A.; CORTI, M. Morphometric analysis of Old World Talpidae (Mammalia, Insectivora) unsing partial-warp scores. Systematic Biology 344–362. p. 1996.

SARNAT, B. G.; WEXLER, M. R. Growth of the face and jaws after resection of the septal cartilage in the rabbit. **Am J Anat**, 118, n. 3, p. 755-767, May 1966.

SAVRIAMA, Y.; KLINGENBERG, C. P. Beyond bilateral symmetry: geometric morphometric methods for any type of symmetry. **BMC Evol Biol**, 11, p. 280, Sep 29 2011.

SCHLICHER, W.; NIELSEN, I.; HUANG, J. C.; MAKI, K. *et al.* Consistency and precision of landmark identification in three-dimensional cone beam computed tomography scans. **Eur J Orthod**, 34, n. 3, p. 263-275, Jun 2012.

SCOTT, J. The cartilage of the nasal septum. Br Dent J. 95**:** 37-43 p. 1953.

SERIFOGLU, I.; OZ, İ.; DAMAR, M.; BUYUKUYSAL, M. C. *et al.* Relationship between the degree and direction of nasal septum deviation and nasal bone morphology. **Head Face Med**, 13, n. 1, p. 3, Feb 2017.

SEVERT, T. R.; PROFFIT, W. R. The prevalence of facial asymmetry in the dentofacial deformities population at the University of North Carolina. **Int J Adult Orthodon Orthognath Surg**, 12, n. 3, p. 171-176, 1997.

SHAH, S. M.; JOSHI, M. R. An assessment of asymmetry in the normal craniofacial complex. **Angle Orthod**, 48, n. 2, p. 141-148, Apr 1978.

SYGOUROS, A.; MOTRO, M.; UGURLU, F.; ACAR, A. Surgically assisted rapid maxillary expansion: cone-beam computed tomography evaluation of different surgical techniques and their effects on the maxillary dentoskeletal complex. **Am J Orthod Dentofacial Orthop**, 146, n. 6, p. 748-757, Dec 2014.

VIG, P. S.; HEWITT, A. B. Asymmetry of the human facial skeleton. **Angle Orthod**, 45, n. 2, p. 125-129, Apr 1975.

VON ELM, E.; ALTMAN, D. G.; EGGER, M.; POCOCK, S. J. *et al.* [The Strengthening the Reporting of Observational Studies in Epidemiology (STROBE) statement: guidelines for reporting of observational studies]. **Internist (Berl)**, 49, n. 6, p. 688-693, Jun 2008.

WEXLER, M. R.; SARNAT, B. G. Rabbit snout growth. Effect of injury to septovomeral region. **Arch Otolaryngol**, 74, p. 305-313, Sep 1961.

YÁÑEZ-VICO, R. M.; IGLESIAS-LINARES, A.; TORRES-LAGARES, D.; GUTIÉRREZ-PÉREZ, J. L. *et al.* Three-dimensional evaluation of craniofacial asymmetry: an analysis using computed tomography. **Clin Oral Investig**, 15, n. 5, p. 729-736, Oct 2011.

8 ANEXOS

8.1 PARECER DO COMITÊ DE ÉTICA EM PESQUISA

UFRJ - HOSPITAL UNIVERSITÁRIO CLEMENTINO FRAGA FILHO DA UNIVERSIDADE FEDERAL DO RIO DE JANEIRO / HUCFF-UFRJ

PARECER CONSUBSTANCIADO DO CEP

DADOS DO PROJETO DE PESQUISA

Título da Pesquisa: Estudo da relação do septo nasal com as características do complexo nasomaxilar.

Pesquisador: Amanda Cunha Regal de Castro
Área Temática:
Versão: 1
CAAE: 27431319.4.0000.5257
Instituição Proponente: UNIVERSIDADE FEDERAL DO RIO DE JANEIRO
Patrocinador Principal: Universidade Federal Do Rio de Janeiro
Financiamento Próprio

DADOS DO PARECER

Número do Parecer: 3.888.756

Apresentação do Projeto:
Protocolo 455-19 recebido em 26.12.2019

Situação do Parecer:
Aprovado

Necessita Apreciação da CONEP:
Não

RIO DE JANEIRO, 28 de Fevereiro de 2020

Assinado por:
Carlos Alberto Guimarães
(Coordenador(a))

8.2 UTILIZAÇÃO DO BANCO DE DADOS DA DISCIPLINA DE ORTODONTIA

UNIVERSIDADE FEDERAL DO RIO DE JANEIRO
FACULDADE DE ODONTOLOGIA
DEPARTAMENTO DE ODONTOPEDIATRIA E ORTODONTIA

UTILIZAÇÃO DO BANCO DE DADOS DA DISCIPLINA DE ORTODONTIA

Eu, Mônica Tirre de Souza Araújo, coordenadora do Programa de Pós-graduação em Odontologia - Ortodontia da Universidade Federal do Rio de Janeiro – UFRJ, autorizo acesso ao arquivo da Clínica da Disciplina de Ortodontia da Faculdade de Odontologia da UFRJ, localizada na Av. Professor Rodolpho Paulo Rocco, 325 Ilha do Fundão – Rio de Janeiro- RJ -Brasil, para fins de pesquisa de Dissertação de Mestrado Intitulada: "Estudo da anatomia do septo nasal e sua relação com a morfologia do complexo nasomaxilar".

Responsabilizo-me, juntamente Amanda Cunha Regal de Castro, Professora Doutora da Faculdade de Odontologia da UFRJ e Sarah Braga Sayão de Paula, aluna do Programa de Pós-Graduação em Odontologia - Ortodontia da UFRJ, a privacidade de seus conteúdos, como preconizam os Documentos Internacionais e a Res.466/12 do Ministério da Saúde e o Código Penal Brasileiro.

Rio de Janeiro, 09 de dezembro de 2019.

Profa. Mônica Tirre de Souza Araújo
Professor Associado
Siape: 6363393

MÔNICA TIRRE DE SOUZA ARAÚJO
Coordenadora do Programa de Pós-graduação em Ortodontia da Faculdade de Odontologia - UFRJ

Amanda Cunha Regal de Castro
Profª Adjunta do Depto.
Odontopediatria e Ortodontia
FO/UFRJ
SIAPE 1389283

AMANDA CUNHA REGAL DE CASTRO
Professora Adjunta do Programa de Pós-graduação em Ortodontia da Faculdade de Odontologia – UFRJ
Pesquisadora Responsável